AD-A083 677 NAVAL OCEAN SYSTEMS CENTER SAN DIEGO CA F/G 17/1
LIRA: A MODEL FOR PREDICTING THE PERFORMANCE OF LOW-FREQUENCY A--ETC(U)
JUN 79 D W HOFFMAN
UNCLASSIFIED NOSC/TD-259 NL

1 OF 2
AD A083677

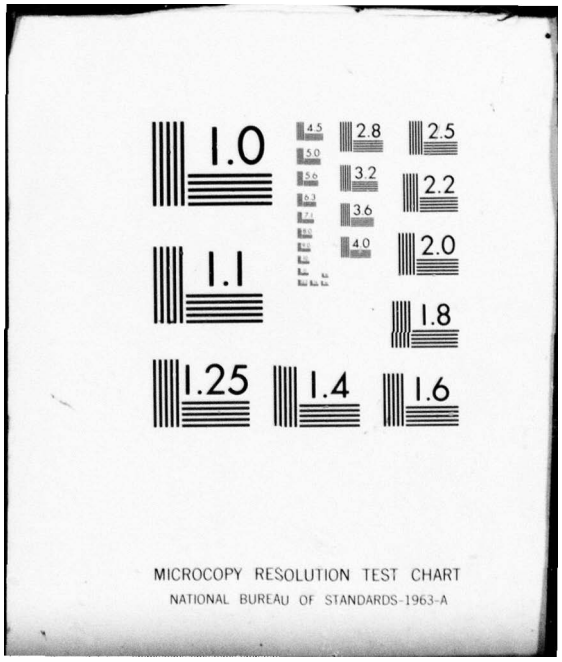
1.0
4.5
5.0
5.6
6.3
7.1
2.8
3.2
3.6
4.0
2.5
2.2
2.0
1.8
1.1
1.25
1.4
1.6
MICROCOPY RESOLUTION TEST CHART
NATIONAL BUREAU OF STANDARDS-1963-A

LEVEL II

12 NW

NOSC

NOSC TD 259

NOSC TD 259

Technical Document 259

LIRA: A MODEL FOR PREDICTING THE PERFORMANCE OF LOW-FREQUENCY ACTIVE-SONAR SYSTEMS FOR INTERMEDIATE SURVEILLANCE RANGES

DW Hoffman

June 1979

Final Report: December 1976 — May 1979

Prepared for
Naval Electronic Systems Command

AD A083677

DTIC FILE COPY

DTIC
ELECTE
S MAY 1 1980

A

Approved for public release; distribution unlimited

NAVAL OCEAN SYSTEMS CENTER
SAN DIEGO, CALIFORNIA 92152

80 4 30 003

NAVAL OCEAN SYSTEMS CENTER, SAN DIEGO, CA 92152

AN ACTIVITY OF THE NAVAL MATERIAL COMMAND

SL GUILLE, CAPT, USN
Commander

HL BLOOD
Technical Director

ADMINISTRATIVE STATEMENT

Initial model development (LORA) was sponsored from 1974 to 1976 by C.D. Smith, NSEA 63R, under the Acoustic Data Bank and Modeling Program, Subproject SF52-552-601, Task 19324. Development continued into early 1978 under the Environmental Acoustic Modeling Program, Project Element 62759N, Task SF52552601, sponsored by A.P. Franceschetti.

The extensive software modifications to LORA which resulted in the present model, LIRA, described in this document, were performed under the Active Acoustic Surveillance Program, Project Element 62711N, Task XF11101100, sponsored by J.N. Bertrand, NELX-320. NOSC sponsors were D.L. Carson, Code 714, and E.D. Chaika, Code 7242.

The author is indebted to many individuals who aided in the work. Melvin A. Pedersen and Dewayne White consulted on the caustic theory. Rawson F. Hosmer supplied the Airy-function subroutine used in the computer program. Dr. James L. Stewart, Dr. Howard M. Wight, and Larry K. Arndt consulted on the signal-processing model. This report was reviewed for technical accuracy by Dr. William H. Marsh and Dr. Harold R. Hall and was edited by Allen N. Saltzman. Most of all the author is indebted to Catherine L.N. Hoffman for her efforts in typing the manuscripts.

Released by
M.R. Akers, Head
System Concepts and Analysis Division

Authorized by
Dr. E.B. Tunstall, Head
Ocean Surveillance Dept.

UNCLASSIFIED
SECURITY CLASSIFICATION OF THIS PAGE (When Data Entered)

REPORT DOCUMENTATION PAGE

READ INSTRUCTIONS BEFORE COMPLETING FORM

1. REPORT NUMBER: NOSC/TD-259
2. GOVT ACCESSION NO.
3. RECIPIENT'S CATALOG NUMBER
4. TITLE (and Subtitle): LIRA: A Model for Predicting the performance of Low-Frequency Active-Sonar Systems for Intermediate Surveillance Ranges
5. TYPE OF REPORT & PERIOD COVERED: Final Report Dec 1976 – May 1979
6. PERFORMING ORG. REPORT NUMBER
7. AUTHOR(s): D.W. Hoffman
8. CONTRACT OR GRANT NUMBER(s): 12) 99
9. PERFORMING ORGANIZATION NAME AND ADDRESS: Naval Ocean Systems Center, San Diego, CA 92152
10. PROGRAM ELEMENT, PROJECT, TASK AREA & WORK UNIT NUMBERS: 62711N, XF11101100
11. CONTROLLING OFFICE NAME AND ADDRESS: Naval Electronic Systems Command, Washington, D.C. 393159 (11)
12. REPORT DATE: June 1979
13. NUMBER OF PAGES: 94
14. MONITORING AGENCY NAME & ADDRESS (if different from Controlling Office): (16) F11101
15. SECURITY CLASS. (of this report): Unclassified
15a. DECLASSIFICATION/DOWNGRADING SCHEDULE
16. DISTRIBUTION STATEMENT (of this Report): Approved for public release; distribution unlimited (17) XF111011 00
17. DISTRIBUTION STATEMENT (of the abstract entered in Block 20, if different from Report)
18. SUPPLEMENTARY NOTES
19. KEY WORDS (Continue on reverse side if necessary and identify by block number)

Active sonar
Underwater surveillance
Ray theory
Propagation simulation
Propagation loss model
Reverberation
Detection

20. ABSTRACT (Continue on reverse side if necessary and identify by block number)

LIRA is a computer model developed to predict the performance of active-sonar systems for intermediate-range surveillance. The program provides a series of outputs as a function of target range. Propagation loss (incoherent and largest arrival), reverberation level, and signal excess are provided in both printed and plotted forms. Other printed outputs are two-way travel time to the target, angle of largest ray arrival at the source, signal level at the output of the beamformer, signal-to-noise ratio, and probability of detection. Reverberation plots show surface, bottom, and volume components as well as total reverberation and competing noise level.

Source and receiver are not required to be at the same depth. Target ranges may extend from 1 yd to (cont)

Go next page

DD FORM 1 JAN 73 1473 EDITION OF 1 NOV 65 IS OBSOLETE
S/N 0102-LF-014-6601

UNCLASSIFIED
SECURITY CLASSIFICATION OF THIS PAGE (When Data Entered)

393159

1000 kyd; a maximum of 500 target ranges are allowed per run. Source frequency is allowed to be between 25 Hz and 25 kHz. Pulse length may be between 10^{-4} and 100 s.

The sound-speed profile is represented by curvilinear segments to eliminate false caustics. The sound-speed profile is assumed to be constant with range and the ocean bottom horizontal.

The propagation loss models are (1) ray theory supplemented with caustic corrections derived by Brekhovskikh, and (2) empirical equations based on the AMOS data and corrected for low frequencies using normal mode theory. Beam patterns for both transmitter and receiver are incorporated into propagation loss. The Hall-Watson model is used for absorption loss.

Surface backscattering strength is a combination of the Chapman-Harris equations, Eckart's equations, and Richter's data. Bottom backscattering strength is derived from Lambert's law and Schmidt's data. Volume backscattering strength is represented as the column strength.

Reverberation is averaged over the pulse length. Contributions from previous pings, if any, are included in the reverberation level for the current ping. Reverberation is corrected for doppler gain due to target motion.

Either recognition differential or detection threshold may be used in computing signal excess; if the latter, reverberation and noise are corrected for signal-processing gain. Signal excess is plotted corresponding to both the incoherent-sum and largest-arrival propagation losses to the target. Five probability-of-detection models for various assumptions of signal distortion and detector characteristics are available.

The computer program uses 10 – 300 s of cpu time per run on the UNIVAC 1110 computer and requires 57,000 words of core storage.

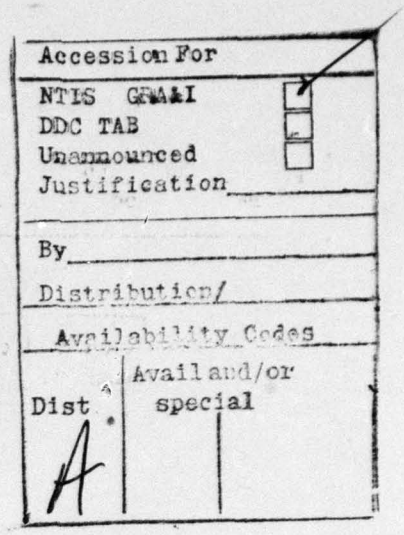

CONTENTS

SUMMARY

OBJECTIVE

Extend the capabilities of LORA (Ref. 1), a computer model for predicting the performance of active sonars, to simulate active-sonar surveillance scenarios. Specifically, include the following additional capabilities:

1. Frequency regime shall be 25 Hz to 25 kHz.
2. Broad bandwidths and long pulse lengths for FM and PRN signals shall be allowed.
3. Target range shall be increased to a 1000-kyd maximum.
4. Source and receiver shall not be restricted to the same depth.
5. Output plots shall be made available.

COMPUTER PROGRAM DESCRIPTION

The new computer program, LIRA, contains many of the capabilities of its predecessor, LORA. The capabilities of LIRA, after incorporating the new additions to the model, include:

1. Active-sonar performance predictions can be obtained for target ranges extending from .001 kyd to 1000 kyd.
2. Source frequencies can be from 25 Hz to 25 kHz.
3. The source and receiver are not restricted to the same depth. (The target can be at still another depth).
4. The scenario of a receiving array mounted on a steeply sloping shelf is modeled.
5. Curvilinear techniques are used with the sound-speed profile to eliminate false caustics.
6. Propagation losses calculated using ray theory are supplemented with caustic corrections derived from wave theory.
7. The spatial positions of caustics are determined by iterative methods.
8. Beam patterns for both transmitter and receiver are allowed.
9. The surface duct propagation loss model is based on the AMOS equations modified for low frequencies using normal mode theory.
10. The Hall-Watson model is used for absorption loss.
11. The surface backscattering strength is derived from the Chapman-Harris equation, Eckart's equations, and Richter's data (the user may also enter his own model).
12. Bottom backscattering strength is derived from Lambert's law and Schmidt's data (the user may also enter his own model).
13. Volume backscattering strength is represented as the water column backscattering strength.

14. Reverberation is averaged over the pulse length.

15. A maximum pulse length of 100 s is allowed.

16. Reverberation contributions from previous pings, if any, are included in the reverberation level for the current ping.

17. Doppler gain against reverberation can be calculated by the program or entered as an input.

18. CW, FM, and PRN signals are allowed.

19. Reverberation and noise are corrected for processing gain.

20. Either recognition differential (at the output of the beamformer) or detection threshold (at the output of the signal processor) may be used to represent the detection-decision process.

21. Signal excess can be calculated using the propagation loss to the target for either the incoherent sum of ray arrivals or the largest arrival.

22. Five probability-of-detection models are available for various assumptions of signal distortion and detector characteristics.

23. Plots are available for propagation loss, reverberation, and signal excess. Reverberation plots display surface, bottom, and volume components as well as total reverberation and competing noise level. Propagation loss and signal excess plots each contain two curves, one for the incoherent sum of ray arrivals and one for the largest arrival.

LIRA has the following limitations:

1. The bottom is assumed to be horizontal.

2. The sound-speed profile cannot vary with horizontal range.

3. The source and receiver cannot be displaced in either range or azimuth.

The LIRA computer program has been executed thousands of times and is able to perform many successive runs without failure. Computer costs are low, from $2 to $15 per run (10 to 300 s of cpu time for the UNIVAC 1110 computer). The average cost for surveillance predictions is $5 with plots extra (about $4 per plot). Computer core storage required is 57,000 words. The program is segmented to allow for plotting.

RECOMMENDATIONS

Caustics in deep submerged ducts give rise to excessively low propagation losses for certain geometries. Either a model to describe leakage of sound from the duct should be developed and validated or another model currently available should be chosen for the incorporation into LIRA.

Separation of source and receiver in range should be modeled as the next step in the development of a bistatic model.

Plots of normalized reverberation vs time should be provided so that comparisons with other reverberation models can be made directly.

The fields at horizontal caustics should be investigated.

INTRODUCTION

LIRA, Low-frequency Intermediate Range Active-sonar performance prediction program is a revision and an extension of LORA, LOng-Range Active-sonar performance prediction program (Ref.1). The LORA computer program was created to predict the performance of active-sonar systems for frequencies above 1 kHz and for ranges not greater than five convergence zones. For active-sonar systems using this frequency regime, three convergence zones is long range.

Stimulated by active-source technologists, the Navy in 1977 renewed its interest in mid- to low-frequency active-sonar surveillance. Two modeling requirements arose:

1. Determine the optimum design parameters of a new-technology active source, i.e., specify source level, bandwidth, and frequency. Highest priority must be given to using current receiver assets.

2. Make performance predictions for combinations of operating environments and system parameters.

LIRA was developed to play a role in satisfying both of these requirements. LORA was inadequate for the following reasons:

1. LORA's active-sonar performance prediction capability is limited to five convergence zones and five bottom bounces. The maximum range for accurate predictions is therefore limited to 75 kyd in upward-refracting areas, such as the Mediterranean, and areas characterized by a submerged double duct.

2. LORA does not have caustic corrections. Below 1 kHz the acoustic fields from caustics extend noticeably into the shadow zones predicted by classical ray theory. Below 100 Hz these fields dominate a curve of propagation loss vs range.

3. LORA does not have the capability to generate output plots.

4. LORA's signal processing model is designed for a short CW pulse. The possibility of using a PRN waveform with a long pulse for active surveillance requires averaging the reverberation over pulse length and correcting both reverberation and noise for the time-correlation gain.

Because of these deficiencies with respect to the modeling requirements, LORA did not impact initial system-design studies. However, the decision was made to extend LORA to low frequencies, longer ranges, and longer pulse lengths. A capability to model bistatic sonar (separation of source and receiver in three dimensions) was also requested, but constraints of time and money allowed only the modeling of depth separation of source and receiver.

The body of this report describes the LIRA model in those aspects in which it differs from its predecessor, LORA, which is described in Ref. 1. Some of the capabilities of the LIRA program that are mentioned in the Summary are not described in the text of this report because they are described in Ref. 1. The topics that are included here are restructured ray tracing, caustics, pulse-averaged reverberation, and source-receiver depth separation.

The first section describes the revised propagation loss model used in LIRA. Basic definitions are given for clarity. The logical order of steps used in the program to calculate propagation loss by merging ray theory with caustic corrections derived from wave theory is presented. The properties of caustics are described and equations are given for the propagation loss at and near caustics. LIRA's methods to isolate caustics and to determine iteratively the caustic parameters are described. The next section describes the reverberation model as it differs from that described in Ref. 1. The addition of long pulse lengths to LIRA's list of options requires that the reverberation be averaged over the time interval (pulse length) that the signal is being received. Pulse-averaged reverberation is described for CW, FM, and PRN signals. The final section deals with the separation of source and receiver in depth. It is shown that propagation loss for all source-target-receiver paths is equivalent to the average of the two-way propagation losses from source to target and from receiver to target. Reverberation is similarly represented, and the errors introduced by using monostatic backscattering strengths instead of bistatic backscattering strengths are estimated. A summary of model and software improvements for LIRA is given. Results of comparisons with other models (Appendix D) are described. Recommendations for further work are given.

Appendix A presents the logical structure of the LIRA program to aid the user in streamlining his inputs. Appendix B gives descriptions of inputs for the LIRA program, i.e., definitions of parameters, acceptable limits of parameters, typical values, etc. Appendix C describes the input format in detail; examples are given. In Appendix D LIRA's propagation loss calculations are compared with those from PLRAY, FACT, and AP2. Appendix E gives an example of using LIRA for predicting performance in a scenario in which the source is located above a receiving array lying on a sloping shelf. Detection ranges are printed and output plots are given for propagation loss, reverberation, and signal excess.

REVISED PROPAGATION LOSS MODEL

The propagation loss model used in LORA has been revised to incorporate caustic corrections. This section explains the approach used in the LIRA program for merging ray theory with the expressions for caustic fields. First, some basic definitions are given to clarify terminology used throughout the report. Then, the procedure used by the LIRA program to trace rays, isolate caustics, and merge ray and caustic propagation losses is presented in a step-by-step format. Following this, the discussion of caustics is greatly amplified. Equations are given for the caustic fields. The iterative procedure to determine caustic parameters exactly is described in detail.

BASIC DEFINITIONS

Throughout this report, reference is made to ray paths, ray segments, ray parameters, ray types, and ray families. Definitions of these terms will facilitate the discussion which follows. The definitions are given in order to avoid confusion with alternative usage by other authors. Because ray tracing is described in detail in the companion document describing LORA (Ref. 1, pp. 25-34), the definitions given here are only supplementary.

A ray path is the path along which sound travels through the water from one point of interest to another. The ray path may contain turning points, i.e., reversals of direction in depth, either refractive or reflective. The depth at which a turning point occurs is called the vertex depth.

A ray segment is a part of a ray path connecting two depths of interest. Ray paths connecting two depths are constructed by assembling ray segments. A ray segment has no complete turning points, although an end of a segment may be at a turning point. In LIRA three basic ray segments are used: upper turning point to source depth, upper turning point to target (or backscattering) depth, and upper turning point to lower turning point. The last segment is one-half of a ray cycle.

Ray parameters comprise the range and its derivatives, travel time, and absorption loss. Ray paths and ray segments may be thought of as vectors with ray parameters as components. A ray path is the vector sum of ray segments appropriately chosen so that the ray path connects two depths of interest.

A ray type is one of four possible ways that ray paths can be constructed using combinations of the same ray segments to connect two depths. The four ray paths so constructed have their end points at the same depths, but the ray parameters are, in general, different. The angles of the ray paths at the starting and ending depths are the four combinations of positive and negative angles, that is,

RAY TYPE	SIGN(ϕ_X)	SIGN(ϕ_T)
1	+	+
2	–	+
3	+	–
4	–	–

where ϕ_X is the starting angle at the source depth, ϕ_T is the ending angle at the target depth, and the signs are positive for angles downward from the horizontal. These four ray types are used for calculating propagation losses to the target and volume backscatterers. Ray paths which terminate at turning points have degenerate ray types, so there are only two unique ray types for paths to the surface or bottom:

RAY TYPE	SIGN(ϕ_X)	SIGN(ϕ_S)	SIGN(ϕ_B)
1	+	+	–
2	–	+	–

where ϕ_S and ϕ_B are the angles at the surface and bottom, respectively. These ray types are used for calculating surface and bottom reverberation.

The ray tracing methods in the LORA computer program have been revised to reduce storage and to include calculations for caustics. Formerly, in the LORA computer program, rays were generated one at a time, with a stored ray path interpolated with the current ray path for target range. The current ray path parameters were then stored over the old ray path parameters, a new ray path for a new starting angle was generated, etc.

The implementation of caustic corrections necessitated scanning families of rays (rays with selected starting angles or vertex sound speeds) to isolate caustics and iterate on vertex sound speed to exactly determine caustic parameters. With the old method of ray path generation, storage would have been increased dramatically.

In the LIRA program calculations are performed in this order:

1. Ray segments are traced from upper vertexing depth to source depth, target depth, and bottom depth for 40 bottom bounce and 40 convergence zone (refractive) rays. Five ray parameters are calculated for each segment: range, travel time, absorption loss, and first and second range derivatives (with respect to vertex sound speed). The total storage required is 2400 cells. The storage areas required for propagation loss to the target and for volume reverberation are overlaid in core.

2. A backscatterer (target is included in this category) is selected.

3. A ray type is selected. There are four basic ray types, with rays either up or down at the source or up or down at the target.

4. A ray family which contains no discontinuities in the range derivative is selected from the set of 40 ray paths.

5. A cycle number (half the number of ray reversals) is selected. This number often corresponds to the number of convergence zones for near-surface source and target.

6. The stored ray segments are used to compute 40 ray paths for the given cycle number and ray type. The minimum and maximum range values are inspected to ensure that they overlap user-specified ranges of interest.

7. The range derivatives are examined to find successive values which straddle zero. Other tests are made by comparing successive ranges and range derivatives to determine possible zeroes for the range derivative.

8. An iterative search is performed to obtain the exact parameters for which the range derivative is zero. Successive values for vertex sound speed C_n are estimated with

$$C_{n+1} = C_n - \frac{\left(\frac{\partial R}{\partial C_n}\right)}{\left(\frac{\partial^2 R}{\partial C_n^2}\right)}$$

where R is range.

9. The propagation loss is calculated for user-specified ranges by using Pedersen's equations (Ref. 2) adapted from Brekhovskikh's treatment (Ref. 4) for a field near a caustic. Minimum and maximum ranges for the caustic field are obtained so that ray interpolation in the range region dominated by the caustic can be excluded.
10. If more than one caustic occurs in this family, Steps 8 and 9 are repeated.
11. The remaining ray paths in this family are used to interpolate for propagation loss at user-specified ranges which lie outside all the caustic intervals of Step 9.
12. The next cycle number is selected and Steps 6–11 are repeated.
13. After all the cycles have been exhausted that allow calculations for user-specified ranges, the next family of rays is selected and Steps 5–12 are repeated.
14. After all the ray families have been exhausted, the next ray type is selected and Steps 4–13 are repeated.
15. After the two or four ray types have been exhausted, the next backscatterer is selected and Steps 3–14 are repeated.

CAUSTICS

Detections at long ranges typically occur only in the regions of caustics. Correct evaluation of caustic fields is therefore essential to estimate detection ranges with any degree of confidence.

A large number of caustics can exist over a range interval of 300 nmi. Usually only one or two main caustic peaks appear within the range interval of a ray cycle, but often enough there are four to eight caustics per ray cycle. The deeper the source and target are below the surface, the greater is the range separation between caustics belonging to different ray types in a given ray cycle and the more the caustics are resolved as individual peaks. A common sound-speed profile is illustrated in Fig. 1, as well as a ray diagram (not to scale). A ray family exists for which four ray types with maximum sound speeds less than the surface sound speed cross the target depth at e, f, g, and h. Each of the four ray types may produce a caustic at the target depth (though not necessarily). Another ray family exists for which four ray types strike the surface and cross the target depth at a, b, c, and d. Again, each of these ray types could produce a caustic at the target depth. For this sound-speed profile, the two ray families, each with four ray types, could produce eight caustics per ray cycle. If a ray cycle is 60 kyd, then a 600-kyd plot of propagation loss could contain contributions from 80 caustics. A more complex sound-speed profile than the one of Fig. 1 could increase the maximum number of caustics.

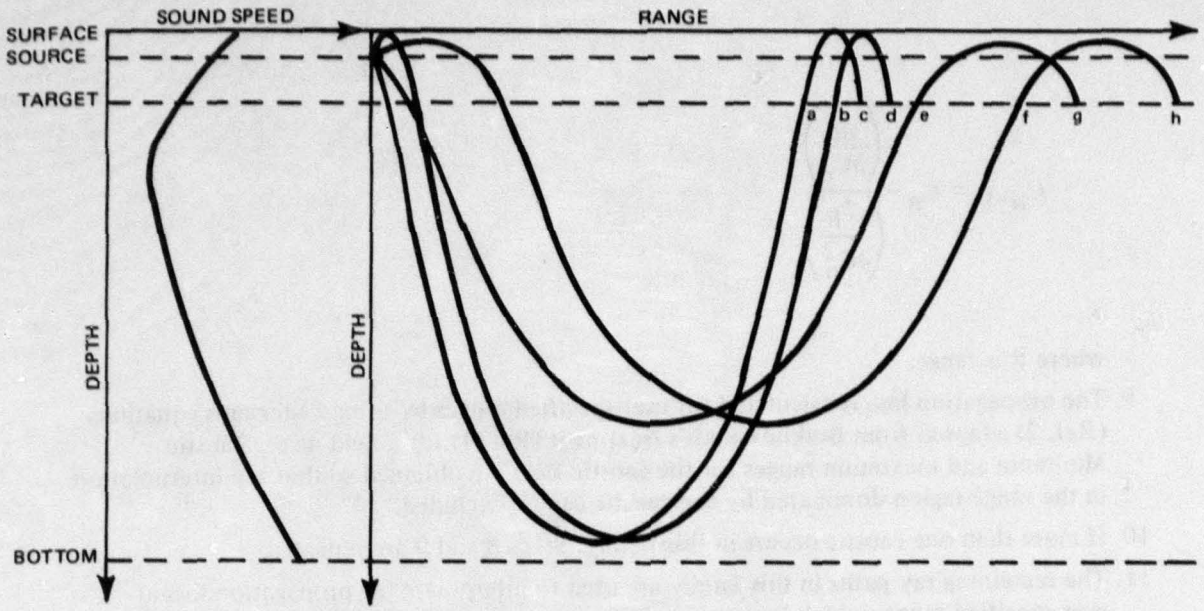

Figure 1. Caustics possible at the target depth.

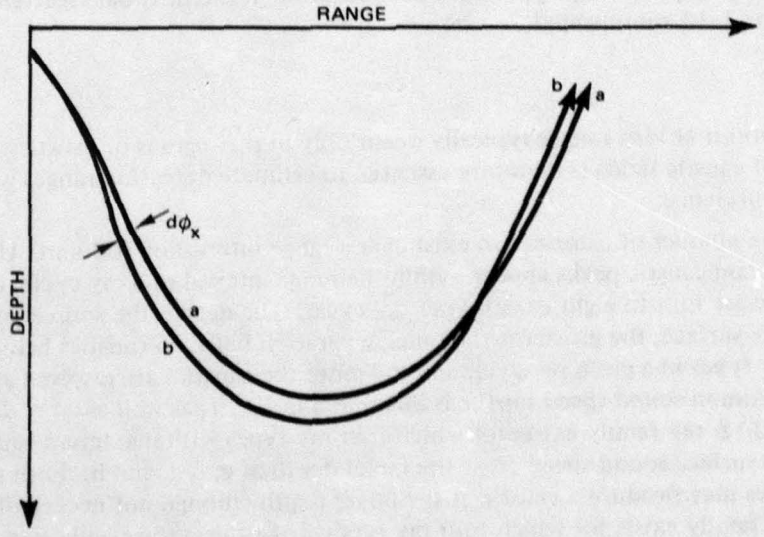

Figure 2. The crossing of neighboring rays.

For high frequencies, say above 1 kHz, standard ray tracing procedures that lack specialized treatment for evaluating fields near caustics still yield adequate predictions for detection ranges. The magnitude of the peaks may be in error, but the ranges at which signal excess crosses zero are reasonably accurate. Above 1 kHz the high absorption of sound limits active-sonar detection to one or, at most, two convergence zones. As frequency decreases, however, the peaks attributed to caustic fields broaden and decrease in magnitude. Unmodified ray theory cannot predict this broadening effect, which is nevertheless known from normal mode calculations for propagation loss. Below 700 Hz the peaks are broadened in range by more than a kyd. At 500 Hz absorption loss is only 1 dB for 500 kyd of path length. Below 500 Hz intermediate-range propagation effective for detection appears to be due to the fields at and near the caustics.

DEFINITION OF A CAUSTIC

In ray theory a caustic occurs when neighboring rays, i.e., rays contained within some differential ray tube, coalesce and cross at some distance from the source (see Fig. 2). A smooth caustic is formed when consecutive neighboring rays in a finite ray tube cross, producing a series of neighboring points constituting a caustic surface (see Fig. 3a). In the geometry of the LIRA model, the vertical range-depth plane, the smooth caustic becomes a line. Figure 3b illustrates schematically how two rays, finitely separated, cross near a caustic. As the rays become arbitrarily close together, point "p" moves onto the caustic surface, represented by the dotted line. All rays forming the caustic are tangent to it. Only the underside of the caustic is illuminated in Fig. 3a. No rays of the family creating the caustic can pass into the shadow region. For this reason the caustic is sometimes referred to as an envelope.

Ray theory predicts that a caustic intensity is zero in the shadow zone and infinite on the envelope. Near the envelope, in the illuminated region, ray theory may predict unreasonably high intensities, depending on the interpolation points.

In ray theory intensity per unit solid angle I/F is easily derived using the concept of solid angle. One of the resulting forms is

$$I/F = \left| R \frac{\partial R}{\partial C_v} \tan \phi_X \tan \phi_Z C_v C_Z / C_X \right|^{-1} \qquad (1)$$

where

R is range,
C denotes sound speed,
ϕ denotes angle down from horizontal,
and X, v, and Z denote source, vertex, and ending depths, respectively.

The partial derivative is evaluated along the horizontal, i.e., depth z is held constant. Obviously, when rays cross at depth z, forming a caustic,

$$\frac{\partial R}{\partial C_v} = 0 \qquad (2)$$

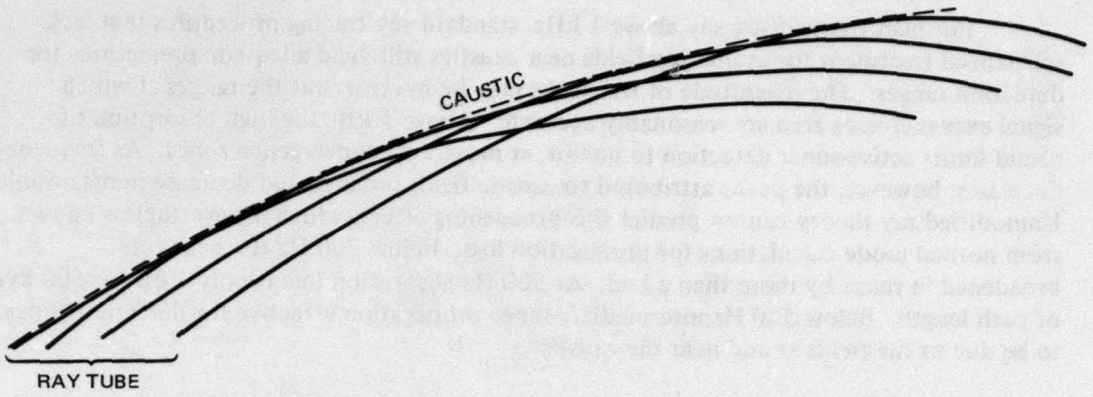

(a) Rays crossing to form a caustic envelope.

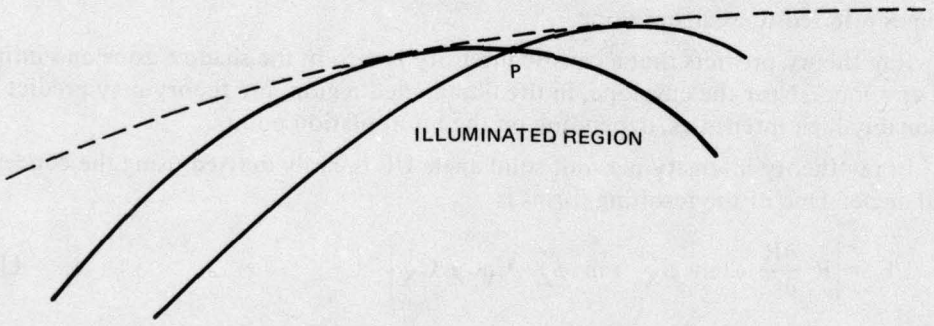

(b) Expanded view of rays crossing.

Figure 3. Pattern of rays crossing to form a caustic.

The intensity on the caustic, by Eq. (1), must be infinity.

Actually the intensity on the caustic is finite. There is also a boundary region or boundary layer on both sides of the caustic in range and depth for which ray theory is in error. The solution to the wave equation exactly describes the pressure field anywhere in the space-time domain. Unfortunately, the wave equation has not, in general, been solved. With some restrictions, the method of normal modes produces exact solutions for special cases. Fortunately, approximation solutions have been derived for the wave equation at and near caustics.

APPROXIMATION FOR THE CAUSTIC FIELD

Requirements for several scientific disciplines, quantum mechanics, electromagnetics, wave guide analysis, and acoustics, have stimulated mathematical development employing normal mode theory (phase integral method), WKB approximation, and uniform and nonuniform asymptotic expansion of integrals to estimate caustic fields. The solutions most amenable to this work were developed by Ludwig (Ref. 3), whose expressions involve the Airy function and its derivative, and by Brekhovskikh (Ref. 4), whose expressions contain the Airy function alone. Both derivations express the field as a superposition of an infinite series of plane waves (as an integral), isolate the caustic, apply the method of steepest descent (with different expressions for the integrand), and keep only the significant terms in frequency (wave number). Brekhovskikh's method has the simplification that the solution to the wave equation is the WKB approximation for geometrical optics. Brekhovskikh's treatment was chosen for use in the LIRA program because expressions in the LIRA coordinate system were readily available, and the difference in estimations in the region of the boundary layer is negligible.

Pedersen's expressions (Ref. 2), derived from Brekhovskikh's treatment, give propagation loss H as a function of range R,

$$H(R) = -10 \log (I/F)_c - 20 \log [Ai(t)/Ai(o)] \tag{3}$$

$$(I/F)_c = 2.32 (C_X/C_T C_v) \left| \cot \phi_X \cot \phi_T \right| f^{1/3} \Big/ \left(R_c \left| C_v \frac{\partial^2 R}{\partial C_v^2} \right|^{2/3} \right) \tag{4}$$

$$t = (R_c - R)/L \tag{5}$$

$$L = 0.2331 C_v \left(C_v \frac{\partial^2 R}{\partial C_v^2} \right)^{1/3} f^{-2/3} \tag{6}$$

where

$(I/F)_c$ is the intensity at the caustic relative to the intensity at 1 yd,

Ai is the absolute value of the Airy function with t as its argument,

C_X is the sound speed at the source depth,

C_T is the sound speed at the target depth,

C_v is the sound speed at the ray vertexing depth,

ϕ_X is the angle from the horizontal at the source depth,

ϕ_T is the angle at the target depth,

f is frequency in Hz,

R_c is the range of the caustic at the target depth,

and $\frac{\partial^2 R}{\partial C_v^2}$ is the second derivative of range with respect to C_v for the ray path starting at the source depth and terminating at the target depth. It is evaluated in this case for the value of C_v such that $\frac{\partial R}{\partial C_v} = 0$

For a sound-speed profile fitted with curvilinear segments, the second derivative of range with respect to vertexing sound speed, with depth held constant, is given (Ref. 5) by

$$\frac{\partial^2 R}{\partial C_v^2} = -(a + 5B + 3R)/C_v^2$$

where

$$a = \Sigma D_i (\alpha_{1i} + \alpha_{2i})$$

$$\alpha_{1i} = B_{1i} (\cot^2 \phi_i + 2D_i)$$

$$\alpha_{2i} = B_{2i} (\cot^2 \phi_{i+1} + 2D_i)$$

$$B = C_v \frac{\partial R}{\partial C_v} = \Sigma [D_i (B_{1i} - B_{2i}) - R_i]$$

$$R = \Sigma R_i$$

The subscript i refers to the i^{th} layer and 1i and 2i refer to the upper and lower boundaries of the i^{th} layer, respectively. Equations for D_i, B_i, and B_{2i} are given in Ref. 1, page 22, or in Ref. 6. Summations include all segments needed to construct a ray path with a given number of cycles and ray type connecting source and target depths.

Figure 4 shows a plot of the term $-20 \log [Ai(t)/Ai(0)]$ used in Eq. (3). Range is related to t by Eq. (5). The caustic envelope, i.e., the position at which the range derivative is zero, corresponds to $t = 0$. The illuminated side of the caustic corresponds to negative t and the shadow zone to positive t.

Figure 5 shows a plot of propagation loss near a caustic derived by standard ray tracing and the corresponding propagation loss obtained by using Eq. (3). The shape of the Airy-integral approximation is reversed from Fig. 4 to Fig. 5. This is because for positive L, t is negative in Eq. (5) for $R > R_c$. The LIRA program uses Eq. (3) in the region

$$-2.2 \leqslant t \leqslant 3$$

Outside this boundary layer, LIRA uses standard ray tracing for derivation of propagation loss.

The LIRA program makes no attempt to smooth the changeover from Airy-function

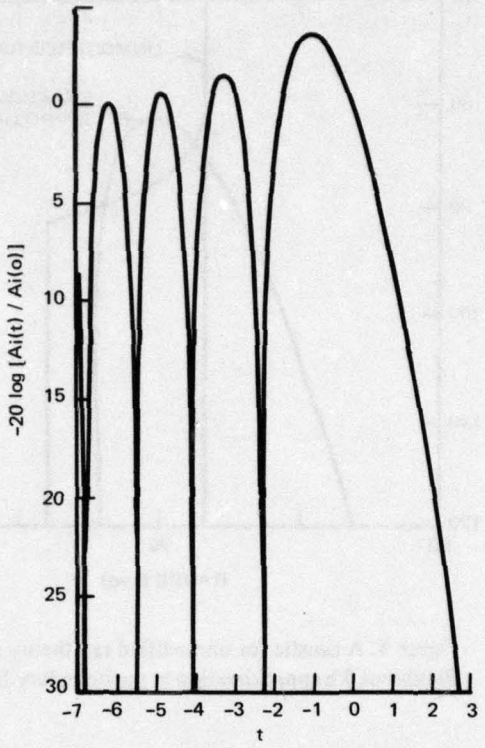

Figure 4. Difference in propagation loss relative to that at the caustic envelope located at t = 0 (from Ref. 2).

caustic curve to the ray tracing interpolation. For small steps in range, interpolation produces a small notch on the illuminated side of the caustic (t = −2.2), a minimum at 72.4 kyd in the curve in Fig. 6. For range increments of 1 kyd or more, the transition is almost always smooth.

The LIRA program does not interpolate the illuminated side of the caustic for ranges at which there are no ray arrivals. Interpolation of a given caustic could be truncated between t = 0 and t = −2.2.

Locating a Caustic

Locating the range of a caustic for a given target depth requires numerically solving Eq. (2) for $C_v = C_c$ such that

$$D(C_c) = \left.\frac{\partial R}{\partial C_v}\right|_{C_c} = 0$$

Since there are many caustics, Eq. (2) must be solved many times to determine C_v, R_c and $\partial^2 R/\partial C_v^2$ for use in Eqs. (4) and (6). It is important not to confuse the solution for one caustic with that of another. For a given caustic certain parameters are fixed: starting and ending depths, ray type, number of ray cycles, and sound-speed limits on ray family. A sequence of ray segments is calculated for the rays in the family for a certain number of preselected vertex sound speeds (C_v's). The ray segments span upper turning depth

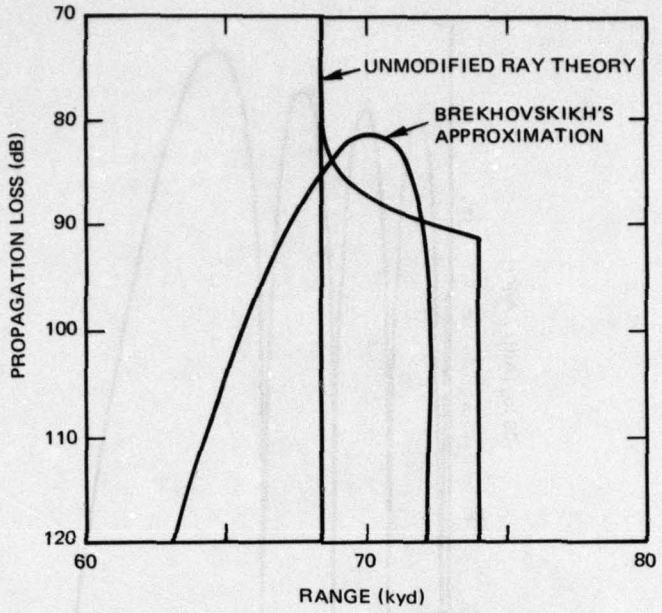

Figure 5. A caustic for unmodified ray theory and the Brekhovskikh approximation in the boundary layer.

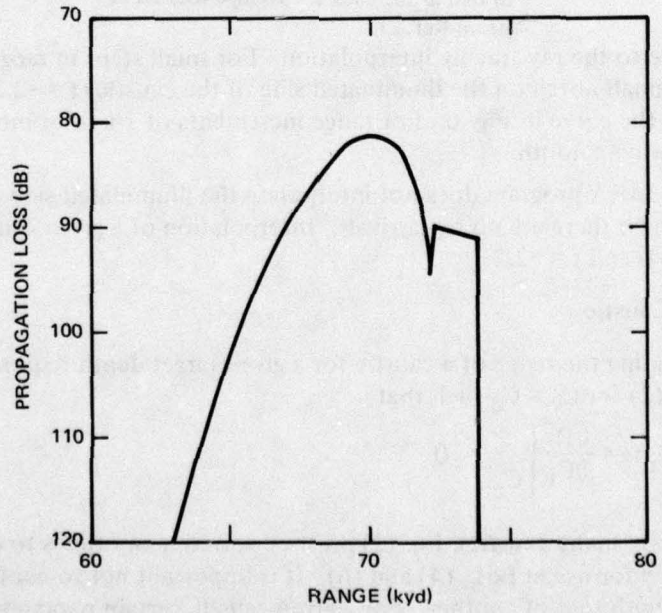

Figure 6. Caustic interpolation merged with standard ray theory outside of the boundary layer (interpolation is at 0.1-kyd intervals).

(either a refractive apex or surface hit) to source, target, and bottom depths. The ray parameters calculated for each segment are range, range derivative, second range derivative, time, and absorption loss. The ray segments are combined in the manner described in Ref. 1, pp. 26-30, to obtain the ray parameters for a path of given cycle number and ray type. The range derivatives for the set of rays in the given ray family are scanned for changes of sign. Whenever a sign change occurs, the range derivative must have crossed zero, and a caustic has occurred. Whenever a caustic is found, its parameters are determined by an iterative procedure described in the next section.

A second scan of the family of rays is performed to try to isolate caustics. Denote iterated ranges by R_i and derivatives by D_i. If $R_{i+1} < R_i$ and D_{i+1} or $D_i \geq 0$ or if $R_i < R_{i+1}$ and D_{i+1} or $D_i \leq 0$, then two or more caustics occur in the interval (R_i, R_{i+1}). An example is given by Fig. 7. The slopes (D_1, D_2) are positive at R_1 and R_2. Therefore, for R_2 to be less than R_1, a negative slope must occur in the interval (R_1, R_2). The derivative must pass through zero twice, first positive to negative, then negative to positive, for R to decrease between R_1 and R_2.

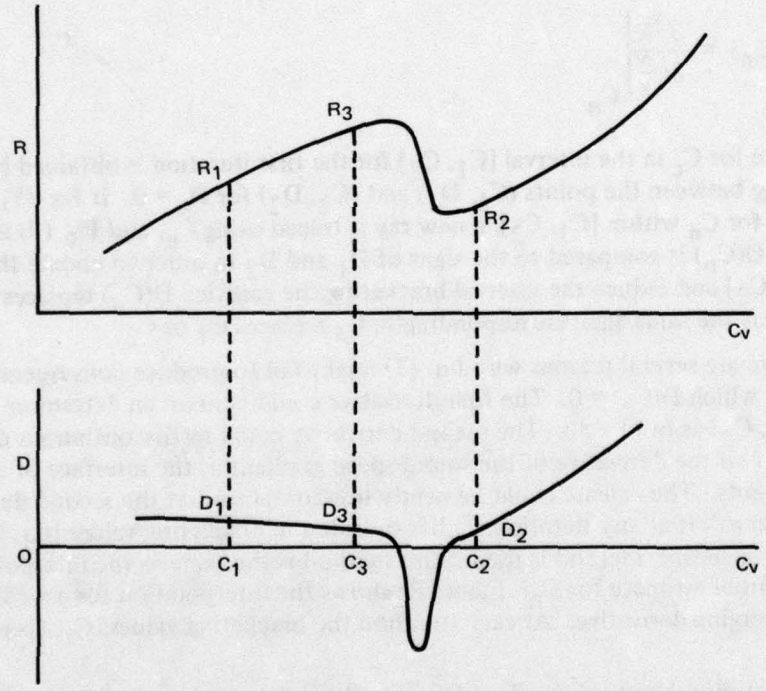

Figure 7. Range R and range derivative D vs vertex sound speed C_v-axis.

In order to isolate the two caustics, it is necessary to find a point on the C_v-axis where the derivative changes sign. The interval (C_1, C_2) is halved to obtain vertex sound speed C_3, and another ray is traced in order to calculate the corresponding range R_3 and derivative D_3. If the derivative has changed sign, then both caustics have been isolated, one on either side of C_3, that is, one each in the intervals (C_1, C_3) and (C_3, C_2). If the

derivative has not changed sign, R is compared to R_1. In Fig. 7 $R_3 > R_1$, so the two caustics must occur to the right of C_3, the interval (C_3, C_2) is halved, and C_3 and R_3 replace C_1 and R_1, respectively. In the LIRA program, this procedure continues until the sign change in the derivative occurs, successive sound speeds are less than 10^{-5} ft/s apart, or 30 iterations have passed. Typically, only one or two iterations are needed.

ITERATION TO EXACTLY DETERMINE CAUSTIC PARAMETERS

Once a caustic has been isolated by finding a sound-speed interval $[C_1, C_2]$ in which the range derivative changes sign, an iterative procedure is used to determine the value C_c for vertex sound speed for which the range derivative is zero. Application of the Newton-Raphson method gives successive approximations C_n for C_c:

$$C_{n+1} = C_n - D(C_n)/D'(C_n) \tag{7}$$

where

$$D(C_n) = \left.\frac{\partial R}{\partial C_v}\right|_{C_n}$$

and

$$D'(C_n) = \left.\frac{\partial^2 R}{\partial C_v^2}\right|_{C_n}$$

The estimate for C_c in the interval $[C_1, C_2]$ for the first iteration is obtained by linearly interpolating between the points (C_1, D_1) and (C_2, D_2) for $D_c = 0$. If Eq. (7) yields an estimate for C_n within $[C_1, C_2]$, a new ray is traced using C_n, and Eq. (7) is reapplied. The sign of $D(C_n)$ is compared to the signs of D_1 and D_2 in order to update the bracketing values $[C_1, C_2]$ and reduce the interval bracketing the caustic. $D(C_n)$ replaces D_1 or D_2, whichever has the same sign; correspondingly, C_n replaces C_1 or C_2.

There are several reasons why Eq. (7) might fail to produce convergence to the value C_c for which $D(C_c) = 0$. The first derivative could contain an extremum in the interval $[C_1, C_2]$ as in Fig. 8b. The second derivative could be discontinuous due to the discontinuity of the derivative of the sound-speed gradient at the interface of sound-speed-profile segments. The caustic could be nearly horizontal so that the second derivative approaches zero. If at any iteration C_n lies outside the bracketing values $[C_1, C_2]$, the *regula falsi*, or secant, method is used. This method is the same as the interpolation to obtain the initial estimate for C_n. Figure 8a shows the interpolation for a well-behaved rapidly converging derivative. At each iteration the bracketing values $[C_1, C_2]$ are updated as before.

Sometimes, Newton's method fails and the *regula falsi* method converges too slowly. An example of this is shown in Fig. 8b. Successive iterations move C_n slowly to the left. A maximum of 30 iterations is allowed per caustic. If the secant method does not produce a sign change in the derivative or reduce the magnitude of the derivative by 0.6 for successive derivatives of the same sign, then the next C_n is selected to be the midpoint of the bracketing interval $[C_1, C_2]$. In Fig. 8b halving the interval four times will produce a C_n for which Eq. (7) will again apply. On every iteration a new attempt is made to predict C_n using Eq. (7). As soon as C_n falls within the updated bracketing values $[C_1, C_2]$,

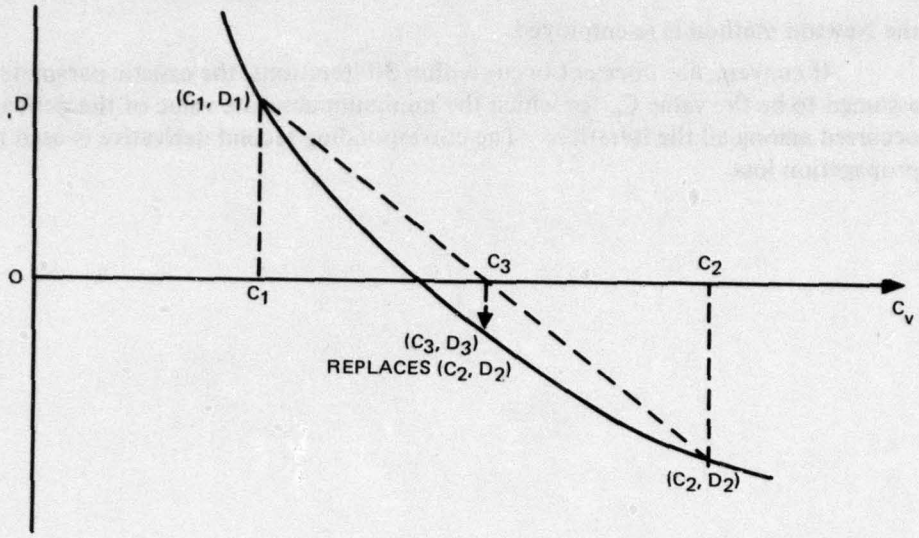

a. Rapid convergence.

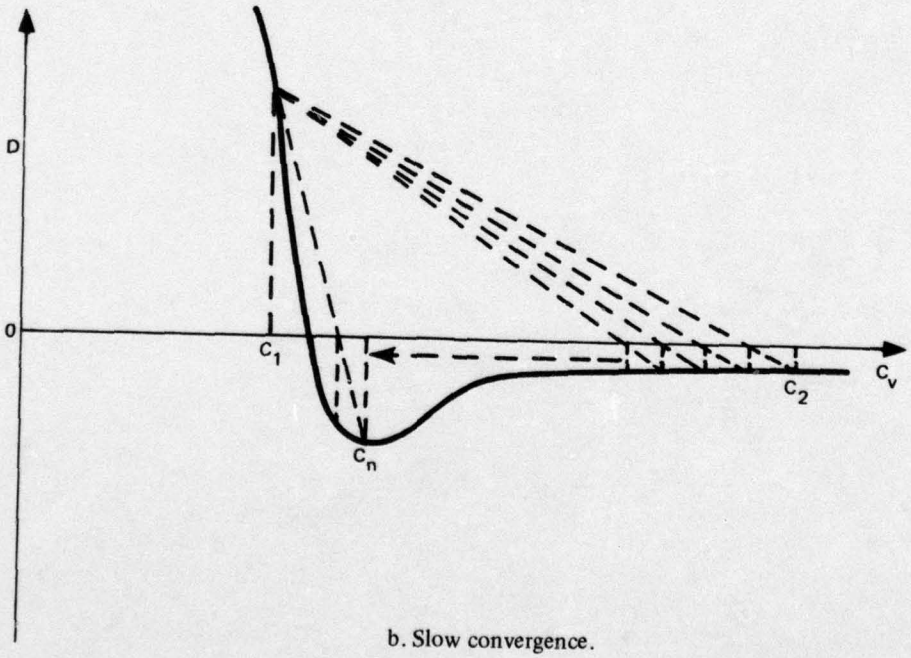

b. Slow convergence.

Figure 8. Constructions for the *regula falsi* method.

the Newton method is re-employed.

If convergence does not occur within 30 iterations, the caustic parameter C_c is assumed to be the value C_n for which the minimum absolute value of the derivative has occurred among all the iterations. The corresponding second derivative is used to calculate propagation loss.

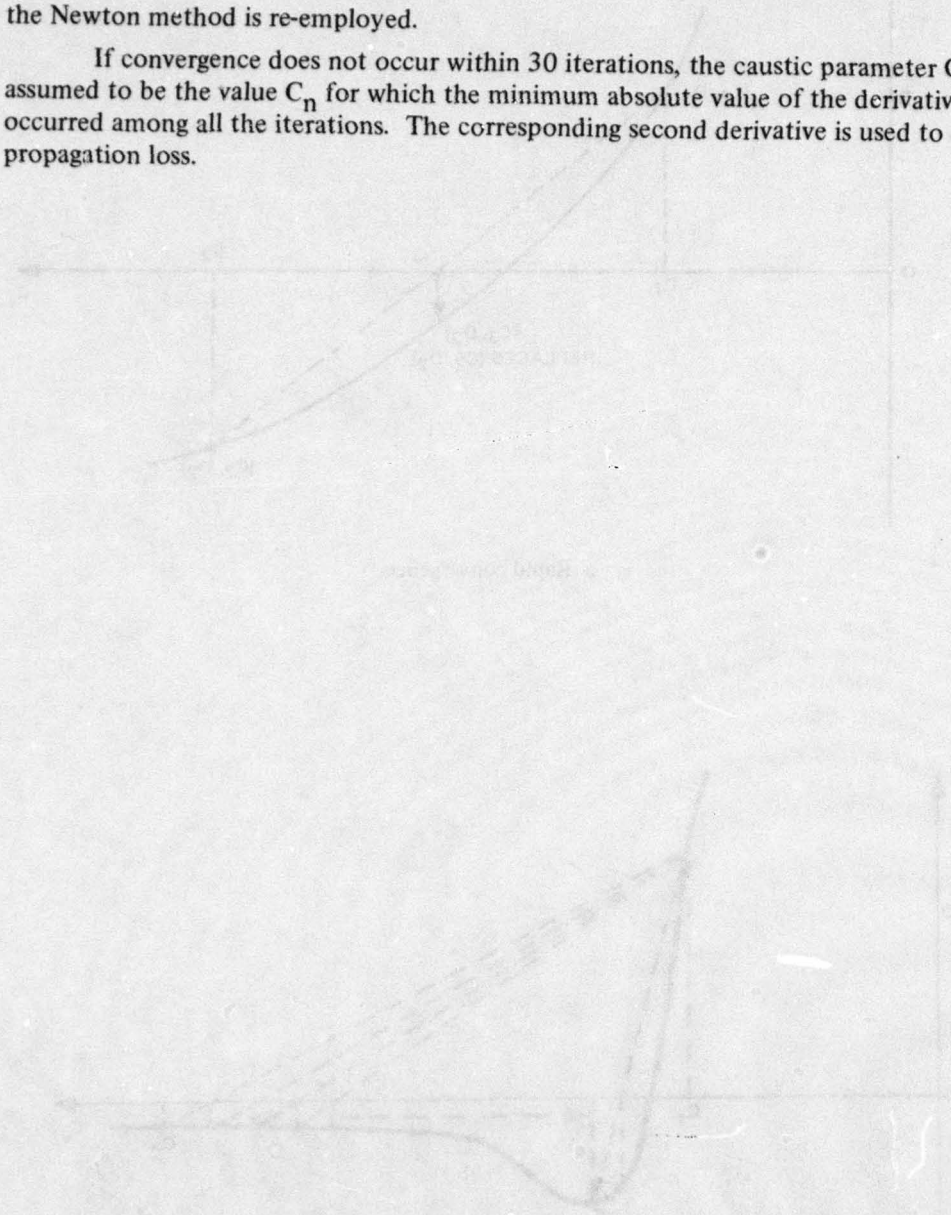

REVISED BACKGROUND NOISE MODEL

PROPAGATION LOSS FOR REVERBERATION CALCULATIONS

Since propagation loss enters into calculation of reverberation, the changes in the propagation loss model described in the previous section impact the calculation of reverberation. The propagation loss model used for reverberation calculation is the same as that used for propagation loss to the target. Target depth is replaced by surface, volume, and bottom depths for surface, volume, and bottom reverberation calculations, respectively. The depth used for the volume backscatterers is one-half of the user-specified column depth. This effectively converts the scattering column to a scattering layer. The set of 40 bottom bounce and convergence zone (refractive) rays is different from that used in calculating propagation loss to the target, because target depth enters into the selection of the rays. It is possible, if one set of rays were used for both cases, to change reverberation results by changing the target depth. Therefore, target depth is replaced by volume reverberation depth and a new set of 80 rays is used for reverberation calculations.

PULSE-AVERAGED REVERBERATION

The LIRA computer program allows a maximum pulse length of 100 s. For this discussion a pulse length τ that is $1 \leqslant \tau \leqslant 100$ is considered to be a long pulse length.

The LORA model allows only short pulse lengths. In LORA the form of the reverberation is (Ref. 1)

$$L_K = L_o + 2H_K + S_K + 10 \log (A_K/A_o) \tag{8}$$

where

L_o is the source strength,

H_K is the propagation loss including beam pattern losses,

S_K is the backscattering strength per A_o,

A_K is the backscattering area,

and A_o is the reference area.

For short pulse lengths H_K does not vary over the area A_K. For long pulse lengths, however, H_K may vary considerably over the range dimension of A_K. In the case of an FM or PRN signal and matched filter processing, range is highly resolved. For a CW pulse length of τ, the range interval used to compute reverberation area is $C\tau/2 \cos \phi_S$. For long pulse lengths and a CW signal, propagation loss for reverberation is averaged over this range interval.

After matched filter processing, the area with FM or PRN signals is $C\tau/2\ W\tau \cos \phi_S = C/2\ W \cos \phi_S$. For large τW products, the range resolution is small. For a 10-s pulse and 100-Hz bandwidth, for example, the range interval contributing to A_K is 25 ft. H_K is assumed not to vary over this interval, and Eq. (8) applies to the LIRA signal waveforms. In the LIRA model this reverberation is referred to as "instantaneous reverberation." An optional plot of "Instantaneous Reverberation vs Target Range" is one of the program outputs.

The instantaneous reverberation corresponds to the time when the leading edge of the target echo arrives at the receiver. Since the signal is correlated for the duration of the pulse length, instantaneous reverberation must be averaged over that interval; that is,

$$\bar{L}(T_2, \tau) = 10 \log \left[\frac{1}{\tau} \int_{T_2}^{T_2 + \tau} 10^{0.1\, L(t)}\, dt\right] \tag{9}$$

where T_2 is two-way travel time to the target, and L is reverberation level in dB. Thus, averaged reverberation is obtained by sliding an averaging window of length τ over the function of instantaneous reverberation vs time. This averaging is performed in the LIRA program for surface, bottom, and volume reverberation for each two-way time to the target corresponding to a user-specified target range. The total pulse-averaged reverberation is the incoherent sum of the bottom, surface, and volume reverberation components. The plot "Averaged Reverberation vs Range" is an optional program output.

Reverberation is computed only for those target-range values (and corresponding time values) entered by the user. The reverberation pressure squared is considered to lie on straight lines connecting these range (time) values. Therefore, Eq. (9) is the integral of reverberation as a piecewise, linear function of time. If the user neglects to enter a closely spaced sequence of range values, the piecewise, linear reverberation function could be greatly in error. Therefore, for values of pulse length which will require integration, that is for $\tau > 1$ s, the user is encouraged to enter his range array incremented in steps of 2 kyd or less. Since instantaneous reverberation values are computed only for range values that the user enters, the pulse averaging near and at the end of the sequence of ranges will not extend over a whole pulse length. In particular, the last value in the pulse-averaged reverberation array will be the value of the instantaneous reverberation at the target range. The averaging at the end is

$$\bar{L}(T_2, T_E) = 10 \log \left[\frac{1}{T_E - T_2} \int_{T_2}^{T_E} 10^{0.1\, L(t)}\, dt\right], \tau > T_E - T_2$$

where T_E is the time corresponding to the ending range. This "edge effect" in averaging appears between target ranges $R_E - 0.83\tau$ and R_E kyd, where R_E is the largest range specified by the user. Thus, a 10-s pulse would have incorrect averaging for the last 8.3 kyd (1/2 range covered by $\tau = 10$ s) before the maximum range, and a 100-s pulse, 83 kyd. The user must be sure that his input maximum range exceeds his maximum range of interest by 0.83τ. This correction applies if a pulse length greater than 1 s is used and if the user is concerned about time-averaged vs instantaneous reverberation values.

SEPARATION OF SOURCE AND RECEIVER IN DEPTH

The LIRA program allows the source and receiver to be separated in depth (one dimension) but not in range or azimuth (two or three dimensions). Propagation loss, travel time, and reverberation for a given target range are obtained by averaging these quantities computed for source/receiver at the source depth and source/receiver at the receiver depth. Justification of this procedure and estimates of the error introduced into the reverberation calculations constitute the remainder of this section. The method employed in LIRA is convenient because

- The complex computational and data storage structure is essentially the same as for the case of source and receiver at the same depth.
- Computation time is drastically reduced for what is otherwise a degenerate case of a bistatic geometry.
- Data storage is correspondingly reduced.

PROPAGATION LOSS

The propagation loss for the principal ray (largest arrival) from the source to the target to the receiver is

$$H_{12} = H_1 + H_2 = (2H_1 + 2H_2)/2$$

where the subscripts 1 and 2 refer to the source-target and target-receiver paths, respectively. The travel time for the source-target-receiver path is

$$T_{12} = T_1 + T_2 = (2T_1 + 2T_2)/2$$

Therefore, propagation loss for the source-target-receiver path can be computed by calculating two-way propagation loss for the source-receiver at the source depth, again at the receiver depth, and averaging. The same can be done with time. No inherent error is introduced into propagation loss or time by using this procedure.

The same arguments apply to propagation loss derived from the incoherent sum of the multipath intensities. Propagation loss from the source to the target is

$$H^X = -10 \log \left(\sum_i 10^{-0.1\, H^X_i}\right)$$

and from the receiver to the target is

$$H^R = -10 \log \left(\sum_j 10^{-0.1\, H^R_j}\right)$$

The propagation loss for a source-target-receiver path is

$$H_{ij} = -10 \log \left[10^{-0.1(H^X_i + H^R_j)}\right]$$

The total propagation loss from all source-target-receiver paths is

$$H = -10 \log\left(\sum_i \sum_j \left[10^{-0.1\left(H_i^X + H_j^R\right)}\right]\right)$$

which is equivalent to

$$H = -10 \log \sum_i 10^{-0.1 H_i^X} \; -10 \log \sum_j 10^{-0.1 H_j^R}$$

$$= H^X + H^R$$

$$= (2H^X + 2H^R)/2$$

Therefore, the total propagation loss for all of the incoherently summed source-target-receiver paths is equivalent to the average of the two-way propagation losses from source to target and from receiver to target.

REVERBERATION

In LIRA the reverberation level is evaluated for the two-way time to target, assuming the path is source-target-source. Again, reverberation level is computed for the receiver-target-receiver path as if the receiver were a source. The reverberation levels for a given target range are averaged, and the result is an approximation for reverberation for separated source and receiver. The following discourse is a justification for using the two-pass approximation for reverberation when source and target are separated in depth.

TRUE REVERBERATION

Quantitatively, reverberation level for a given target-echo-return time for source and receiver separated in depth is expressed by

$$L = \sum_k L_k$$

$$L_k = L_o + B_X(\phi_X) + B_R(\phi_R) - H_k^X - H_k^R + S_k(\phi_k^i, \phi_k^r) + 10 \log (A_k^{XR}/A_o) \qquad (10)$$

where

L_o is the source level,

k is the index of the backscattering element,

B_X is the source beam-pattern response for

ϕ_X the ray angle with respect to the horizontal of the source,

B_R is the receiver beam pattern response for

ϕ_R the ray angle at the receiver,

H_k^X is the one-way propagation loss between source and the k^{th} backscatterer,

H_k^R is the one-way propagation loss between the receiver and the k^{th} backscatterer,

S_k is the bistatic backscattering strength in dB per unit area, where ϕ_k^i and ϕ_k^r are angles of incidence and scattering (return), respectively,

A_o is a reference area which has the same spatial units as the backscattering area, and

A_k^{XR} is the effective scattering area of the k^{th} scattering surface or cross-sectional areas associated with column volume scattering.

TWO-PASS APPROXIMATION FOR REVERBERATION

The two-pass method computes reverberation L_k^X for the source at source depth, reverberation L_k^R for the source at receiver depth, and averages the result.

$$L_k^X = L_o + B_X(\phi_X) + B_X(\phi_X) - 2H_k^X + S_k(\phi_k^i, \phi_k^i) + 10 \log (A_k^X / A_o)$$

$$L_k^R = L_o + B_R(\phi_R) + B_R(\phi_R) - 2H_k^R + S_k(\phi_k^r, \phi_k^r) + 10 \log (A_k^R / A_o)$$

Adding and dividing by 2 gives the reverberation level L_k^{XR} for the k^{th} backscatter obtained by the two-pass method:

$$L_k^{XR} = L_o + B_X(\phi_X) + B_R(\phi_R) - H_k^X - H_k^R + 1/2 \left[S_k(\phi_k^i, \phi_k^i) + S_k(\phi_k^r, \phi_k^r)\right] + 10 \log \left[(A_k^X A_k^R)^{1/2} / A_o\right] \quad (11)$$

The true reverberation level for separated source and receiver is given by Eq. (10); the reverberation predicted by LIRA is given by Eq. (11). The two equations differ only in the scattering strengths and backscattering areas.

ERROR IN THE BACKSCATTERING AREA FOR THE TWO-PASS METHOD

True Backscattering Area. The true backscattering area is illustrated in Fig. 9. Paths a and b are incident upon the surface with angle ϕ_r. The difference in path length between paths a and b is $C(\tau_1 + \tau_2)$, where $\tau = \tau_1 + \tau_2$ is the ping length. All points on the surface over length Δr will make a scattering contribution to the reverberation at the receiver at time T_2, the time at which the leading edge of the target-echo pulse arrives at the receiver. Path b is traveled by the leading edge of the transmitted pulse, path a the trailing edge.

The backscattering area for the geometry of Fig. 9 is $r \Delta \theta \Delta r$, where r is the horizontal range from source/receiver to the backscattering area, and $\Delta \theta$ is the azimuthal angle containing significant source energy. The true backscattering area is derived by calculating the value for Δr. From Fig. 9

$$\Delta r = C\tau_1 \sec \phi_i = C\tau_2 \sec \phi_r$$

where

$$\tau = \tau_1 + \tau_2.$$

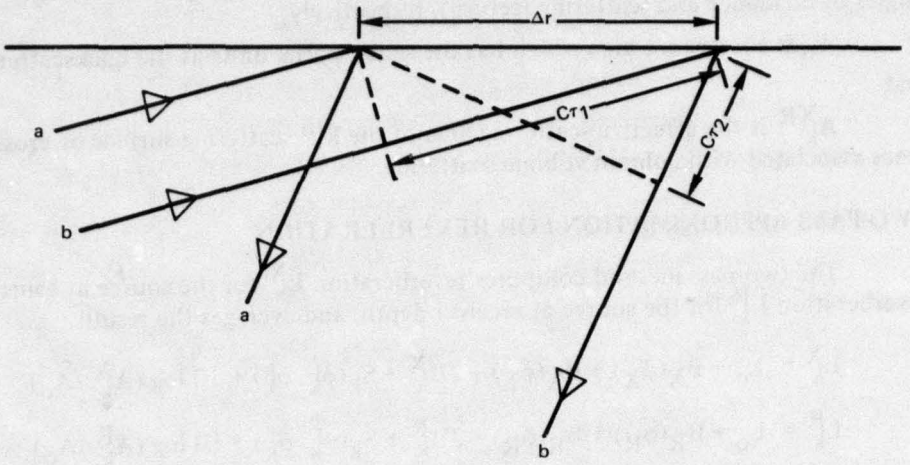

Figure 9. Bistatic backscattering geometry.

Therefore,

$$\Delta r = \frac{C\tau \sec \phi_i \sec \phi_r}{\sec \phi_i + \sec \phi_r}$$

The true backscattering area to be used in Eq. (10) is therefore

$$A_k^{XR} = r \Delta \theta \Delta r = r \Delta \theta \, C \tau \sec \phi_i \sec \phi_r / (\sec \phi_i + \sec \phi_r) \qquad (12)$$

Two-pass Backscattering Area. With source and receiver separated in depth, LIRA calculates reverberation as if the source and receiver were both located at source depth and then as if both source and receiver were at receiver depth and averages the results. The geometry of Fig. 9 does not apply to this case. Instead the two passes require the geometry of Fig. 10 to explain the reverberation backscattering area.

The two areas of Eq. (11) are

$$A_k^X = r \Delta \theta \Delta r_1 \text{ and } A_k^R = r \Delta \theta \Delta r_2$$

Since $\Delta r_1 = 1/2 \, C\tau \sec \phi_i$ and $\Delta r_2 = 1/2 \, C\tau \sec \phi_r$, the geometric mean used in Eq. (11) is

$$(A_k^X A_k^R)^{1/2} = r \Delta \theta (\Delta r_1 \Delta r_2)^{1/2} = 1/2 r \Delta \theta \, C \tau (\sec \phi_i \sec \phi_r)^{1/2}$$

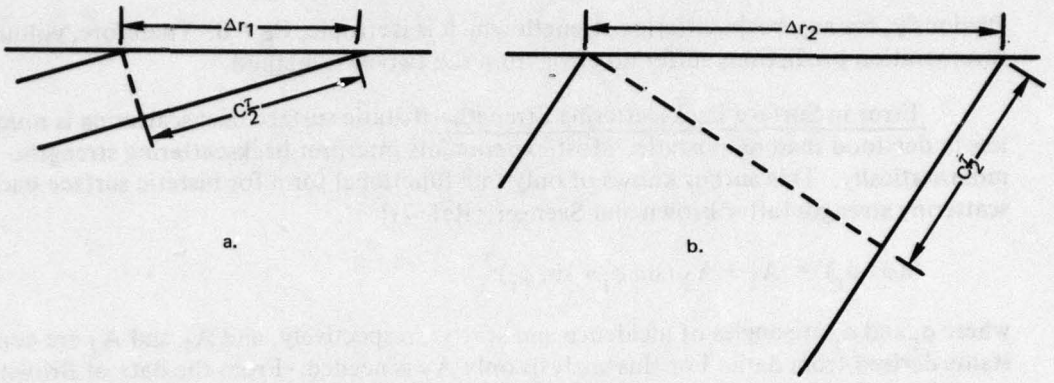

Figure 10. Monostatic backscattering geometry for: (a) ray path from source depth; (b) ray path from receiver depth.

This approximated area is to be compared with the true reverberation area of Eq. (12) used in Eq. (10). The error in reverberation level E_A due to approximating backscattering area with the two-pass method is

$$E_A = 10 \log \left\{ \frac{1}{2} \left[\left(\frac{\cos \phi_i}{\cos \phi_r} \right)^{1/2} + \left(\frac{\cos \phi_r}{\cos \phi_i} \right)^{1/2} \right] \right\}$$

Obviously, when source and receiver are at the same depth, $\phi_i = \phi_r$ and $E_A = 0$. For shallow angles of incidence and return, E_A is also very nearly zero. The greatest discrepancy occurs when one angle is small and the other is large. For an extreme case, say $\phi_i = 0$ and $\phi_r =$ 60 deg, $E_A = 0.26$ dB. Only for very short ranges, in the order of 1 kyd, could the transmit and return paths of significance be greatly different; yet even if they are, the error in approximating backscattering area is small when using the two-pass method.

ERROR IN BACKSCATTERING STRENGTH FOR THE TWO-PASS METHOD

The true backscattering strength used in Eq. (10), $S_k (\phi_k^i, \phi_k^r)$, is bistatic. The approximated backscattering strength used in Eq. (11) for the two-pass method

$$\frac{1}{2} \left[S_k (\phi_k^i, \phi_k^i) + S_k (\phi_k^r, \phi_k^r) \right]$$

is the average of two monostatic backscattering strengths, i.e., the angle of incidence equals the angle of return. The error in backscattering strength E_S in dB introduced in reverberation level by using the two-pass method is

$$E_S = \frac{1}{2}\left[S_k\left(\phi_k^i, \phi_k^i\right) + S_k\left(\phi_k^r, \phi_k^r\right)\right] - S_k\left(\phi_k^i, \phi_k^r\right) \tag{13}$$

Obviously, for any backscattering strength which is isotropic, $E_S = 0$. Therefore, volume reverberation predictions suffer no error from the two-pass method.

Error in Surface Backscattering Strength. Bistatic surface backscattering is much less understood than monostatic. Most experiments interpret backscattering strengths monostatically. This author knows of only one functional form for bistatic surface backscattering strength [after Brown and Saenger, (Ref. 7)]:

$$S(\phi_i, \phi_r) = A_1 + A_2 (\sin \phi_i + \sin \phi_r)^2 \tag{14}$$

where ϕ_i and ϕ_r are angles of incidence and scatter, respectively, and A_1 and A_2 are constants derived from data. For this analysis only A_2 is needed. From the data of Brown and Saenger, which spans frequencies from 62.5 to 5000 Hz and angles 20 deg $\leq \phi_i \leq$ 70 deg and 1.5 deg $\leq \phi_r \leq$ 70 deg, A_2 has a maximum value of 10 dB for a weakly shadowed surface and 15 dB for a strongly shadowed surface.

The error E_S in evaluating the backscattering strength using the two-pass (monostatic) method is derived by substituting Eq. (14) into Eq. (13).

$$\begin{aligned} E_S &= \frac{1}{2}\left[A_2 (2 \sin \phi_i)^2 + A_2 (2 \sin \phi_r)^2\right] - A_2 (\sin \phi_i + \sin \phi_r)^2 \\ &= A_2 (\sin \phi_i - \sin \phi_r)^2 \end{aligned} \tag{15}$$

Figure 11 shows the maximum error for maximum angle differences, i.e., one angle is 0 deg and the other is at the maximum. Figure 12 shows the error if ϕ_i and ϕ_r are not more than 10 deg apart. These two figures are based on Eq. (15). Errors for values of $\phi_i < 20$ deg are not computed because of the limits of the data upon which the bistatic function is based. For ranges at one convergence zone and greater, angles of incidence and return are limited by the bottom; they are less than 15 deg and tend to be about 5 deg. Figure 11 indicates that for very short ranges at steep angles, significant error could be induced in surface backscattering strength if the two-pass method is used. For long ranges, however, the worse case would be less than 1.8 dB. Figure 12 shows that if the angles are not greater than 10 deg apart, the maximum error is 0.42 dB. It is very unlikely that this spacing in bistatic angles would be exceeded for any source/receiver configuration in any ocean. Much more likely, the angles will be within 2 deg of each other with negligible induced error.

Error in Bottom Backscattering Strength. The Lambert's law approximation for bottom backscattering strength is of the form [after MacKenzie (Ref. 8)]:

$$S_B = B_1 + 10 \log (\sin \phi_i \sin \phi_r)$$

where ϕ_i and ϕ_r are angles of incidence and return, respectively, and B_1 is a constant. The error E_B induced in reverberation level by using the two-pass method in place of the bistatic geometry is

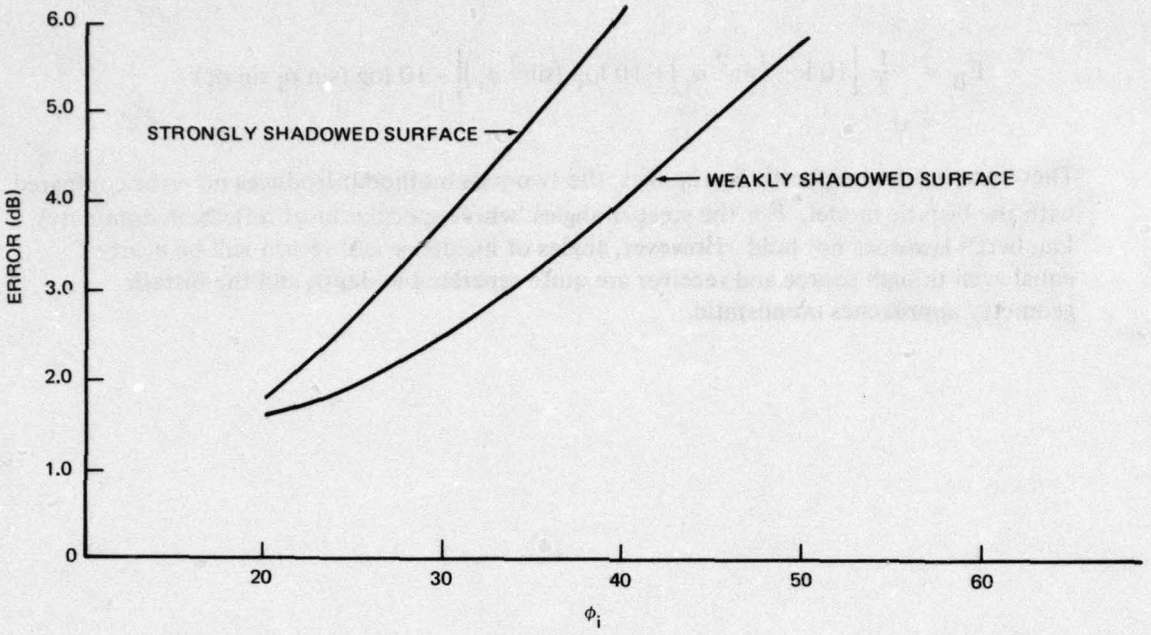

Figure 11. Maximum error in computing surface backscattering strength using the monostatic approximation for the bistatic function ($\phi_r = 0$).

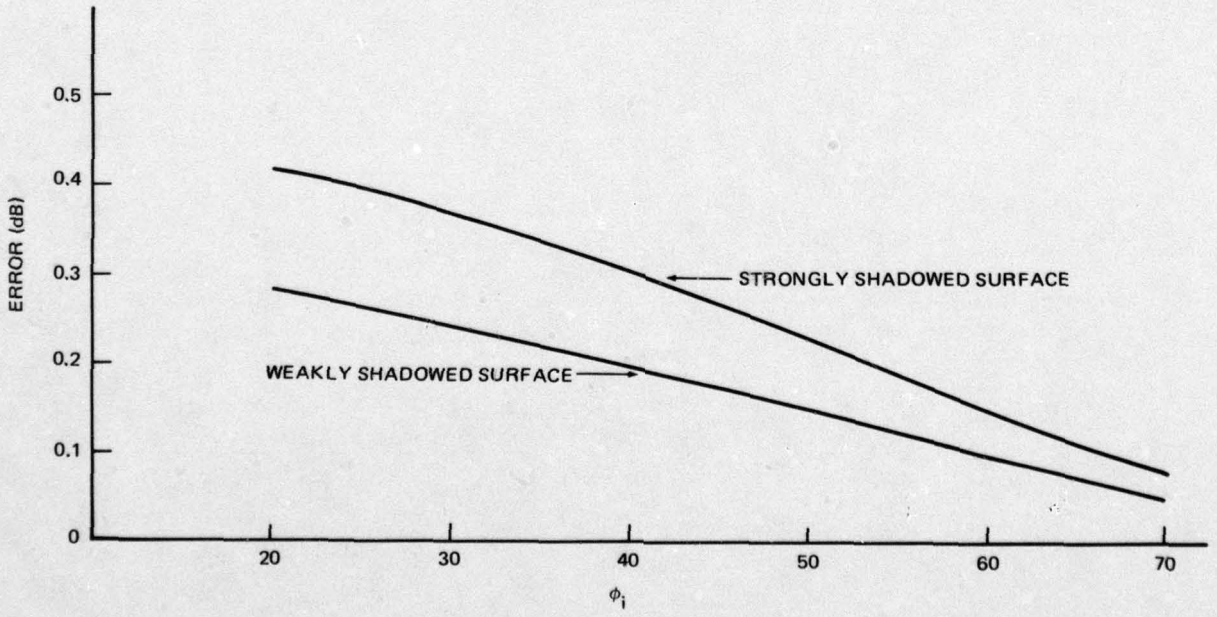

Figure 12. Realistic error in computing surface backscattering strength using the monostatic approximation for bistatic function ($\phi_r = \phi_i - 10^\circ$).

$$E_B = \frac{1}{2}\left[10 \log \left(\sin^2 \phi_i\right) + 10 \log \left(\sin^2 \phi_r\right)\right] - 10 \log \left(\sin \phi_i \sin \phi_r\right)$$
$$= 0$$

Therefore, where Lambert's law applies, the two-pass method introduces no error compared with the bistatic model. For the steeper angles, where specular facet reflection dominates, Lambert's law does not hold. However, angles of incidence and return will be nearly equal even though source and receiver are quite separated in depth and the bistatic geometry approaches monostatic.

RESULTS

In Appendix D LIRA is compared with three other models, PLRAY, FACT and AP2, with regard to propagation loss. For most cases all the models agree well. Differences are usually explainable. The importance of the comparison is to show that LIRA produces a reasonable propagation loss curve. LIRA's propagation loss examples exhibit no pathological excursions from the norm of the other models, nor trends, nor biases. LIRA's caustic correction algorithm performed without idiosyncracies.

Reverberation is calculated by means of the same algorithm used for propagation loss. Because of the way in which reverberation is represented, it is difficult to make meaningful comparisons with other models and with experimental measurements.

The LIRA program has been executed thousands of times and is a reliable performer. Inputs and outputs are user oriented, designed for clarity. Active-sonar performance predictions for targets from 1 to 600 kyd from the source cost $2 to $15 using a UNIVAC 1110 computer, with plots costing extra (about $4/plot). The four example runs in Appendix E cost $25, with 10 min of cpu time used. The 14 propagation loss curves for the cases in Appendix D cost $4.70 and used 107 s of cpu time. Thus, one case averaged $0.34 for 7.64 s of cpu time.

LIRA uses 57,000 words of computer core storage. The program must be segmented (overlaid in core) in order to incorporate the plotting routines.

SUMMARY OF MODEL AND SOFTWARE IMPROVEMENTS

LIRA surpasses LORA's capabilities in the following ways:

1. Allowable frequencies are from 25 Hz to 25 kHz.

2. Maximum range is 1000 kyd.

3. Brekhovskikh's caustic corrections are applied to propagation losses to the target and all backscattering elements which produce reverberation.

4. Linear FM and PRN signals are modeled by averaging the reverberation time sequence over the pulse length.

5. The source and receiver are not restricted to being at the same depth.

Outputs are modified in the following ways:

1. Calcomp plots can be made for propagation loss, reverberation (including components from bottom, surface, and volume backscattering), and signal excess. These are displayed vs range from source to target.

2. Target ranges are user specified. Formerly, the user specified the number of convergence zones and bottom bounces, and the output included all ranges encompassed by the ray paths generated.

3. The output is tabulated for the user-specified target ranges. Formerly the output heading described the mode of propagation (i.e., direct path, convergence zone, bottom bounce, etc.), and the output was broken up into various zones.

New inputs available to the user are:

1. Arrays of surface and bottom backscattering strengths vs grazing angle. (Formerly, an internal model had to be used.)

2. Array of target ranges.

3. A new array of flags for special intermediate printout for debugging purposes.

4. Array of recognition differential vs reverberation-to-noise ratio.

5. Flag to turn on or off the caustic corrections.

6. Flag to suppress any or all portions of printing or plotting.

7. Flags to exclude up- or down-going rays at the source and/or the receiver (to model the array on a steeply sloping bottom).

8. Flags to select CW, FM, or PRN signal waveform.

9. Receiver depth (when different from source depth).

RECOMMENDATIONS

LIRA experiences the same difficulties with submerged ducts that LORA did. Study should be undertaken to develop or choose a model which corresponds in normal mode theory to weak trapping of modes.

A big step toward true bistatic simulation of active sonar is to allow source and receiver to be separated in the range dimension. With this modification LIRA would have source and receiver separated in two of the three dimensions (azimuth, the remaining dimension).

Representation of reverberation at the output of the signal processor causes awkwardness in comparing LIRA's reverberation with that of other reverberation models. A plot of normalized reverberation vs time would be useful.

Fields near horizontal caustics cannot be represented by Brekhovskikh's methods. A study should be performed to derive the fields for these cases. The equations for fields near horizontal cusped caustics are available (implemented in the FACT model) (Ref. 9). These equations could be included in LIRA, but the rather rare occurrence of horizontal cusped caustics (source and target must be at the same depth) reduces the priority of this effort.

REFERENCES

1. D.W. Hoffman. "LORA: A Model for Predicting the Performance of Long-Range Active Sonar Systems," NUC TP 541 (1976).

2. Melvin A. Pedersen and David F. Gordon, "Normal-Mode and Ray Theory Applied to Underwater Acoustic Conditions of Extreme Downward Refraction," *J. Acoust. Soc. Amer.*, Vol. 51:323-368 (1972).

3. Donald Ludwig, "Uniform Asymptotic Expansions at a Caustic," *Comm. on Pure and Appl. Math*, Vol. XIX, 215-250 (1966).

4. Leonid M. Brekhovskikh, *Waves in Layered Media*, New York, Academic Press, 1960.

5. Available only to authorized requestors. (Pedersen and Anderson).

6. M.A. Pedersen and D.F. Gordon. "Comparison of Curvilinear and Linear Profile Approximation in the Calculation of Underwater Sound Intensities by Ray Theory," *J. Acoust. Soc. Amer.*, 41:419-438 (1966).

7. M. Vertner Brown and R. Alfred Saenger, "Bistatic Backscattering of Low-Frequency Underwater Sound from the Ocean Surface," *J. Acoust. Soc. Amer.*, Vol. 52, 944-960 (1972).

8. K.V. MacKenzie, "Bottom Reverberation for 530- and 1030-cps Sound in Deep Water," *J. Acoust. Soc. Amer.*, Vol. 33, 1498-1504 (1961).

9. C.W. Spofford, "The FACT Model, Acoustic Environmental Support Detachment," Maury Center Report 109, (November 1974).

10. M.M. Holl, "Technical Notes on Sound Propagation in the Sea," Volume 2, Meteorology International Report on Project M-153, (June 1968).

11. C. Bartberger, "PLRAY - A Ray Propagation Loss Program," Naval Air Systems Command, Report No. NADC-77296-30, (October 1978).

APPENDIX A

LOGICAL STRUCTURE OF THE LIRA COMPUTER PROGRAM

The LIRA computer program consists of two segments, one for calculations and one for plotting. The MAIN routine (See Fig. A-1) calls SUBROUTINE LIRA, which causes segment 1 to be loaded. It is in this segment that the user enters his inputs in SUBROUTINE READIN. After all of the user-specified calculations have been completed and if plot flags have been set, control returns to MAIN, and segment 2 is loaded. All storage areas except those common to both segments are lost. The appropriate plots are created in segment 2, and control is returned to the user in READIN after passing through MAIN to reload segment 1.

All inputs are entered through SUBROUTINE READIN. The input parameters are flagged to determine if they belong to sound-speed-profile (SSP), environmental, reverberation, or detection categories. Depending on the inputs, redundant calculations are skipped on successive runs performed during the same program execution.

If a user on a demand terminal executes the program, and after a given run decides that he would like to plot his previous calculations, he can set the appropriate plot flags, type the data literal "GOPL," and the segment swapping and plotting will be performed. Control returns to the user in READIN in segment 1, with the input values the same as before he typed "GOPL." He can continue to make runs with his data, but unless he changes the plot flags, plotting will still be performed after each run.

The flag ISPLIT is initialized as 0. If source depth ZX and receiver depth ZR are different, ISPLIT is set to 1 for the first pass for calculating propagation loss and reverberation. For the first pass ZR replaces ZX (ZX is temporarily stored as ZXX). The first-pass propagation loss and reverberation arrays are stored. ISPLIT is set to 2. The second pass is performed with ZX restored to the original source depth (ZXX). Propagation loss and reverberation arrays are combined after both passes. ISPLIT is reset to 0.

Special outputs are allowed for propagation loss and reverberation if the user enters values for the flags OUTP and OUTR, respectively. If OUTP = 1, all reverberation and detection calculations are skipped and two-way travel time to the target, angle of the largest arrival, the propagation loss of the largest arrival, and the propagation loss for the incoherent sum of all of the ray arrivals are printed for all of the user-specified target ranges.

If OUTR = 1 or 2, bottom, surface, and volume components of reverberation as well as contributions from each previous ping are printed for the times corresponding to two-way travel time for the user-specified target ranges. If OUTR = 1, the detection calculations are performed; if OUTR = 2, they are skipped.

Unless the user enters NOPR, the LIRA program prints detection outputs under the following headings:

- RANGE, all user-specified target ranges in kyd.
- TIME, two-way travel time for the ray which gives minimum loss to the target.
- LOSS, minimum two-way propagation loss (or incoherent sum), including beam pattern corrections.

- ANGLE, angles at source depth for rays which give minimum loss to the target.
- SIGNAL, level of the return signal at the output of the signal processor.
- REVERB, reverberation level at the output of the beamformer (corrected for pulse averaging) or at the output of the signal processor (corrected for target doppler, pulse averaging, and processing gain), depending on whether recognition differential or detection threshold is used.
- REV LIM, "YES" to indicate if reverberation exceeds noise by more than 3 dB; "NO" otherwise.
- S/MN, signal-to-masking-noise ratio in dB.
- EXCESS, signal excess in dB, with zero corresponding to 50% probability of detection if recognition differential is used or the probability of detection for a given detection threshold if that is used.
- PROB DETECT, probability of detection, with 0.5 corresponding to signal excess = 0 (not applicable for other probabilities of detection at signal excess = 0).

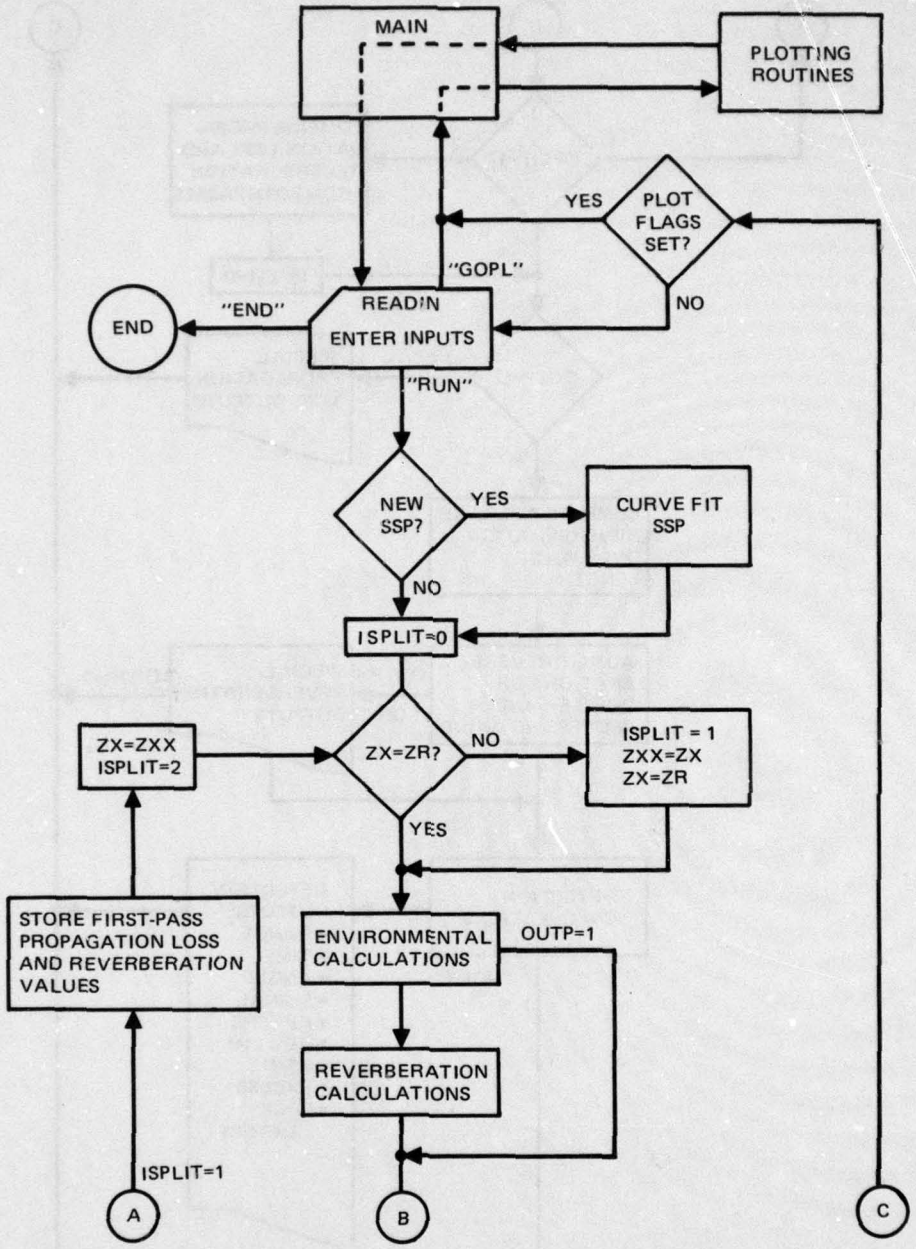

Figure A-1 (a). Flow chart for LIRA input, output, and calculations.

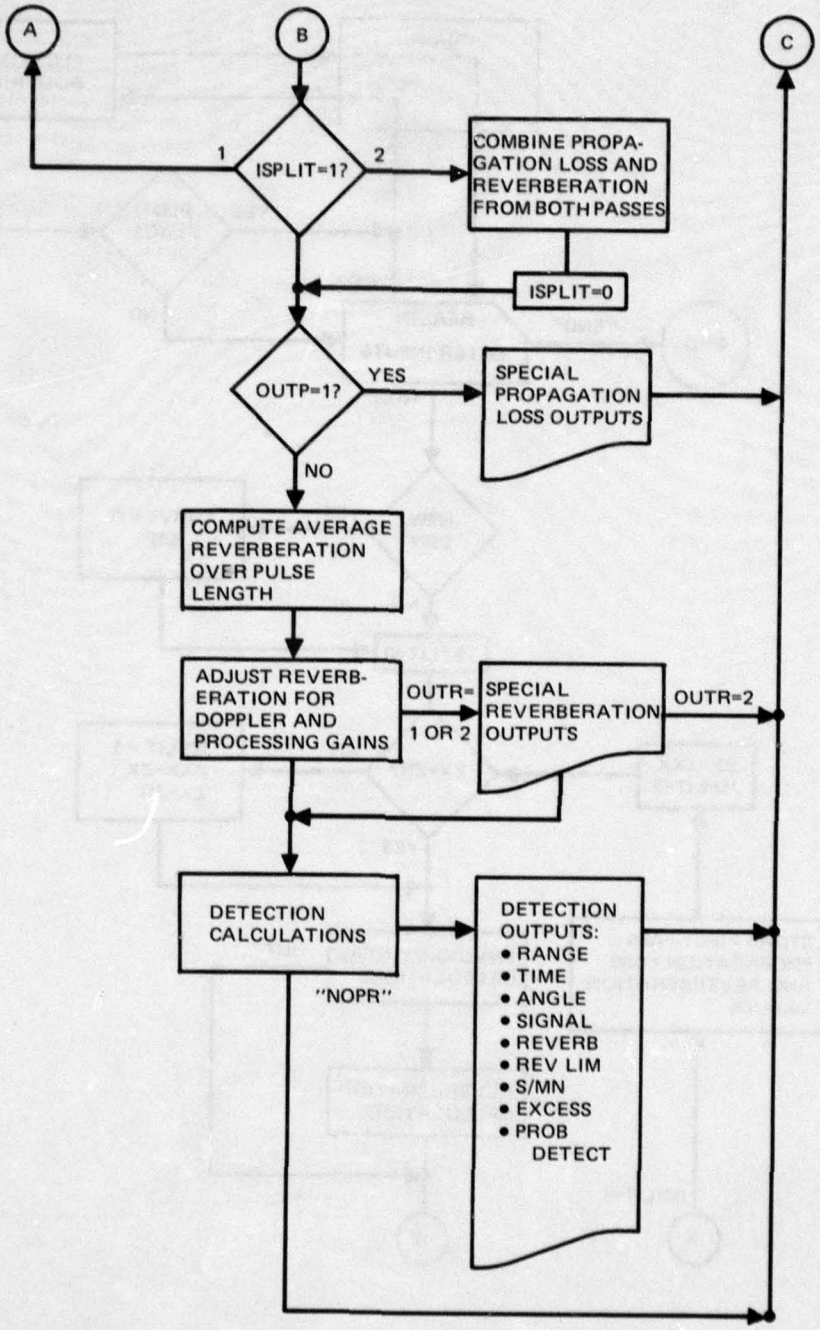

Figure A-1 (b). Flow chart for LIRA input, output and calculations.

APPENDIX B

INPUTS TO THE LIRA COMPUTER PROGRAM

Table B-1 contains a list of the most commonly used inputs to the LIRA computer program. Following Table B-2, the inputs are described in greater detail along with other inputs not needed by the general user.

The column under "Name" in Table B-1 contains the name of the variable or array to be typed by the user when he enters data according to the format described in Appendix C. Some variables have optional names. The column under "Description" contains brief definitions of the input parameters. "Range" is the range of values a given parameter is allowed. Any value outside this range is either set to a "Typical Value" or calculated in the program.

Table B-2 contains a list of data literals used to exert specific control over the program.

Not all of the input parameters need to be entered by the user. The only input required for the program to run is sound-speed profile (SSP). Typical or calculated values are used for every input parameter not entered by the user.

Input parameters fall into three categories, environmental, reverberation, and detection. The computational structure of the LIRA program may be thought of as three nested loops, with the environmental loop on the outside and the detection loop on the inside. During a single program execution, many runs can be made. On the first run, unless otherwise specified by the user through the inputs, the environmental, reverberation, and detection loops are all performed. Thereafter, only those loops are performed that are required by category of inputs entered by the user. If he enters only detection parameters, only the detection loop is performed. If he enters reverberation parameters, the reverberation and detection loops are performed. Savings in computer time and cost are obtained by looping on detection and/or reverberation parameters rather than environmental parameters. Table B-1 groups the input parameters into environmental, reverberation, and detection categories so that the user can choose the order to enter his data and reduce his computer costs.

ADDITIONAL DESCRIPTION OF INPUTS

Certain inputs need to have their descriptions elaborated to clarify their meanings or to acquaint the user with additional options:

BD, ZBM. If bottom depth (ft) is not entered, it is assumed to be the maximum depth in the sound-speed profile. If BD is entered, the sound-speed profile is either linearly interpolated or extrapolated to find the sound speed for the bottom depth.

FREQ, F. Frequency may be entered in units of Hz or kHz. The program tests the value to determine the units. If $25 \leqslant \text{FREQ} \leqslant 100{,}000$, the program assumes Hz. If $0.0001 \leqslant \text{FREQ} < 25$, the program assumes kHz.

R, RANGE. Range of target in kiloyards; an array of ranges and range increments for which propagation loss, reverberation, signal excess, and probability of detection are calculated. The elements of array R are scanned in order to generate the range array internal to the program. Each successive set of three elements in R is examined to see if the third

Table B-1. Most commonly used LIRA inputs.

ENVIRONMENTAL PARAMETERS

Name	Description	Units	Range	Typical Value; Comments
SSP	Sound-speed profile. Array of alternating depth and sound-speed values or depth and temperature values	ft, ft/s m, m/s ft, °F m, °C	4750 to 5160 1440 to 1590 30 to 85 0 to 30 at the surface	no typical value – user must enter SSP for program to run
BD, ZBM	Bottom depth	ft	1 to	largest depth in SSP
SD, ZX	Source (transmitter) depth	ft	1 to 10^{30}	20
RD, ZR	Receiver depth	ft	1 to 10^{30}	20
TD, ZTG	Target depth	ft	1 to 10^{30}	50
FREQ, F	Frequency of transmitter; center frequency of receiver bandwidth	Hz kHz	25 to 10^{5} 10^{-4} to 24.99	– 3.5
WAVE, LWA	Wave height (crest to trough)	ft	0 to 20	4
WIND, VWI	Wind speed	knots	0.1 to 35	15
SLPB, HS	Signal loss per bounce at the surface	dB	-2 to 20	3, calculated internally if negative
LAT	Latitude	deg	-90 to 90	0
BRLP, AHB	Bottom-reflection-loss profile. Array of alternating grazing-angle and bottom-reflection-loss values	deg, dB	not checked	zero loss at any grazing angle
XVRP, BEAMX	Transmit vertical response pattern (i.e., beam pattern) – array of alternating angle and response values, where response is given as positive dB down from the maximum response, defined as 0 dB at an angle of 0 deg	deg, dB	not checked	omnidirectional (i.e., 0 dB for all angles); if the array contains one element only, the response pattern sin(x)/x for a continuous line is calculated (XVBM needed)
RVRP, BEAMR	Receive vertical response pattern	same as for XVRP		(RVBM needed for sin(x)/x response pattern)
XVBM, DELPX	Effective vertical beamwidth – transmit	deg	0.1 to 180	180
RVBM, DELPR	Effective vertical beamwidth – receive	deg	0.1 to 180	180
XDE, PHDX	Transmit depression-elevation angle of the main axis of the beam pattern	deg	-85 to 85	5
RDE, PHDR	Receive depression – elevation angle of the main axis of the beam pattern	deg	-85 to 85	5

Table B-1. Continued

ENVIRONMENTAL PARAMETERS

Name	Description	Units	Range	Typical Value; Comments
R, RANGE	Array of target ranges – may be entered as single values or in groups of 3: 3rd successive value may be used to step between two preceding values	kyd	.001 to 1000	1 10 1
PLOT	Array of plot flags – enter as PLOT = A B C A: plot propagation loss = 1: incoherent sum and largest arrival = 2: incoherent sum only = 3: largest arrival only B: plot reverberation = 1: pulse-averaged reverb = 2: instantaneous reverb = 3: both on separate graphs C: plot signal excess = 1 incoherent sum and largest arrival = 2 incoherent sum = 3 largest arrival	–	–	all flags 0
OUTP	= 1: limit calculations to propagation loss – skip reverberation and detection	–	0 to 1	0

REVERBERATION PARAMETERS

BBS, MUB	Bottom-backscattering strength if internal function is used	dB/yd^2//1 yd	-40 to -5	-27
ABBS	Array of alternating grazing angle and bottom-backscattering strength values – internal function not used	deg, dB/yd^2//1 yd	not checked	array all zeroes
ASBS	Array of alternating grazing angle and surface-backscattering strength values – do not use if internal surface-backscattering model is desired	deg, dB/yd^2//1 yd	not checked	array all zeroes

Table B-1. Continued

REVERBERATION PARAMETERS

Name	Description	Units	Range	Typical value; Comments
VBS, MUV	Volume-backscattering strength of the water column 1 yd^2 in area at surface extending to depth ZC	dB/yd^2//1 yd	-300 to 0	-49
SLD, ZC	Scattering layer depth; maximum depth of the water column	ft	0 to 10,000	2000
SL	Source level	dB//1 μPa//1 yd	40 to 300	240
HBM, DELTH	Horizontal beamwidth	deg	0.1 to 360	360
TBP	Time between pings	s	1 to 200	10
PULS, PULSE	Pulse length	s	10^{-4} to 100	0.1
BWR	Bandwidth of receiver	Hz	10^{-4} to 1000	100
GDOP	Doppler gain	dB	-2 to 300	-1, internal model is used if GDOP is negative
TCV, TVC	Target closing velocity – used only with internal doppler model when GDOP = -1	knots	-60 to 60	0
OUTR	Reverberation output flag = 1: print special reverberation outputs = 2: do above and skip detection section	–	0 to 2	0

DETECTION PARAMETERS

DI	Directivity index	dB	0 to 70	0
NIN, NSPEC	Spectrum level noise into the receiving array (not needed if NOUT is used)	dB/1 Hz//1 μPa	-80 to 100	55
NOUT, NBWR	Noise in the receiver bandwidth at the output of the beamformer (supercedes NIN)	dB//1 μPa	-105 to 129	65
TGS	Target strength	dB	0 to 40	15
RDN	Recognition differential for noise-limited detection (corrected by program for reverberation-limited detection)	dB	-20 to 20	-2

Table B-1. Continued

DETECTION PARAMETERS

Name	Description	Units	Range	Typical Value; Comments
ARD	Array of alternating reverberation-to-noise-ratio and recognition-differential values	dB, dB	not checked	RDN = --2
ADT	Array of alternating reverberation-to-noise-ratio and detection-threshold values	dB, dB	not checked	RDN = --2
CLIP	=:1 reduces signal level 2 dB for clipping in the signal processor (= 0, no clipping loss)	–	0 to 1	0
SIG, SIGMA	Standard deviation of signal differential (only used with SP = 5)	dB	0.5 to 6	6
PFA	Probability of false alarm	–	10^{-12} to 0.1	0.001
SP	Flag to denote signal processing model = 1: linear correlator, known signal = 2: linear correlator, constant signal = 3: quadrature correlator, constant-amplitude signal = 4: quadrature correlator, random-amplitude-and-phase signal = 5: energy detector for gaussian signal	–	1 to 5	5

Table B-2. Data Literals.

Data literal	Resulting control
RUN	Perform calculations for the values of the current input parameters and return control to input section.
END	End program execution.
HEADER	Use the next card image for output headings.
ABUT	Abut the characters in the next card image to the current characters in the heading.
TTY	Reduce output for demand terminal.
NOTT*	Print normal outputs, defeat TTY.
NOPR	Eliminate most printed outputs.
PRIN*	Allow printed outputs, defeat NOPR.
DR	Print detection ranges.
DRONLY	Print detection ranges only, eliminate other outputs.
NODR*	Defeat DR and DRONLY.
GOPL	Plot previously calculated arrays (appropriate plot flags must be set).
NOPL	Allow no plotting at the end of this run, clear plot flags.
CW	Label the plots for a CW signal.
FM	Label the plots for an FM signal.
PRN*	Label the plots for a PRN signal.
LA*	Use the propagation loss for the largest arrival to compute detection ranges.
SUM	Use the propagation loss for the incoherent sum to compute detection ranges.
SAVY	Write outputs in Unit 11 (disk).
SAVN*	Do not write outputs on a disk.
CAUN	Use standard ray tracing without caustic corrections.
CAUY*	Use caustic corrections.
XSUR	Exclude up-going rays at the source.
XBOT	Exclude down-going rays at the source.
RSUR	Exclude up-going rays at the receiver.
RBOT	Exclude down-going rays at the receiver.
TSUR	Exclude up-going rays at the target.
TBOT	Exclude down-going rays at the target.

* The program is initialized to this condition at the beginning of execution.

is less than half the difference of the first two. If so, the third element is used as a stepping increment between the first two elements. Thus, R = 4 11 2 will generate the sequence 4, 6, 8, 10, 11. Values in R which do not satisfy the stepping principle are used singly. Thus,

R = 1 5 1 4.5 7 10 2

yields the sequence

1, 2, 3, 4, 4.5, 5, 7, 9, 10

The same range sequence is generated by

R = 7 10 2 4.5 1 5 1.

"7 10 2" is taken as a stepping sequence, and none of its values can participate in another sequence, such as "2 4.5 1." A maximum of 90 values can be used in R and the maximum number of values that can be generated for range in LIRA is 500. For plotting purposes it is necessary to generate range values closely and evenly spaced.

PLOT. Array of plot flags. If "PLOT" is entered with no values following, then "PLOT = 1 1 1" is assumed.

PLOT (1) = 1: plot propagation losses for incoherent sum and largest arrival
= 2: plot propagation loss for incoherent sum
= 3: plot propagation loss for largest arrival

PLOT (2) = 1: plot pulse-averaged reverberation*
= 2: plot instantaneous reverberation*
= 3: plot both pulse-averaged and instantaneous reverberation on separate graphs

PLOT (3) = 1: plot signal excess for the incoherent sum and the largest arrival on the same graph
= 2: plot signal excess for the incoherent sum
= 3: plot signal excess for the largest arrival

OUTR. Reverberation output flag.

= 0: no effect
= 1: prints bottom, surface and volume reverberation components, total contribution from each ping (if more than one ping) and total reverberation vs target range (and corresponding two-way travel time)
= 2: same as OUTR = 1 but detection calculations are skipped.

ADT. Detection threshold (DT) vs reverberation-to-noise ratio (RNR); array of

---

* Included in the reverberation plots are the total reverberation, the surface, volume, and bottom components of reverberation, and the ambient noise level.

alternating RNR and DT values, both in dB. A single value in the array signifies that DT is constant at that value. The values for DT are measured at the output of the signal processor. Detection threshold in dB is the ratio of the signal-plus-noise power to the noise power in the receiver bandwidth needed to achieve a specified level of correct decision with a specified probability of false alarm (PFA). For the probability-of-detection models in LIRA to apply, the specified level of correct decision is probability of detection = 0.5 for signal excess = 0 for user-specified PFA. The user may use a DT corresponding to another probability of detection (at which plotted signal excess = 0), but the printed values for probability of detection vs range will not apply. The entering of the ADT array nullifies previous entries of either RDN or ARD.

ARD. Recognition differential (RD) vs reverberation-to-noise ratio (RNR); array of alternating RNR and RD values, both in dB. A single value in the array signifies that RD is constant at that value. The values for RD are measured at the output of the beamformer. RD is the signal-to-masking-background ratio in the receiver bandwidth needed to achieve 50% probability of detection for a given probability of false alarm. ARD is a curve representing the uniting of the signal processing and the decision processes into one. In general the values of PFA used for ARD and ADT inputs are different for a given receiver because the signal and noise distributions are different before and after the signal processor. Signal excess is zero for 50% probability of detection. Reverberation plots are for reverberation in the receiver bandwidth at the output of the beamformer. The entering of the ARD array nullifies previous entry of either RDN or ADT.

Additional Inputs

Other inputs exert specific control not needed by the general user.

NBBB, REFLS. Maximum number of bottom bounce ray cycles for which ray tracing calculations will be performed. If this parameter is not entered, a maximum of 100 cycles is assumed, but calculations are limited by the end points of the input ranges to increase program efficiency.

ZONE, ZONES. Maximum number of convergence zone ray cycles for which ray tracing calculations will be performed. If this parameter is not entered, a maximum of 100 cycles is assumed, but calculations are limited by the end points of the input ranges to increase program efficiency.

DUMP. Flag for intermediate printout.

= 0: no effect

= 1: lists sound-speed maxima and subsurface ducts; lists sound speeds used for ray tracing to the target; lists surface duct propagation loss, surface and volume reverberation, and two-way travel time to the target.

FLAG. Array containing flags which control diagnostic printouts.

FLAG (N) = 0, N = 1, . ., 6: no effect.

FLAG (1) applies to caustics generated in both the propagation loss and reverberation calculations.

=1: print parameters for each caustic

= 2 : add calculations for each iteration for each caustic

= 3 : add details for each iteration

FLAG (2) applies to ray interpolations for propagation loss to the target.

= 1 : print parameters for individual rays for both bottom bounce and convergence zone paths

= 2: add the interpolations for range after each successive ray

= −1: only print backscattering strengths for each ray

= −2: print a dump of array "ARP," the array containing the ray segment parameters for all rays (all bottom bounce and convergence zone ray segments for bottom surface and volume backscatterers and for the target)

FLAG (3) ⩾1 : allow FLAG (1) to apply to reverberation caustics.

⩾2 : add printing of minimum and maximum two-way travel times for each family of rays, ray cycle, and ray type for each backscatterer.

⩾3 : add printing of lengthy reverberation interpolations as they are being calculated vs time.

FLAG (4) = 1 : print a dump of arrays "ABB" and "ACZ," the arrays containing the bottom bounce and convergence zone vertex sound speeds used in ray tracing.

FLAG (5) limits calculations to a particular backscatterer; all other calculations are shunted.

= 1 : bottom

= 2 : bottom bounce paths to the surface

= 3 : refractive paths to the surface

= 4 : bottom bounce paths to the volume or target

= 5 : refractive paths to the volume or target

FLAG (6) = K ; K = 1, 2, 3, 4. Limit calculations to ray type "K" for both propagation loss to the target and reverberation.

APPENDIX C

INPUT FORMAT

The LIRA program accepts all inputs through SUBROUTINE READIN. READIN contains only two read statements. The input characters are scanned in a manner similar to NAMELIST to determine if a string of characters is an input name or an input parameter value (a number). READIN does not use NAMELIST for the following reasons:

- It is important to keep track of the variables which are changed from run to run in order to reduce redundant calculations.
- Column 1 on the input record can now be used.
- Data literals which have no numerical value can be entered.

The user enters single-value variables by typing the name of the variable, followed by a space or an equal sign "=" and then by the numerical value in F, I, E, or D format. All input values are converted to single-precision floating point numbers. There can be no imbedded blanks in either the name or value, although there may be more than one blank separating the name and value. A name and its value must be on the same line. If more than one name-value set occurs on a line, the sets are to be separated by a comma "," or a slash "/". There is no need to use a comma or a slash as a separator between sets occurring on different lines. The parameters can be input in any order or not input at all, as the user desires.

The user enters arrays in a fashion similar to that used for single-value variables, by first typing the name, then a space or equal sign "=", and then the array values in F, I, E, or D format. Successive array values are separated by one or more spaces. If the array is too long for one line, as many lines as are required can be used by typing the continuation symbol "* ", that is, an asterisk and a space, as the first characters on the successive lines. An array is terminated by a comma or a slash or by starting a new line without the continuation symbol.

Data literals are names which are not followed by values. To enter the name is to set a flag or to follow some instructions before reading the next input.

Figure C-1 illustrates some of the possible ways data may be entered. Column 1 is indicated by the arrow. The line numbers are merely for reference in this discussion. Line 1 in Fig. C-1 shows several examples of separators and spacings and the use and non-use of the equal sign. Line 2 contains the data literal "DR," which will cause a flag to be set so that detection ranges will be calculated. Line 3 is another data literal, "HEADER," which causes the next card to be read as heading information. Line 5 shows how an array of target ranges might be entered. The user need not specify the number of values in an array; the program automatically counts them. Lines 7-10 illustrate the entering of values in array "AHB", employing continuation cards. The latest entry of any parameter supersedes any value it may have been assigned by previous entries. On card 11 "TGS = 15" is superseded by "TGS = 20." On Line 12 PFA is assigned value in E format and on Line 13 in D format. The data literal on Line 12 ("RUN") will cause immediate exit from the READIN subroutine, calculations will be performed with the current data set, and control will be returned to READIN to read the new value for PFA on Line 13. The "RUN" on Line 14

will again cause calculations to be performed, this time only in the detection section, since PFA is a detection parameter. Line 15 ends the program with "END," and control is returned to the executive.

```
Col. 1
     ↓
1    FREQ=1., ZX=20/ZTG 300.,PHDX=5 ,PHDR .5
2    DR
3    HEADER
4    THIS IS A HEADING
5    R 1 10 1 10 20 2 19 17 11 15 2
6    SSP 0 5000 100 5001.8 3000 4950 10000 5050
7         AHB 0 5 5.0 8.5 10. 12
8       *  20  13  40  14
9    * 55  15
10          * 90 15
11        TGS=15, TTY, TGS=20
12   PFA=1.E-5, RUN
13              PFA=1.D-4
14   RUN
15   END
```

Figure C-1. Example of some options in the input format.

A data set equivalent to that represented in Fig. C-1 is shown in Fig. C-2.

```
Col. 1
     ↓
     HEADER
     THIS IS A HEADING
     FREQ=1, ZX=20, ZTG=300, TGS=15
     PFA=.00001, PHDX=5, PHDR=-5
     DR, TTY
     R = 1  20  1
     SSP=0  5000  100  5001.8  3000  4950  10000  5050
     AHB=0 5 5 8.5 10 12 20 13 40 14 55 15 90 15
     RUN
     PFA=.0001, RUN
     END
```

Figure C-2. Rewritten form of the data in Figure C-1.

APPENDIX D

COMPARING LIRA WITH OTHER MODELS

The most sensitive aspect of active-sonar performance prediction is the calculation of propagation loss. Predictions are equally sensitive to underlying theory and algorithms implementing the theory. Within any practical application (i.e., computer program) of a theoretical approach for calculating propagation loss, a host of idiosyncratic cases exist. Each case requires individual treatment and numerical approximation when no analytical solution exists (usually the case). Because of the great complexity of the calculations, some of the idiosyncracies inherent in the method are often overlooked. Comparison of a propagation loss program's outputs with data often looks good when the variance of the data is considered. A program is sometimes rejected when it fails to agree with data and vice versa.

There is no simple way of validating a program. Perhaps the most significant factors in the validating of a propagation loss program are

- Recognition of the validity of the theoretical approach.
- Lack of obvious spurious predictions.
- Good comparison with data.
- Wide range of use in the acoustic propagation community.
- Agreement with other validated programs.

The FACT* program easily falls into the category of a validated program. It has its shortcomings, as does every propagation loss program, but it is a useful and much used tool for passive-sonar applications.

---

* FACT (Fast Asymptotic Coherent Transmission model), developed by the former AESD (Acoustic Environmental Support Detachment) at Office of Naval Research (Ref. 9), computes incoherent and semi-coherent propagation losses using ray theory with corrections for both smooth and cusped caustics. FACT is the "Navy Standard" model for ray models. FACT represents the sound-speed profile by straight lines connecting the points. Because of the discontinuous gradients at the profile-segment interfaces, numerous false caustics would be generated by standard ray theory. Instead, for a particular ray family, FACT fits range vs starting angle (R-Θ points) with a curve (R-Θ curve) that is limited to, at most, one extremum. The relatively small extrema in the R-Θ curves caused by the gradient discontinuities are washed out by the dominating effect of the real caustic. FACT therefore forces the condition of, at most, one caustic per ray family. Other real caustics in a ray family are truly obliterated because FACT uses the fitted R-Θ curve to calculate propagation loss rather than the R-Θ points. FACT is perhaps the only ray program to calculate the acoustic field at and near horizontal cusps. FACT uses a surface duct model developed for FNWC (Ref. 10). For receivers below the surface layer, FACT uses the surface duct propagation loss plus a constant. When source and receiver are located near the deep sound channel axis, FACT uses a wave correction for the rays which obtain. The maximum angle for ray tracing in FACT is 30 deg; thereafter an approximation method is used for propagation loss. Only the internal bottom loss functions may be used in FACT; there is no provision for entering a new one. Neither can a beam pattern be entered.

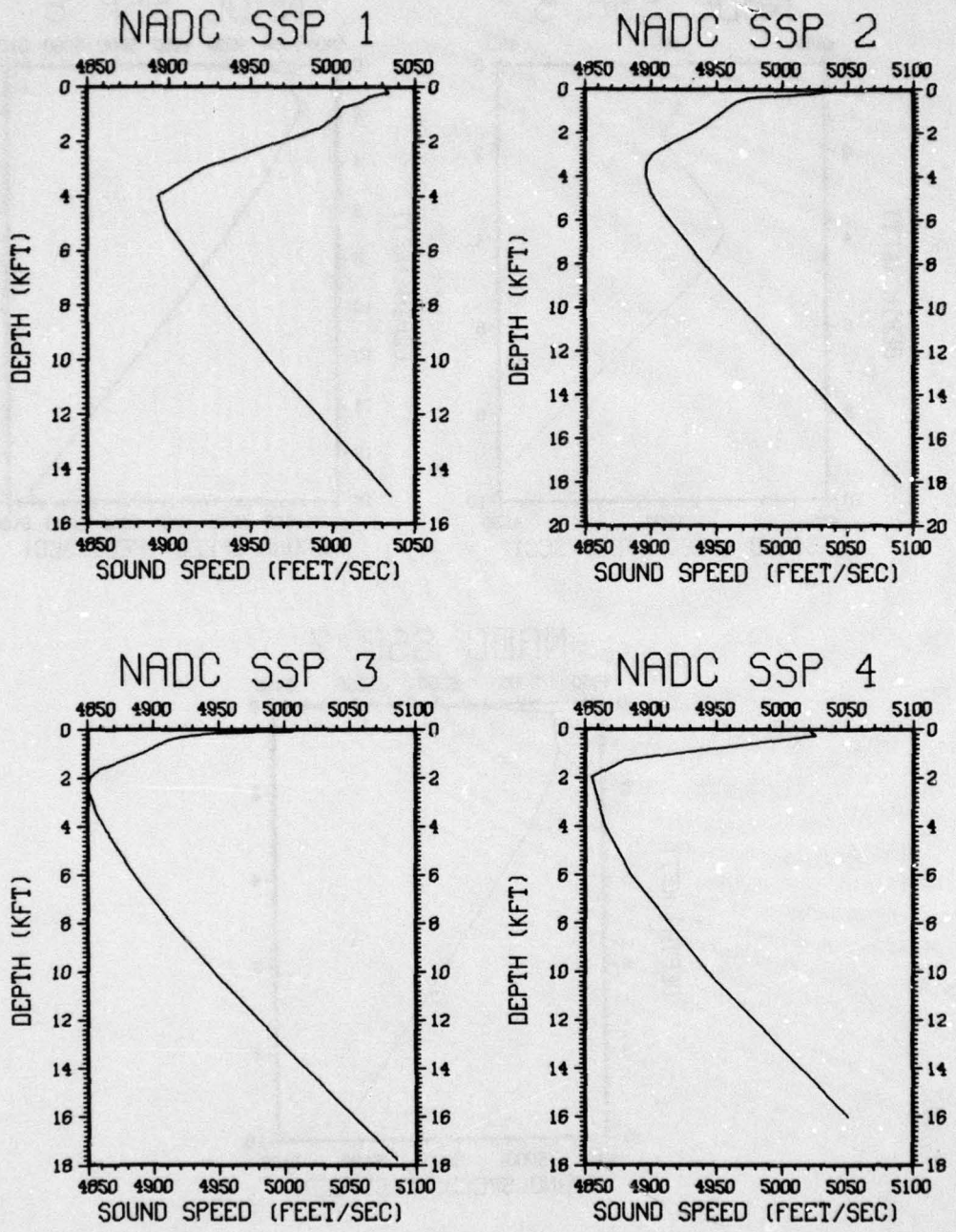

Figure D-1 (a). Sound-speed profiles used to compare LIRA, PLRAY, FACT and AP2 (from Ref. 11).

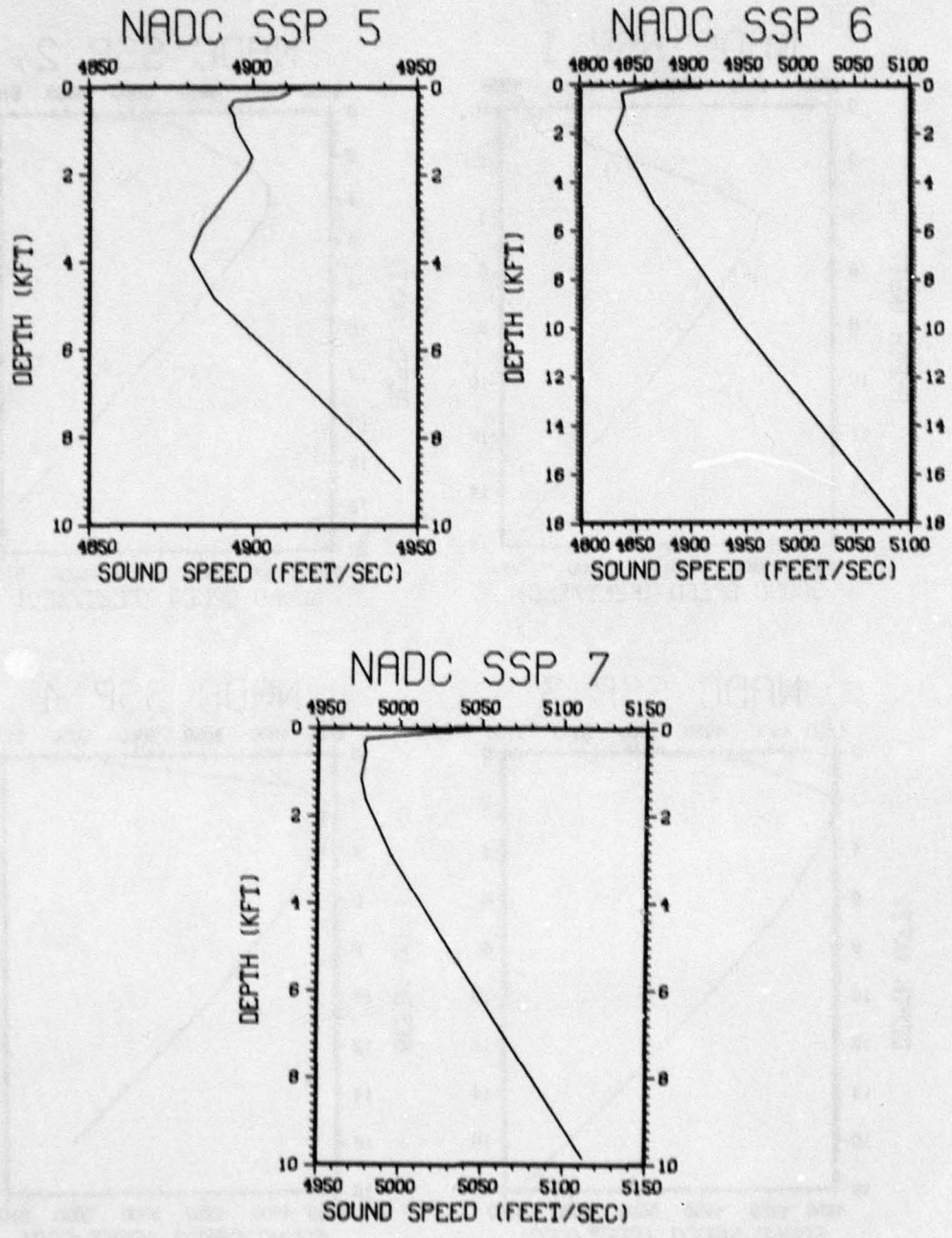
NADC SSP 5
DEPTH (KFT)
SOUND SPEED (FEET/SEC)
NADC SSP 6
DEPTH (KFT)
SOUND SPEED (FEET/SEC)
NADC SSP 7
DEPTH (KFT)
SOUND SPEED (FEET/SEC)

Figure D-1 (b).

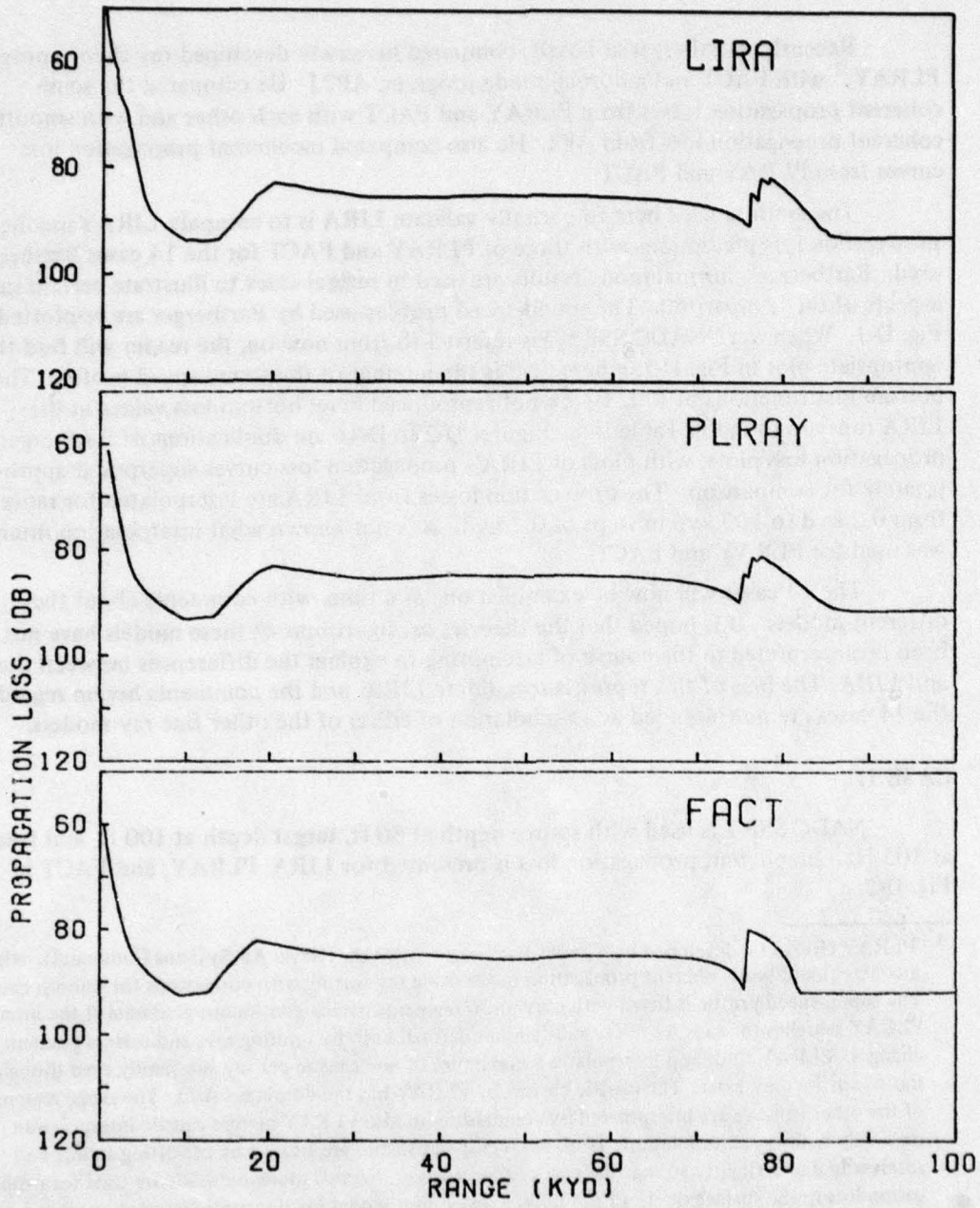

Figure D-2. Incoherent propagation loss, CASE 1 (NADC SSP 1, frequency 105 Hz, source depth 100 ft, target depth 80 ft).

Recently, Bartberger at NADC compared his newly developed ray theory program, PLRAY,* with FACT and a normal mode program, AP2.† He compared the semi-coherent propagation losses from PLRAY and FACT with each other and with smoothed coherent propagation loss from AP2. He also compared incoherent propagation loss curves from PLRAY and FACT.

The method used here to partially validate LIRA is to compare LIRA's incoherent propagation loss predictions with those of PLRAY and FACT for the 14 cases Bartberger used. Bartberger's normal mode results are used in several cases to illustrate certain salient aspects of the comparison. The sound-speed profiles used by Bartberger are re-plotted in Fig. D-1. Whenever "NADC SSP N" is referred to from now on, the reader will find the appropriate plot in Fig. D-1, where "N" is the number of the sound-speed profile. The bottom loss functions of Ref. 10 are not reproduced here; bottom loss values in the LIRA runs are found in Table D-1. Figures D-2 to D-16 are duplications of Bartberger's propagation loss plots, with plots of LIRA's propagation loss curves superposed appropriately for comparison. The propagation losses from LIRA are interpolated for ranges from 0.2 kyd to 100 kyd in steps of 0.2 kyd. It is not known what interpolation interval was used for PLRAY and FACT.

The 14 cases will now be examined one at a time, with comments about the different models. It is hoped that the theories or algorithms of these models have not been misinterpreted in the course of attempting to explain the differences between them and LIRA. The bias of this report is to validate LIRA, and the comments herein regarding the 14 cases are not intended as a repudiation of either of the other fine ray models.

CASE 1.

NADC SSP 1 is used with source depth at 80 ft, target depth at 100 ft, and frequency at 105 Hz. Incoherent propagation loss is presented for LIRA, PLRAY, and FACT in Fig. D-2.

---

* PLRAY (Ref. 11), developed by Charles Bartberger at NADC (Naval Air Systems Command), calculates incoherent and semi-coherent propagation losses using ray tracing with corrections for smooth caustics. The sound-speed profile is fitted with curvilinear segments having continuous gradients at the interfaces. PLRAY searches for caustics in ray sub-families defined both by limiting rays and certain gradient changes. PLRAY finds and interpolates a maximum of one caustic per ray sub-family even though more caustics may exist. The caustic chosen by PLRAY has the dominant field. The range regions of the other caustics are interpolated by standard methods. PLRAY merges caustic interpolation smoothly with ray interpolation. Horizontal cusped caustics are treated by offsetting source and receiver in depth slightly so that the cusps cannot occur. Normal mode methods are used for propagation loss in the surface duct. PLRAY has a leaky duct model for transition between good and no propagation in the surface duct. PLRAY has an internal set of bottom loss curves, which it interpolates for frequency. Bottom loss may also be read in. PLRAY accepts beam-pattern inputs.

†AP2 is a normal mode program newly developed at NADC, still undocumented (Ref. 11). AP2 uses a maximum of 500 modes to calculate coherent propagation loss. For comparison with semi-coherent models, AP2's curve of intensity vs range is smoothed with a weighted sliding window spanning nine terms. AP2 is compatible with ray programs in that it can take as inputs arbitrary sound-speed profiles and bottom loss functions. AP2 was compared with other normal mode programs and gave identical results for the same cases.

```
HEADER
NADC SSP 1
SSP 0 5030.55 233.5 5033.83 395.6 5021.67 433.4 5021.44 597.1 5016.64
* 755.9 5007.44 777.9 5005.64 1098.2 5001.75 1214.8 4999.05
* 1520.7 4992.35 3005.3 4920.79 4011.7 4893.38 5014.1 4898.32
* 8027.9 4934.36 10000 4960 12000 4990 14000 5020 15000 5035
HS 0
OUTP 1
R .2 100 .2
FREQ 105
AHB 0 0 5 0 15 2 25 2 35 15 45 17 65 13 75 12 90 11.5
ZTG 80,ZX 100,RUN
HEADER
NADC SSP 2
SSP 0 5045 200 5025 400 4975 600 4965 800 4960 1600 4943 2000 4932
* 2400 4918 3000 4902 3400 4897 4000 4896 4800 4900 6000 4914
* 8000 4940 14000 5030 18000 5040
FREQ 100
AHB 0 2 10 2 20 6 30 7.5 40 10 55 12 90 12
ZTG 300,ZX 60,RUN
ZX 200,RUN
HEADER
NADC SSP 3
SSP 0 5005.9 32.8 5004.91 65.6 5005.9 98.4 4990.15 164.0 4948.81
* 246.1 4933.39 328.1 4921.91 410.1 4914.69 492.1 4909.44
* 984.2 4892.05 1640.4 4859.57 1968.5 4852.35 2296.6 4850.06
* 2624.7 4850.71 3608.9 4857.93 4921.2 4872.04 5741.5 4881.55
* 6561.7 4892.05 8202.1 4916.33 9842.5 4942.58 13123.3 4999.33
* 16404.2 5059.64 17762.4 5084.96
AHB 0 0 10 0 20 3 35 7 45 8 50 10 90 10
ZTG 300,ZX 60,RUN
ZX 1000,RUN
FREQ 300
AHB 0 2 10 2 12 2.5 20 4.5 35 7.5 45 9.5 55 11 90 11
RUN
HEADER
NADC SSP 4
SSP 0 5019 275 5025 450 5000 1300 4880 2000 4855 4000 4865 6000 4885
* 10000 4943 16000 5050
FREQ 150
AHB 0 0 20 0 25 2 30 4 55 8 90 8
ZTG 200,ZX 60,RUN
ZX 300,RUN
ZX 1000,RUN
HEADER
NADC SSP 5
SSP 0 4921.91 32.8 4915.67 65.6 4911.08 98.4 4911.06 160.8 4910.1
* 242.8 4908.13 321.5 4894.02 485.6 4892.38 646.3 4893.69 967.8 4894.68
* 1607.6 4899.6 1932.4 4897.63 3231.6 4884.18 3881.2 4880.57
* 4852.4 4888.11 6456.7 4910.75 8067.6 4933.06 9005.9 4944.54
FREQ 100
AHB 0 0 10 0 20 3 35 7 45 8 50 10 90 10
ZTG 300,ZX 100,RUN
ZX 1000,RUN
```

Table D-1. LIRA's inputs for the 14 cases in this Appendix.

```
HEADER
NADC SSP 6
SSP 0 4910.8 98.4 4910.7 124.7 4869.75 377.3 4837.6 984.2 4839.9
* 1535.7 4832.30 4921.3 4867.5 9842.3 4943.6 17782.2 5083.7
FREQ 50
AHB 0 6 90 6
ZTG 300,ZX 1000,RUN
HEADER
NADC SSP 7
SSP 0 5062.99 32.8 5063.65 98 5028.76 98.4 5023.62 246.1 4979.33
* 360.9 4977.69 574.2 4978.67 1148.3 4976.05 1640.4 4979
* 2952.8 4995.41 5000 5029.18 7000 5062.85 9842.5 5111.88
FREQ 100
AHB 0 0 10 0 20 3 35 7 45 8 50 10 90 10
ZTG 300,ZX 100,RUN
ZX 1000,RUN
END
```

Table D-1. Continued.

The three programs agree in the bottom bounce region ($4 < R < 75$ kyd and $R > 85$ kyd). There are, however, subtle differences in the direct-path and convergence zone regions.

All three models use their own specialized surface duct models derived from data and normal mode theory. The surface duct propagation losses for ranges less than 4 kyd are slightly different for each model.

At 75 kyd there appears to be the onset of a convergence zone. Actually, the decrease in propagation loss is produced by rays which converge but do not cross; that is, there are no caustics at all produced by this geometry, at least for LIRA. The shape of the FACT curve looks like part of an Airy function curve that has been cut off. It is likely that the FACT program established the presence of a reversed caustic (i.e., range vs starting angle has a maximum) and interpolated for that caustic on the illuminated side for only those ranges which had rays arriving. The shadow zone extends past 50 kyd, and again rays contributing to the field are excluded because they fall within the boundaries of the caustic field.

In contrast, LIRA and PLRAY have not established the presence of a caustic and use standard ray tracing for the acoustic field. For this reason the tail of the zone extends farther than FACT's.

It is not the purpose of this discussion to make a choice between models. Because of the different representations of the sound-speed profile, one model can certainly establish the presence of a caustic and others not. Indeed, there is cause for encouragement that the fundamentally different algorithms agree so well in their predictions.

CASE 2.

NADC SSP 2 is used with source depth at 60 ft, target depth at 300 ft and frequency at 100 Hz. Incoherent propagation loss for LIRA, PLRAY, and FACT is presented in Fig. D-3.

There is good agreement between the three models in the direct path and bottom bounce regions as well as the leading edge (shadow side) of the convergence zone. Slight variations in sound-speed profile representation can cause the shifting of the intensity of the acoustic pressure field in the caustic regions. Both PLRAY and FACT use approximations for the position of the caustics rather than the iterative method of LIRA, probably causing slight changes in the positions and shapes of the several caustic fields which make up the composite field. The average magnitudes are the same over the region of the convergence zone from 68 to 74 kyd.

All three models forbid interpolation of a caustic on the illuminated side for those ranges not reached by rays in the same ray family from which the caustic is derived. This results in the sharp increase in propagation loss at 73-74 kyd for all three programs. For LIRA and PLRAY two caustics were truncated in this manner, resulting in the small notch at 74 kyd. FACT truncated one caustic at the tail of the convergence zone. Perhaps if FACT had determined the other caustic at the tail of the zone, the shape of the zone would have been more like PLRAY's.

60

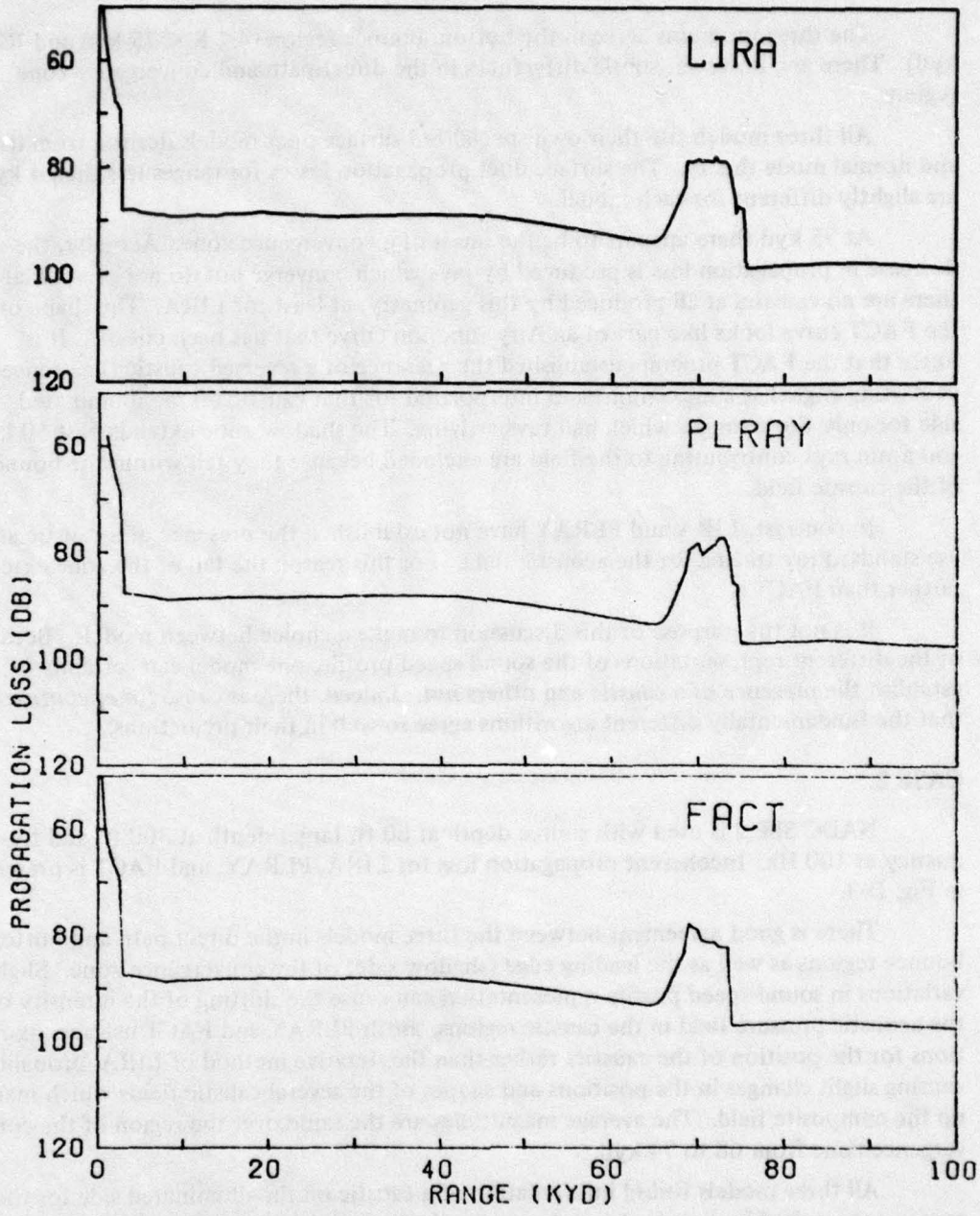

Figure D-3. Incoherent propagation loss, CASE 2 (NADC SSP 2, frequency 100 Hz, source depth 60 ft, target depth 300 ft).

CASE 3.

The incoherent propagation losses in Fig. D-4 are for the same sound-speed profile as CASE 2; source depth is changed to 200 ft. The same remarks apply, approximately, to this case as CASE 2, since there are no novel differences.

CASE 4.

NADC SSP 3 is used with source depth at 60 ft, target depth at 300 ft and frequency at 100 Hz. Incoherent propagation loss for LIRA, PLRAY, and FACT is presented in Fig. D-5.

The small peak at 4 kyd in LIRA is not a caustic, just a narrow bundle of rays. No novel differences occur at convergence zone ranges.

Neither PLRAY nor FACT traces bottom bounce rays steeper than 30 deg. They both use the same approximation to compute propagation loss for ranges corresponding to bottom bounce with steeper rays. LIRA traces rays at angles up to 89 deg, nearly vertical. This can account for the slight discrepancy in bottom bounce propagation loss between LIRA and the other two models for ranges between 5 and 10 kyd.

CASE 5.

Incoherent propagation loss for NADC SSP 3, for a frequency of 100 Hz, source depth at 1000 ft and target depth at 300 ft, is presented in Fig. D-6 for LIRA, PLRAY, and FACT. Smoothed coherent propagation loss for AP2 is presented in Fig. D-7.

The most noteworthy differences between LIRA, PLRAY, and FACT are the heights, widths, and numbers of the caustic peaks in the convergence zone region. PLRAY's leftmost peak is narrower, higher, and slightly to the left of the corresponding peak in LIRA and FACT. FACT's leftmost peak follows the opposite trend, leaving LIRA's leftmost peak an intermediate between those of PLRAY and FACT. A comparison with the normal mode curve for CASE 5 in Fig. D-7a shows that LIRA's prediction conforms better to the AP2's prediction than those of PLRAY and FACT. The same is true of the caustic peak at 59 kyd in the LIRA curve.

The peak at 56 kyd between the two most prominent peaks in the LIRA curve does not have any counterpart in the normal mode curve. It may be that secondary caustics in a ray family which occur because of slight sound-speed profile nuances should be excluded from interpolation. In PLRAY the secondary caustic occurs at 54 kyd. From its shape it appears to have escaped the caustic search. The small peak was probably obtained by ray interpolation. FACT's treatment of this secondary caustic is consistent with the theory that more than one caustic exists in this ray family. Assuming that the secondary caustic does occur in the ray family, FACT would fit a curve with a single maximum through the R-Θ points containing both the primary and secondary maxima. FACT then would use the fitted curve to calculate the parameters of a single caustic, resulting in a wider, lower peak than if the secondary caustic did not exist.

CASE 6.

The environment and geometry are the same as the previous case. The only

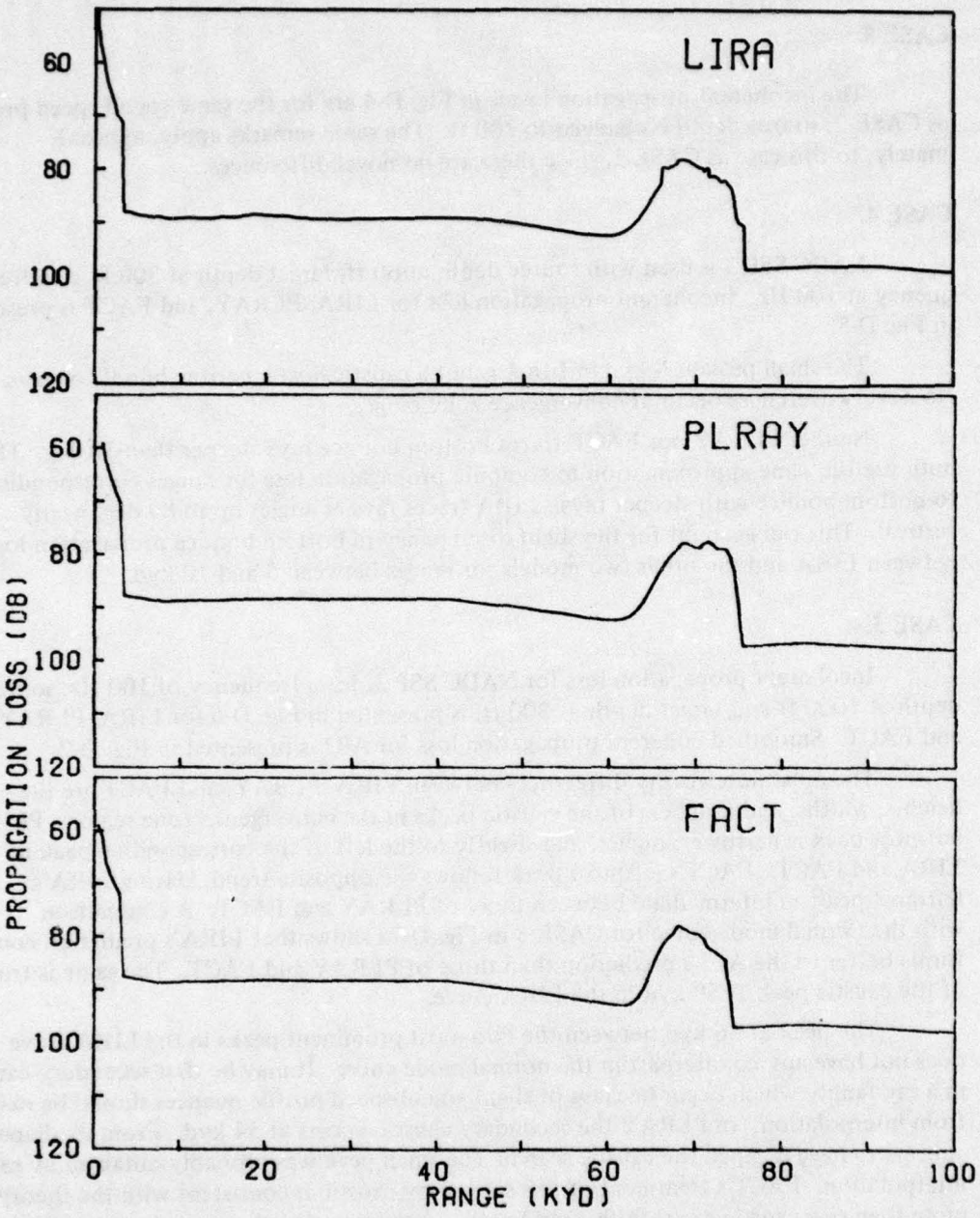

Figure D-4. Incoherent propagation loss, CASE 3 (NADC SSP 2, frequency 100 Hz, source depth 200 ft, target depth 300 ft).

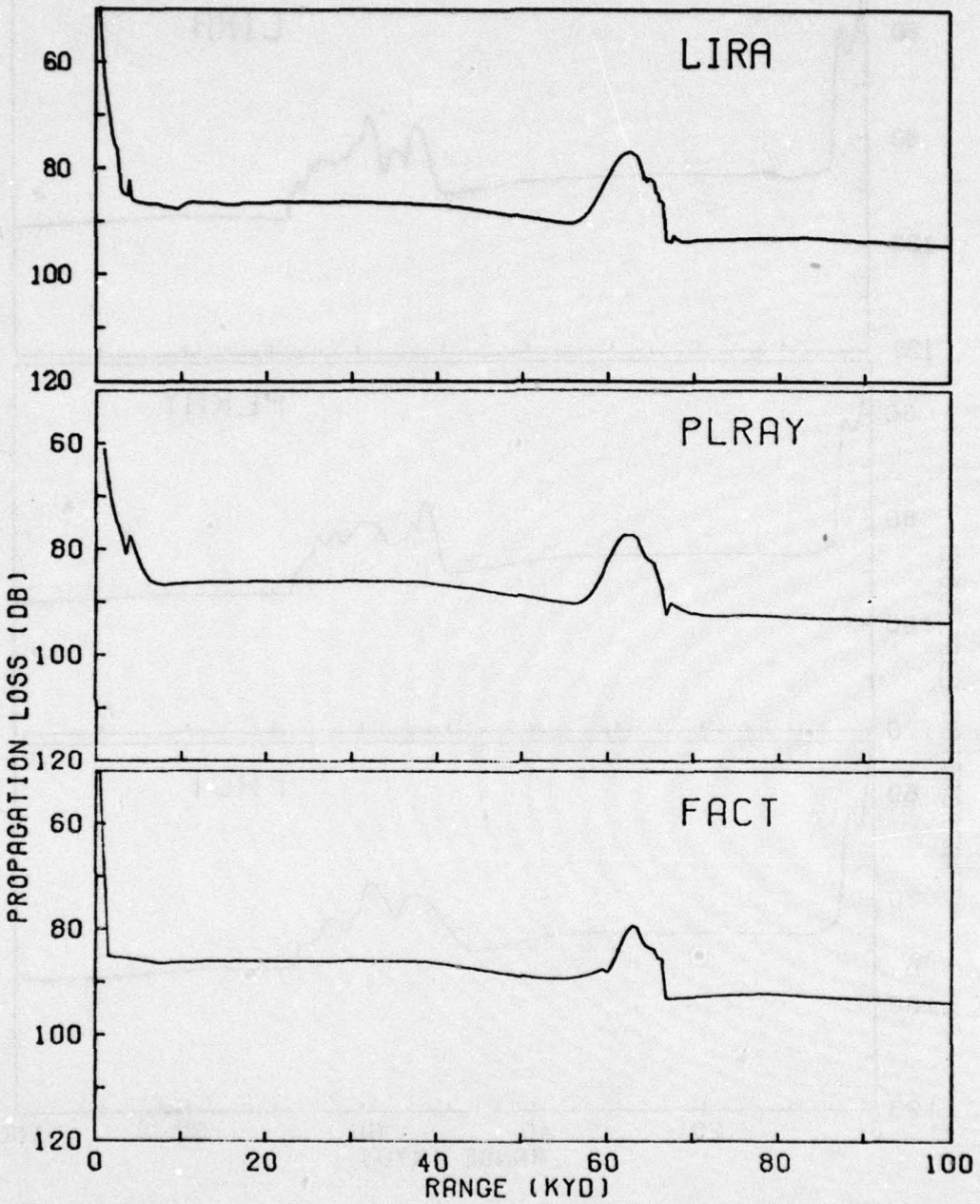

Figure D-5. Incoherent propagation loss, CASE 4 (NADC SSP 3, frequency 100 Hz, source depth 60 ft, target depth 300 ft).

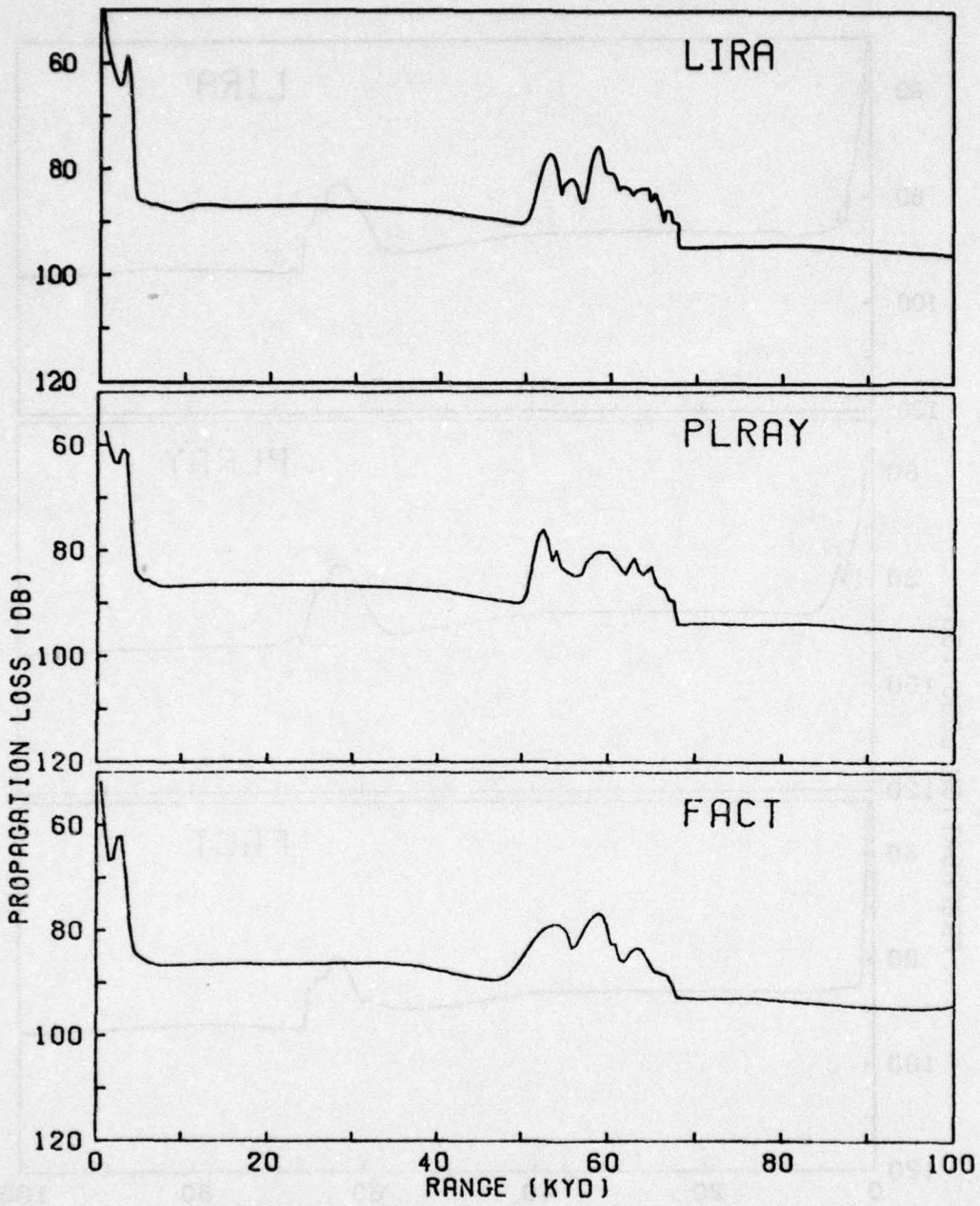

Figure D-6. Incoherent propagation loss, CASE 5 (NADC SSP 3, frequency 100 Hz, source depth 1000 ft, target depth 300 ft).

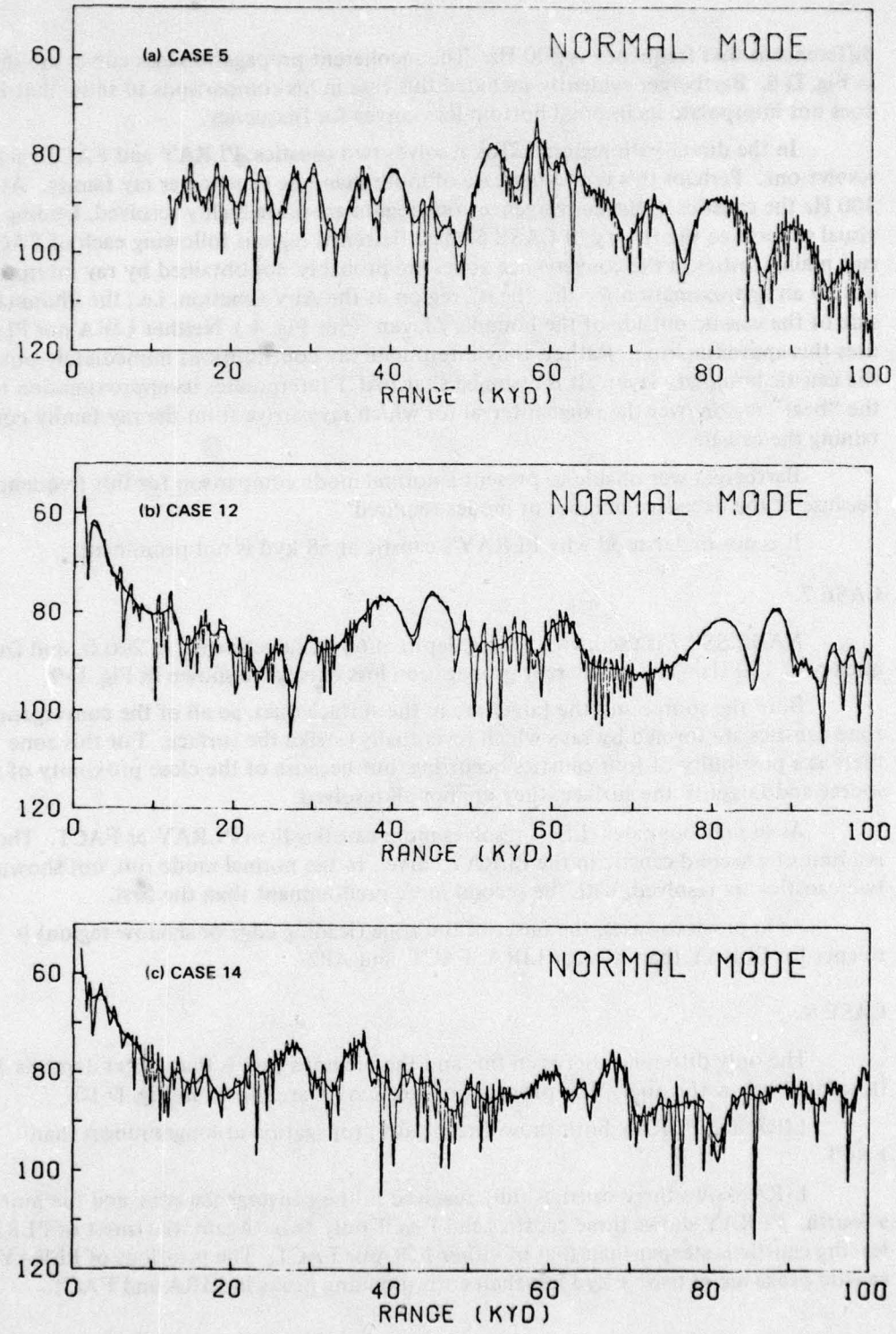

Figure D-7. Normal mode propagation loss from AP2 for CASES 5, 12, and 14.

difference is that frequency is 300 Hz. The incoherent propagation loss curves are shown in Fig. D-8. Bartberger evidently included this case in his comparisons to show that FACT does not interpolate its internal bottom-loss curves for frequency.

In the direct-path region, LIRA resolves two caustics; PLRAY and FACT each resolve one. Perhaps this is another case of more than one caustic per ray family. At 300 Hz the caustics in the convergence zone region are more highly resolved, lending visual support to the theory of CASE 5. The flattened regions following each of FACT's two main caustics in the convergence zones are probably not obtained by ray interpolation but by an approximation for the "beat" region of the Airy function, i.e., the illuminated side of the caustic outside of the boundary layer. (See Fig. 4.) Neither LIRA nor PLRAY uses this approximation. Rather, they interpolate ray contributions immediately outside the caustic boundary layer. It is assumed that FACT interpolates its approximation for the "beat" region over the range interval for which rays arrive from the ray family containing the caustic.

Bartberger was unable to present a normal mode comparison for this frequency because of the excessive number of modes required.

It is not understood why PLRAY's caustic at 58 kyd is not prominent.

CASE 7.

NADC SSP 7 is used with source depth at 60 ft, target depth at 200 ft, and frequency at 150 Hz. The incoherent propagation loss curves are shown in Fig. D-9.

Both the source and the target are in the surface duct, so all of the convergence zone caustics are formed by rays which (eventually) strike the surface. For this zone there is a possibility of four caustics occurring, but because of the close proximity of the source and target to the surface, they are not all resolved.

As in previous cases LIRA resolves more caustics than PLRAY or FACT. There is a hint of a second caustic in the PLRAY curve. In the normal mode run, not shown, two caustics are resolved, with the second more predominant than the first.

As in previous cases, the onset of the zone (leading edge or shadow region) is steeper for PLRAY than it is for LIRA, FACT, and AP2.

CASE 8.

The only difference between this and the previous case is that target depth is 300 ft, located below the duct. The propagation loss curves are shown in Fig. D-10.

LIRA and PLRAY both show direct-path propagation at longer ranges than FACT.

LIRA shows three caustics fully resolved in the convergence zone and the hint of a fourth. PLRAY shows three caustics and FACT only two. Again, the onset of PLRAY's leading caustic is steeper than that of either LIRA or FACT. The positions of PLRAY's caustic peaks are at least 1 kyd less than corresponding peaks in LIRA and FACT.

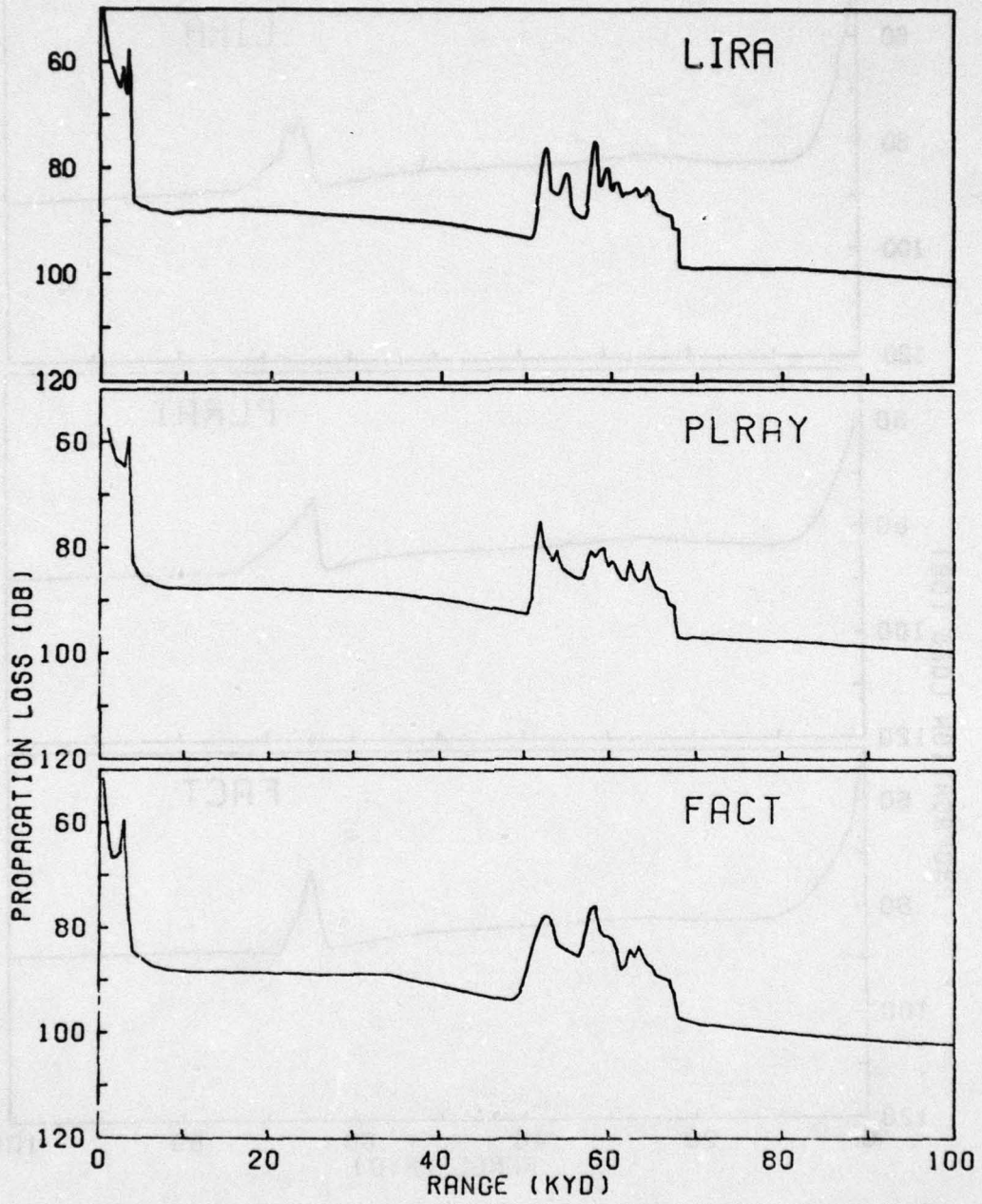

Figure D-8. Incoherent propagation loss, CASE 6 (NADC SSP 3, frequency 300 Hz, source depth 1000 ft, target depth 300 ft).

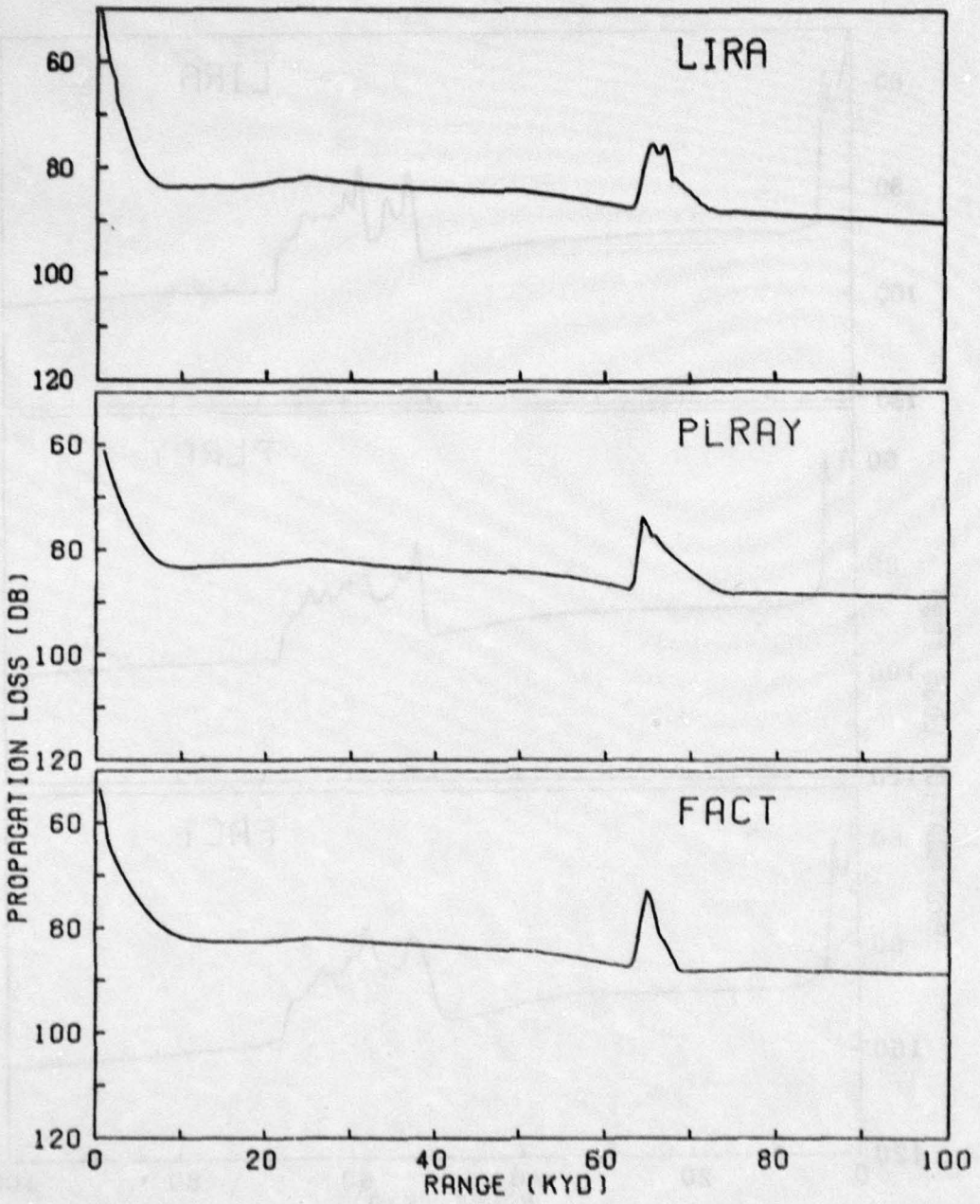

Figure D-9. Incoherent propagation loss, CASE 7 (NADC SSP 4, frequency 150 Hz, source depth 60 ft, target depth 200 ft).

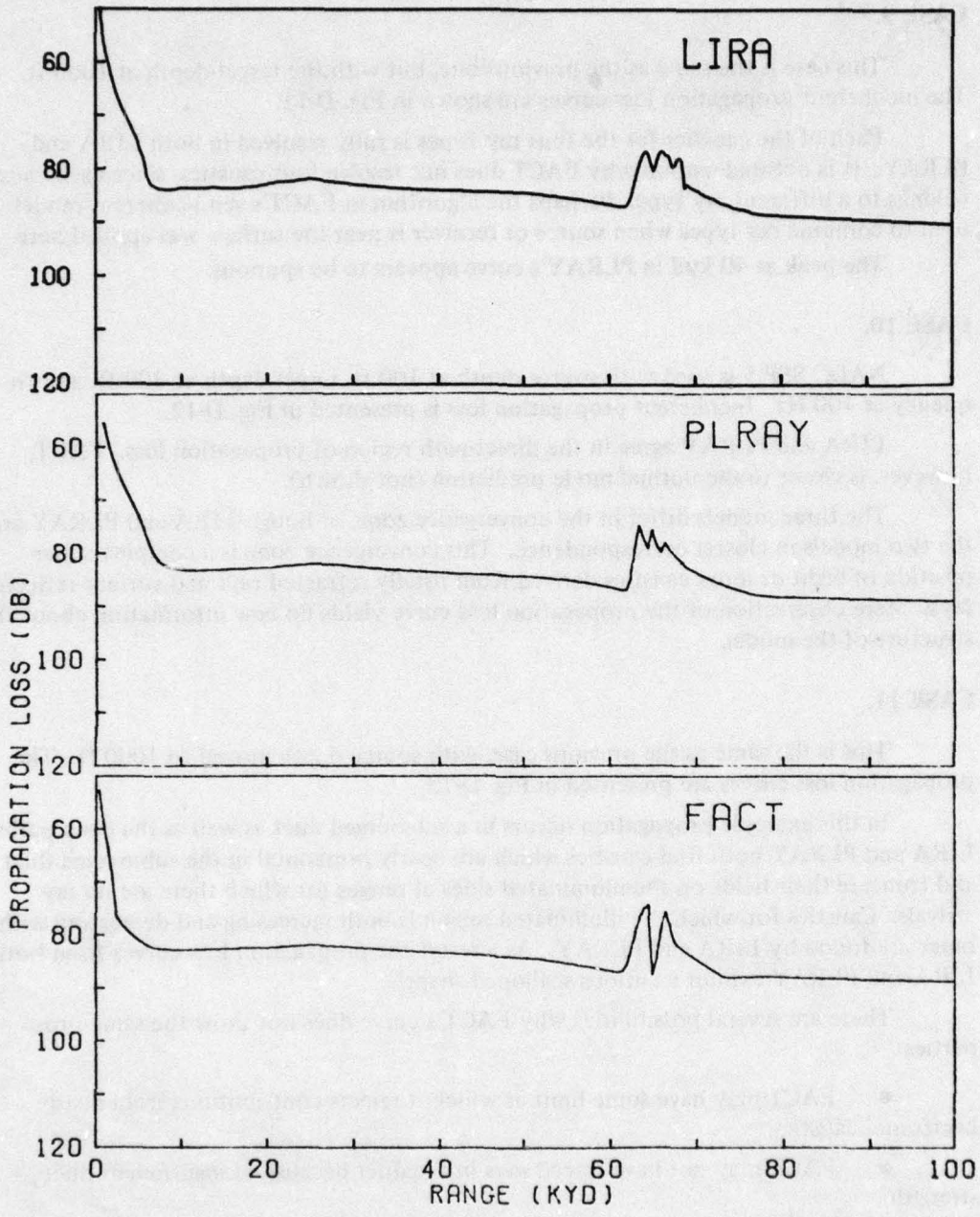

Figure D-10. Incoherent propagation loss, CASE 8 (NADC SSP 4, frequency 150 Hz, source depth 300 ft, target depth 200 ft).

CASE 9.

This case is the same as the previous one, but with the target depth at 1000 ft. The incoherent propagation loss curves are shown in Fig. D-11.

Each of the caustics for the four ray types is fully resolved in both LIRA and PLRAY. It is not understood why FACT does not resolve four caustics, since each caustic belongs to a different ray type. Perhaps the algorithm in FACT's semi-coherent model used to combine ray types when source or receiver is near the surface was applied here.

The peak at 40 kyd in PLRAY's curve appears to be spurious.

CASE 10.

NADC SSP 5 is used with source depth at 100 ft, target depth at 300 ft, and frequency at 100 Hz. Incoherent propagation loss is presented in Fig. D-12.

LIRA and PLRAY agree in the direct-path region of propagation loss. FACT, however, is closer to the normal mode prediction (not shown).

The three models differ in the convergence zone, although LIRA and PLRAY are the two models in closest correspondence. This convergence zone is a complex superposition of eight or more caustics derived from totally refracted rays and surface-reflected rays. Mere observation of the propagation loss curve yields no new information about the structure of the model.

CASE 11.

This is the same as the previous case, with source depth moved to 1000 ft. The propagation loss curves are presented in Fig. D-13.

In this example propagation occurs in a submerged duct as well as the deep paths. LIRA and PLRAY both find caustics which are nearly horizontal in the submerged duct and truncate their fields on the illuminated sides at ranges for which there are no ray arrivals. Caustics for which the illuminated region is both increasing and decreasing with range are found by LIRA and PLRAY. As a result the propagation loss curves from both LIRA and PLRAY exhibit a curious scalloped shape.

There are several possibilities why FACT's curve does not show the same properties:

- FACT may have some limit at which it rejects contributions from nearly horizontal caustics.
- FACT may not have traced rays in the duct because of insufficient duct strength.
- FACT may have used its wave approximation for a deep duct.

Whatever the approach FACT used, its curve matches the normal mode curve (not shown) better than LIRA or PLRAY.

The peak at 21 kyd in the curve for LIRA is due to rays that converge but do not cross. No caustic solution is obtainable.

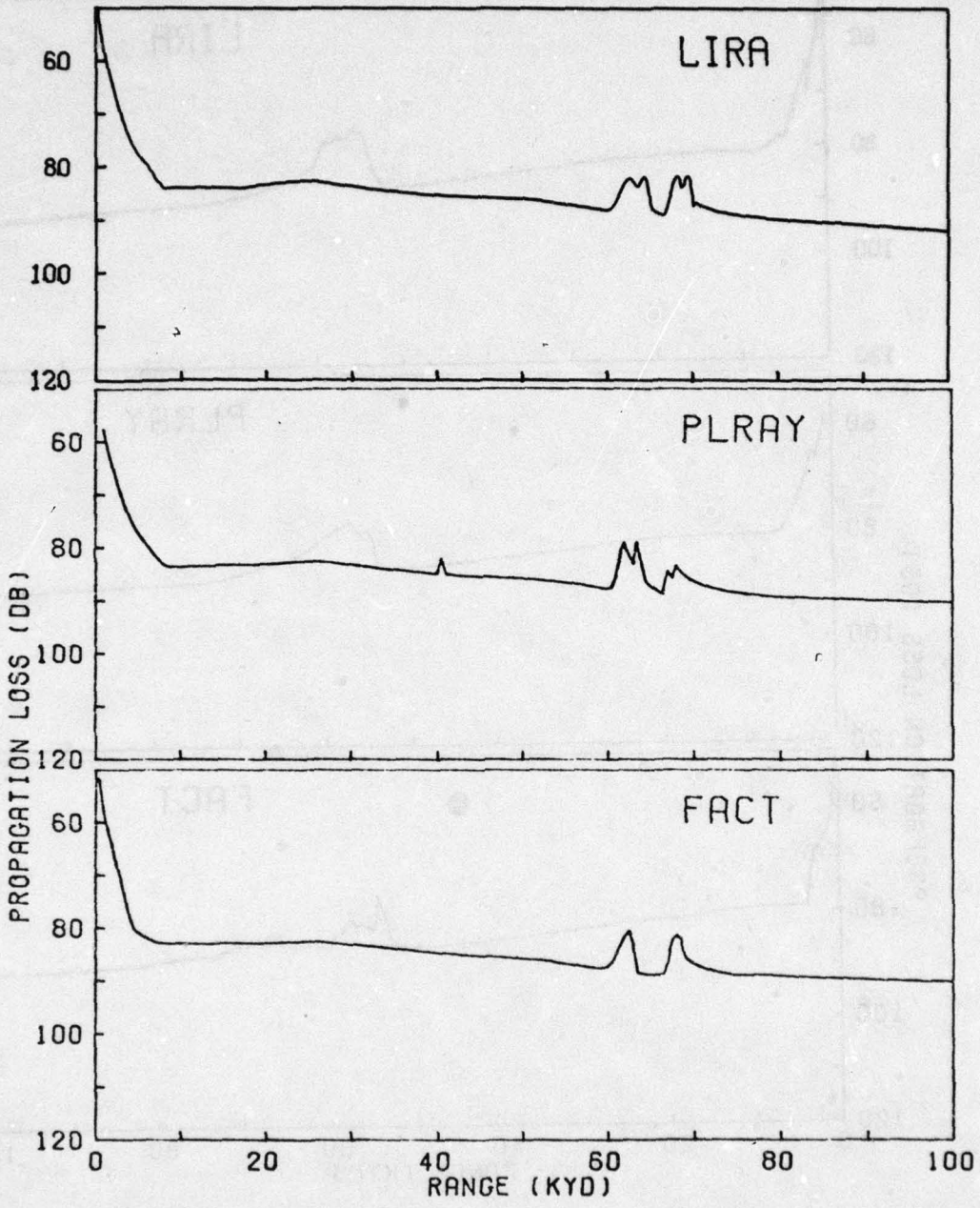

Figure D-11. Incoherent propagation loss, CASE 9 (NADC SSP 4, frequency 150 Hz, source depth 1000 ft, target depth 200 ft).

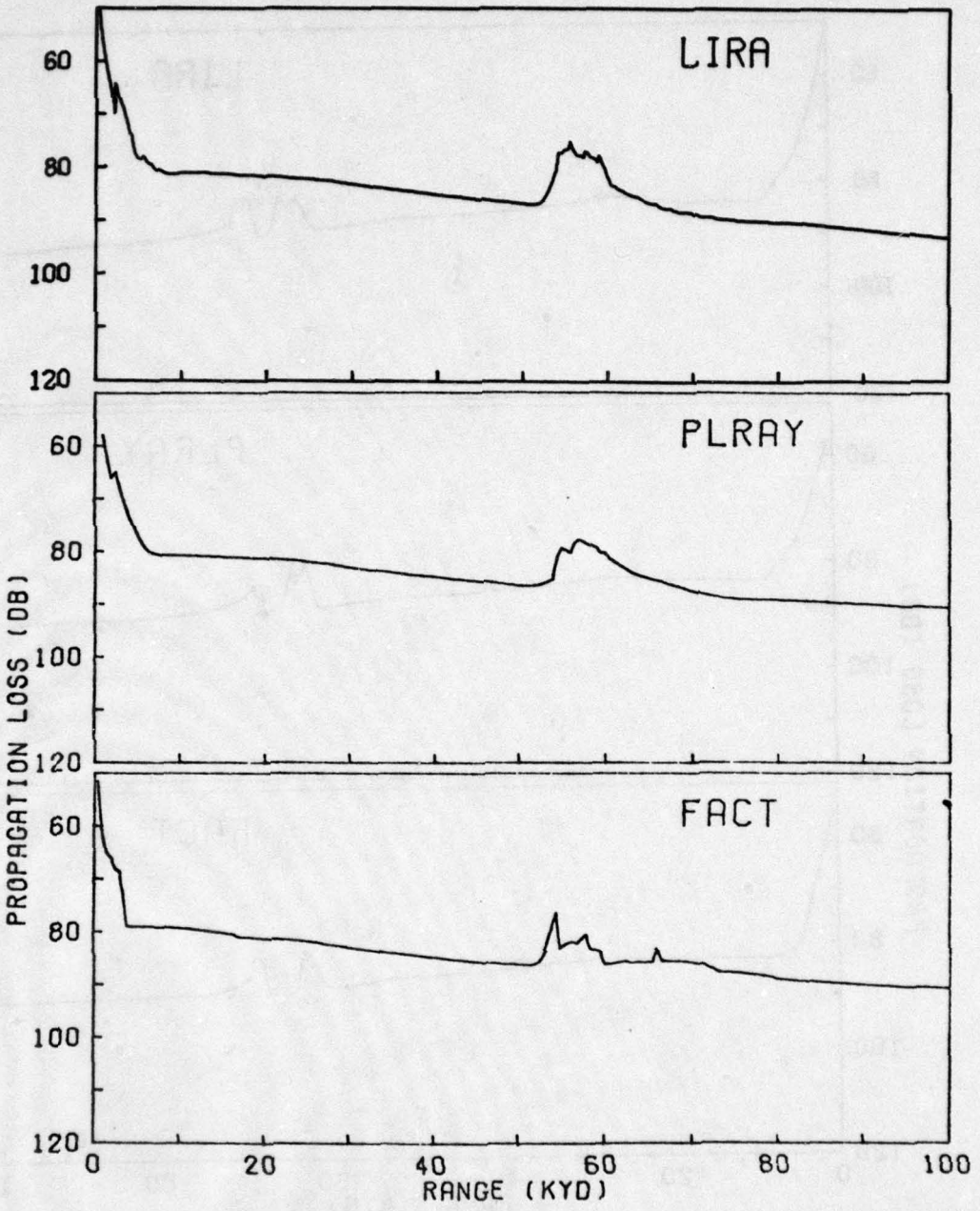

Figure D-12. Incoherent propagation loss, CASE 10 (NADC SSP 5, frequency 100 Hz, source depth 100 ft, target depth 300 ft).

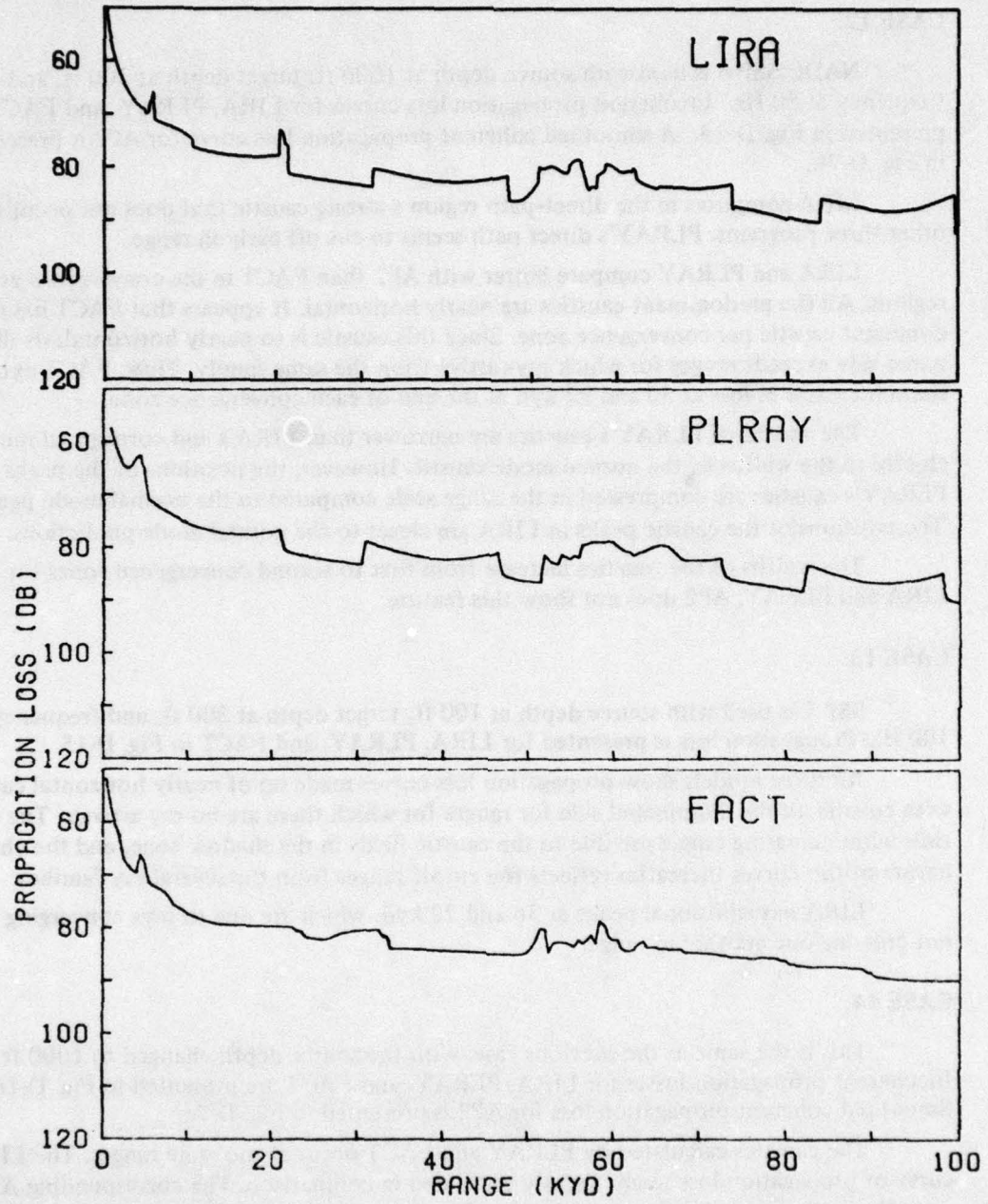

Figure D-13. Incoherent propagation loss, CASE 11 (NADC SSP 5, frequency 100 Hz, source depth 1000 ft, target depth 300 ft).

CASE 12.

NADC SSP 6 is used with source depth at 1000 ft, target depth at 300 ft, and frequency at 50 Hz. Incoherent propagation loss curves for LIRA, PLRAY, and FACT are presented in Fig. D-14. A smoothed coherent propagation loss curve for AP2 is presented in Fig. D-7b.

LIRA computes in the direct-path region a strong caustic that does not occur in the other three programs. PLRAY's direct path seems to cut off early in range.

LIRA and PLRAY compare better with AP2 than FACT in the convergence zone regions. All the predominant caustics are nearly horizontal. It appears that FACT has one dominant caustic per convergence zone. Since this caustic is so nearly horizontal, its illuminated side exceeds ranges for which rays arrive from the same family. Thus, FACT exhibits sharp increases in loss at 50 and 97 kyd at the end of each convergence zone.

The widths of PLRAY's caustics are narrower than LIRA's and correspond more closely to the widths of the normal mode caustic. However, the positions of the peaks of PLRAY's caustics are compressed in the range scale compared to the normal mode peaks. The positions of the caustic peaks in LIRA are closer to the normal mode predictions.

The widths of the caustics increase from first to second convergence zones for both LIRA and PLRAY; AP2 does not show this feature.

CASE 13.

SSP 7 is used with source depth at 100 ft, target depth at 300 ft, and frequency at 100 Hz. Propagation loss is presented for LIRA, PLRAY, and FACT in Fig. D-15.

All three models show propagation loss curves made up of nearly horizontal caustics with cutoffs on the illuminated side for ranges for which there are no ray arrivals. The slow rises with increasing ranges are due to the caustic fields in the shadow zone, and the choppy nature of the curves thereafter reflects the cutoff ranges from the several ray families.

LIRA has additional peaks at 36 and 72 kyd, which are due to rays converging but not crossing one another in range.

CASE 14.

This is the same as the previous case, with the source depth changed to 1000 ft. Incoherent propagation losses for LIRA, PLRAY, and FACT are presented in Fig. D-16. Smoothed coherent propagation loss for AP2 is presented in Fig. D-7c.

The caustics calculated by PLRAY and FACT occur at the same ranges. The LIRA curve of propagation loss seems slightly expanded in comparison. The corresponding AP2 smoothed coherent propagation loss curve places the caustics at the same ranges as LIRA.

LIRA and FACT show the direct path extending out to at least 15 kyd; PLRAY achieves only 3 kyd. There is a caustic at 3 kyd, which LIRA merges with the other ray contributions. Unfortunately, the tail of the illuminated side of the caustic is not well merged with the corresponding ray arrivals for that family, giving the dip at 5 kyd and a bump at 6 kyd. LIRA's bump at 6 kyd does not correspond to FACT's small peak at 3 kyd, which is the correct position of the caustic. From the shape of FACT's peak, it appears that

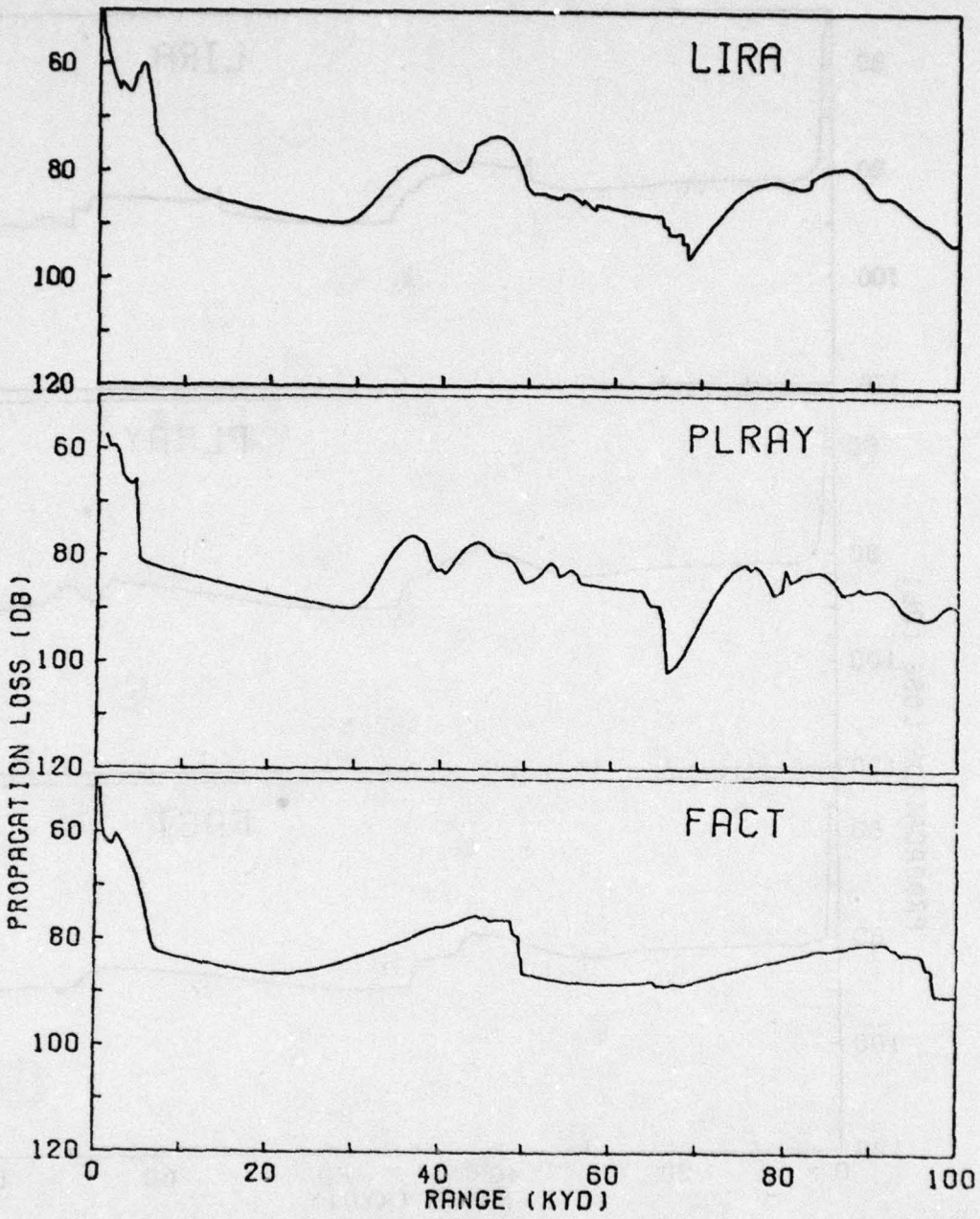

Figure D-14. Incoherent propagation loss, CASE 12 (NADC SSP 6, frequency 50 Hz, source depth 1000 ft, target depth 300 ft).

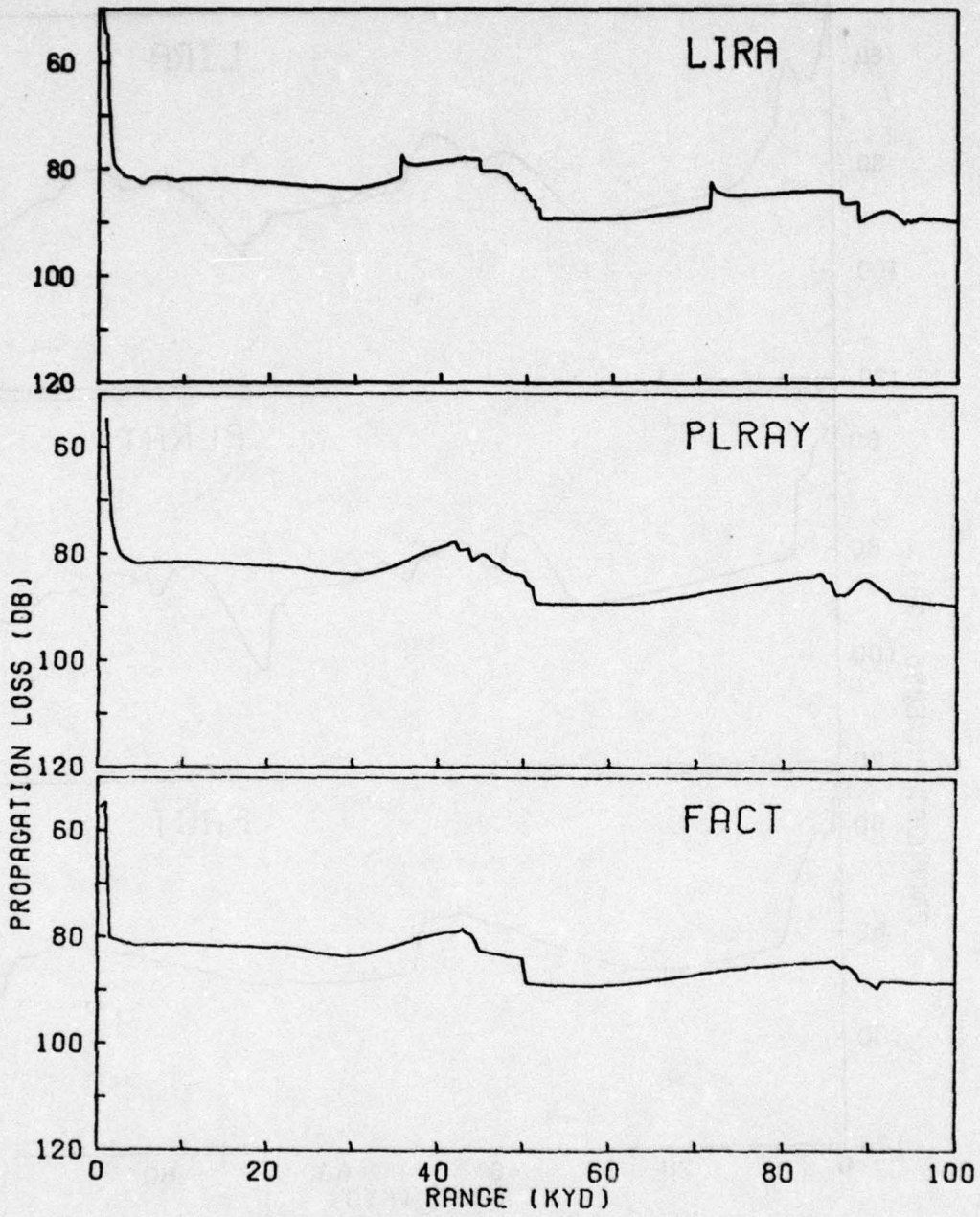

Figure D-15. Incoherent propagation loss, CASE 13 (NADC SSP 7, frequency 100 Hz, source depth 100 ft, target depth 300 ft).

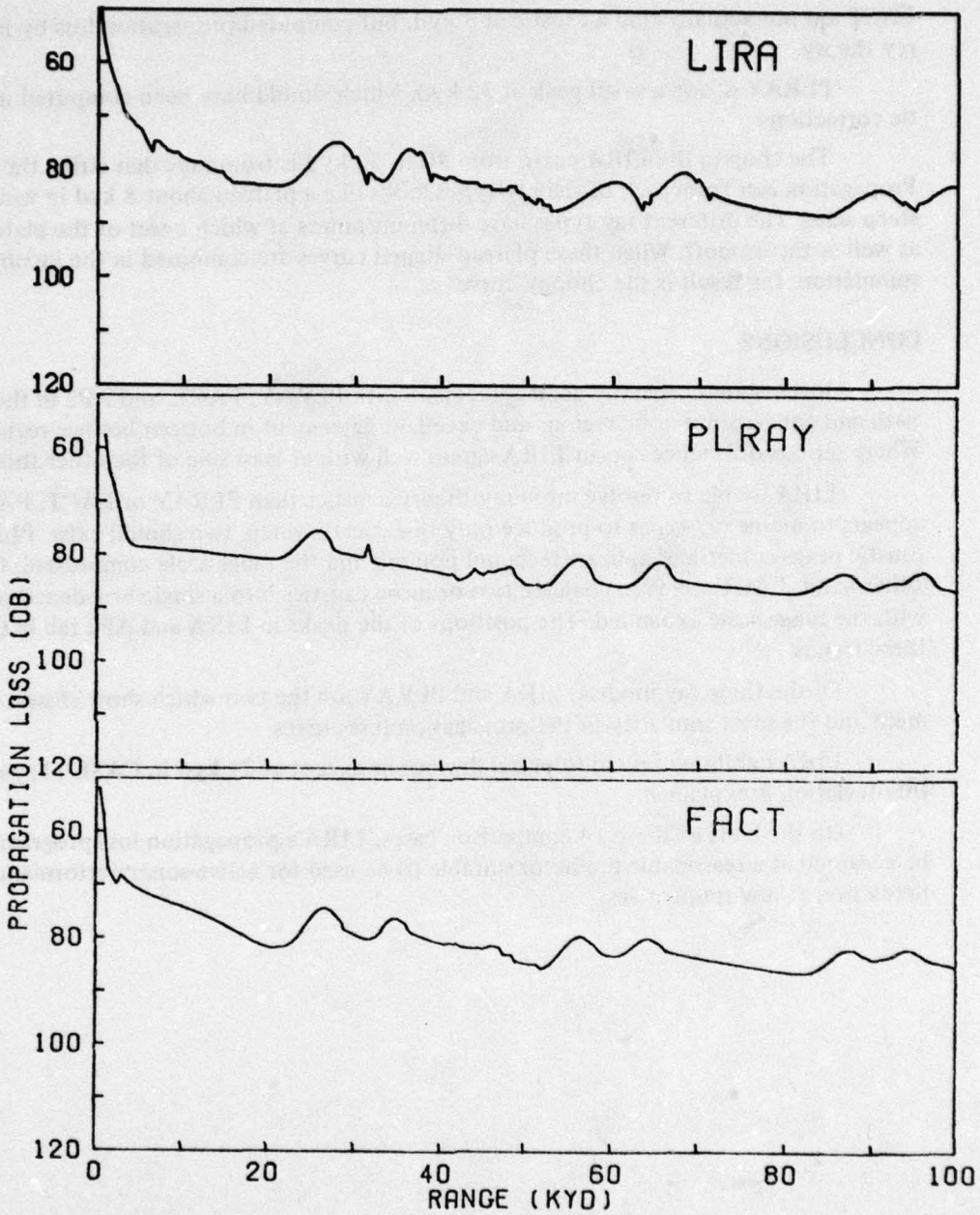

Figure D-16. Incoherent propagation loss, CASE 14 (NADC SSP 7, frequency 100 Hz, source depth 1000 ft, target depth 300 ft).

FACT did not actually find a caustic at 3 kyd, but computed propagation loss by means of ray theory.

PLRAY shows a small peak at 32 kyd, which should have been computed using caustic corrections.

The chop in the LIRA curve from 40 to 52 kyd is from rays that strike the surface. Propagation loss from each of the ray types looks like a plateau about 8 kyd in width with steep sides. The different ray types have different ranges at which onset of the plateau occurs as well as the dropoff. When these plateau-shaped curves are combined in the incoherent summation, the result is the choppy curve.

CONCLUSIONS

LIRA shows generally good agreement with PLRAY, FACT, and AP2 in the direct-path and convergence zone regions and excellent agreement in bottom bounce regions. Where serious differences occur LIRA agrees well with at least one of the other three models.

LIRA is able to resolve more ray theory caustics than PLRAY or FACT. FACT appears to merge ray types to produce only one caustic where two should exist. PLRAY's caustic peaks sometimes appear steep and pointed and the range scale compressed. On the other hand, FACT seems to coalesce two or more caustics into a single broadened peak, with the range scale expanded. The positions of the peaks in LIRA and AP2 fall between these trends.

Of the three ray models, LIRA and PLRAY are the two which show closest agreement and the most similarity in the propagation loss curves.

LIRA exhibited no pathological deviations except at 21 kyd in CASE 11; yet this deviation is explained.

On the basis of these 14 comparison cases, LIRA's propagation loss program should be accepted as a reasonable predictor suitable to be used for active-sonar performance prediction at low frequencies.

APPENDIX E

EXAMPLES OF OUTPUT PLOTS FROM LIRA

The following plots demonstrate the use of LIRA to analyze an active-surveillance scenario. The winter and summer sound-speed profiles in Figs. E-1 and E-2 are representative of an area at the edge of a continental shelf, where the bottom drops sharply from 3600 to 17600 ft. An active source at 700 ft is positioned above a horizontal receiving array on the bottom at 3600 ft.

Four cases are investigated:

CASE	SSP	TARGET DEPTH (FT.)
E-1	Winter	60
E-2	Winter	400
E-3	Summer	60
E-4	Summer	400

Three plots are produced for each case: propagation loss, pulse-averaged reverberation, and signal excess.

The input card images used to run the LIRA program are given in Table E-1, an example of one execution of LIRA containing four runs. Input parameters of interest are:

- Frequency is 250 Hz (FREQ)
- Surface loss per bounce is 0.015 dB (HS)
- Volume column backscattering strength is -70 dB/yd^2//1 yd (MUV)
- Surface backscattering strength is a function of grazing angle; for low angles it is -60 dB/yd^2//1 yd (ASBS).
- Bottom backscattering strength is a function of grazing angle; for low angles it is -35 dB/yd^2// 1 yd (ABBS).
- Source level is 240 dB // 1 μPa at 1 yd (SL).
- Source vertical beam pattern is that of a continuous line array (BEAMX = 0).
- Vertical beamwidth of the main lobe of the source beam pattern is 20 deg (VBM).
- The signal waveform is PRN.
- The pulse length is 10 s (PULSE).
- Receiving array gain is 13 dB (AG).
- Receiving array vertical beam pattern is omnidirectional.
- Receiver bandwidth is 100 Hz (BWR).
- Spectrum level noise is 64 dB/1 Hz // 1 μPa (NIN).
- Target strength is 15 dB (TGS).
- Detection threshold is 14.5 dB (ADT) for 0.9 probability of detection and 10^{-4} probability of false alarm.
- Only up-rays are allowed at the receiver (RBOT).

Propagation loss vs target range for the four cases is presented in Figs. E-3 to E-6. The propagation loss shown is the average of the one-way losses from source to target and from target to receiving array. The solid curve is the incoherent sum of all ray arrivals, and the dashed curve is the propagation loss for the largest arrival (single path with least loss). The beam-pattern effects are included in the loss curves.

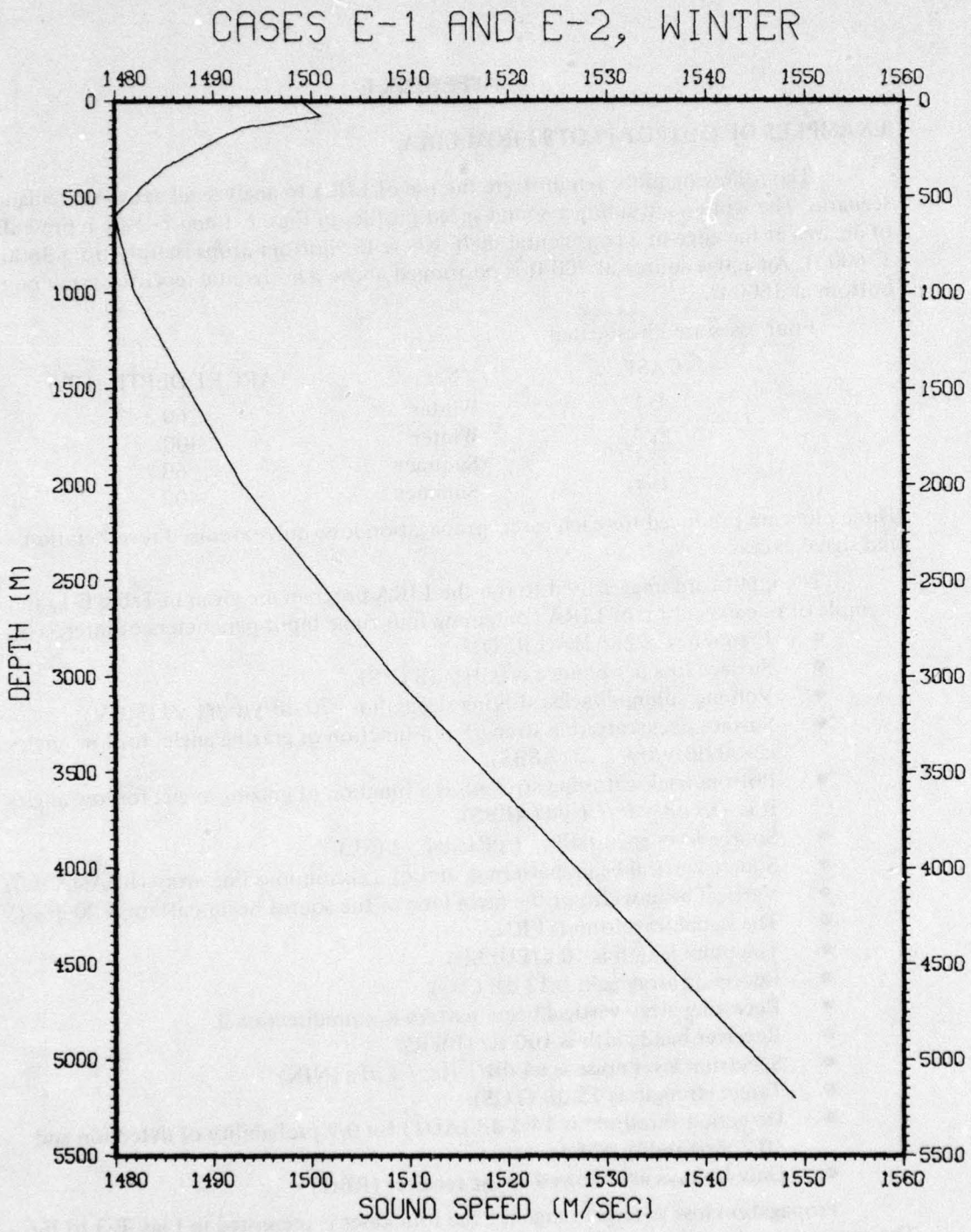

Figure E-1. Sound-speed profile for CASES E-1 and E-2.

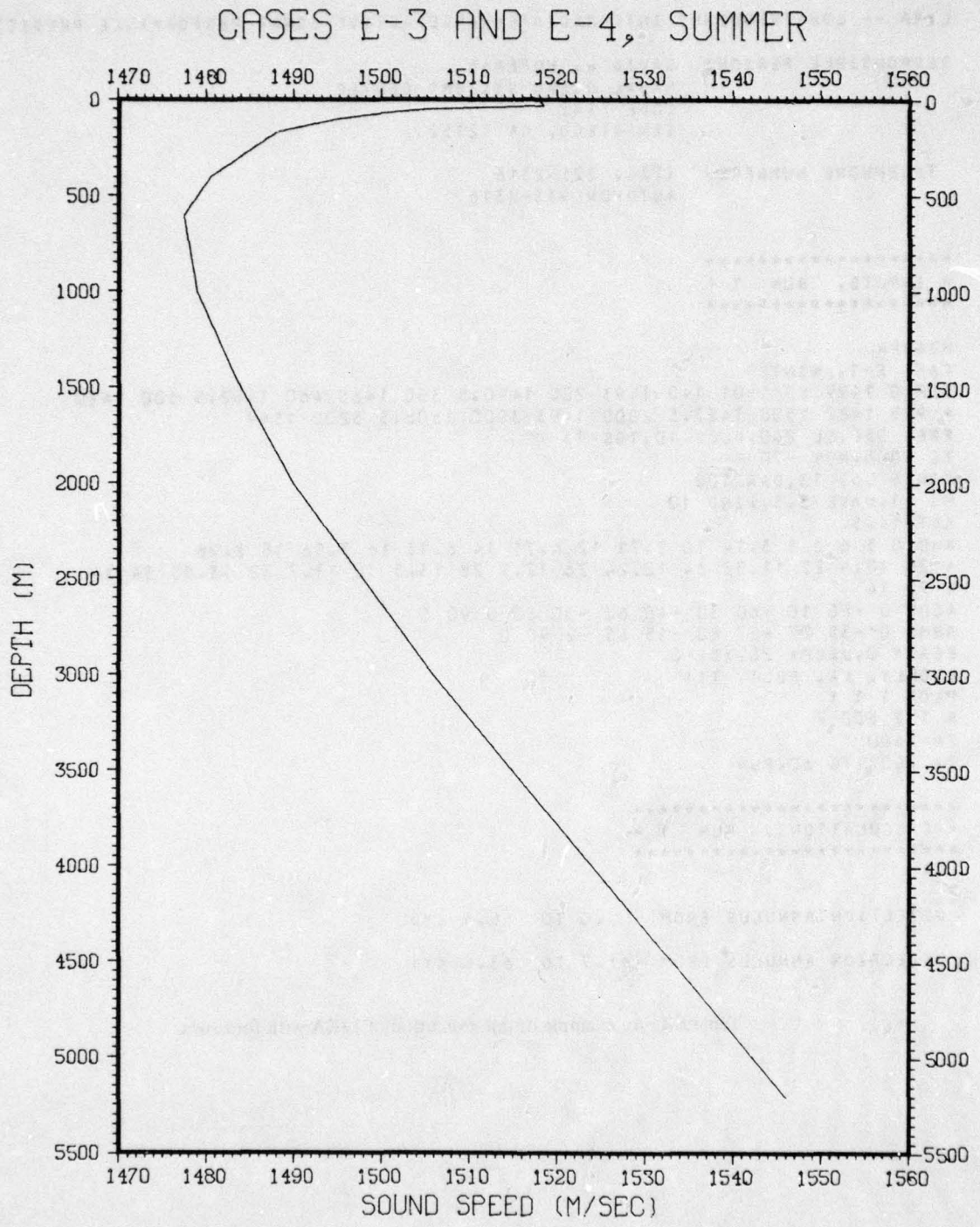

Figure E-2. Sound-speed profile for CASES E-3 and E-4.

```
LIRA -- LOW-FREQUENCY INTERMEDIATE-RANGE ACTIVE-SONAR PERFORMANCE PREDICTIONS

RESPONSIBLE PERSON:   DAVID W. HOFFMAN
                      NAVAL OCEAN SYSTEMS CENTER
                      CODE 7142
                      SAN DIEGO, CA 92152

 TELEPHONE NUMBERS    (714) 225-2316
                      AUTOVON 933-2316


********************
* INPUTS,  RUN  1 *
********************

HEADER
CASE E-1, WINTER
SSP 0 1499 60 1501 140 1493 200 1490.5 350 1485 460 1482.5 600 1480
* 995 1482 1500 1487.5 2000 1493 3000 1508.5 5200 1549
FREQ 250,SL 240,PULS 10,TGS 15
ZC 1000,MUV -70
NIN 67,DI 13,BWR 100
HS -1,WAVE 3.5,WIND 10
ADT 14.5
AHB 0 3 6 3 8 3.14 10 3.71 12 4.71 14 6.13 16 7.56 18 8.98
* 20 10.4 22 11.32 24 12.24 26 12.9 28 13.3 30 13.7 32 13.85 34 14
* 90 14
ASBS 0 -60 10 -60 30 -40 60 -30 80 0 90 5
ABBS 0 -35 77 -27 80 -15 85 -2 90 0
BEAMX 0,DELPX 20,XDE 0
DRONLY, LA, RBOT, TTY
PLOT 1 1 1
R 1 2 600 2
ZR 3600
ZX 700,ZTG 60,RUN

**************************
* CALCULATIONS,  RUN  1 *
**************************


 DETECTION ANNULUS FROM     .0 TO   5.5 KYD

 DETECTION ANNULUS FROM  61.7 TO  63.8 KYD
```

Table E-1. An example of one execution of LIRA with four runs.

```
********************
* INPUTS,  RUN  2 *
********************

HEADER
CASE E-2, WINTER
ZTG 400,RUN

*************************
* CALCULATIONS,  RUN  2 *
*************************

 DETECTION ANNULUS FROM     .0 TO   5.8 KYD
 DETECTION ANNULUS FROM  41.8 TO  43.3 KYD
 DETECTION ANNULUS FROM  47.7 TO  62.0 KYD
 DETECTION ANNULUS FROM  99.7 TO 101.7 KYD
 DETECTION ANNULUS FROM 103.3 TO 107.2 KYD
 DETECTION ANNULUS FROM 109.9 TO 113.5 KYD
 DETECTION ANNULUS FROM 117.9 TO 119.2 KYD
 DETECTION ANNULUS FROM 155.1 TO 157.9 KYD
 DETECTION ANNULUS FROM 161.5 TO 165.6 KYD
 DETECTION ANNULUS FROM 215.7 TO 217.4 KYD
 DETECTION ANNULUS FROM 225.8 TO 229.2 KYD
```

Table E-1. Continued.

```
********************
* INPUTS,  RUN  3 *
********************

HEADER
CASE E-3, SUMMER
SSP 0 1518 30 1518.5 50 1505 70 1500 100 1495 170 1488 400 1480.5 500 1479
* 600 1477.5 1000 1479 1500 1484 2000 1490 3000 1506 5200 1546
ZX 700,ZTG 60,RUN

********************
* CALCULATIONS,  RUN  3 *
**************************

 DETECTION ANNULUS FROM     .0 TO    5.3 KYD

 DETECTION ANNULUS FROM  55.6 TO  57.9 KYD

 DETECTION ANNULUS FROM  59.1 TO  61.3 KYD

 DETECTION ANNULUS FROM  63.7 TO  65.7 KYD

 DETECTION ANNULUS FROM 113.8 TO 115.4 KYD

 DETECTION ANNULUS FROM 117.7 TO 119.2 KYD

 DETECTION ANNULUS FROM 121.7 TO 123.4 KYD
```

Table E-1. Continued.

```
********************
* INPUTS,  RUN  4 *
********************

HEADER
CASE E-4, SUMMER
ZTG 400,RUN

*************************
* CALCULATIONS,  RUN  4 *
*************************

 DETECTION ANNULUS FROM     .0 TO   5.2 KYD

 DETECTION ANNULUS FROM   41.9 TO  43.3 KYD

 DETECTION ANNULUS FROM   47.6 TO  59.6 KYD

 DETECTION ANNULUS FROM   99.5 TO 107.9 KYD

 DETECTION ANNULUS FROM 109.0 TO 113.7 KYD

 DETECTION ANNULUS FROM 115.5 TO 117.3 KYD

 DETECTION ANNULUS FROM 149.9 TO 158.0 KYD

 DETECTION ANNULUS FROM 159.5 TO 164.0 KYD

 DETECTION ANNULUS FROM 165.9 TO 167.1 KYD

 DETECTION ANNULUS FROM 201.6 TO 209.2 KYD

 DETECTION ANNULUS FROM 213.1 TO 215.5 KYD

 DETECTION ANNULUS FROM 253.4 TO 255.8 KYD

 DETECTION ANNULUS FROM 263.8 TO 265.7 KYD

 DETECTION ANNULUS FROM 303.9 TO 305.1 KYD

 DETECTION ANNULUS FROM 307.9 TO 309.1 KYD

 DETECTION ANNULUS FROM 410.0 TO 411.1 KYD

********************
* INPUTS,  RUN  5 *
********************

END
```

Table E-1. Continued.

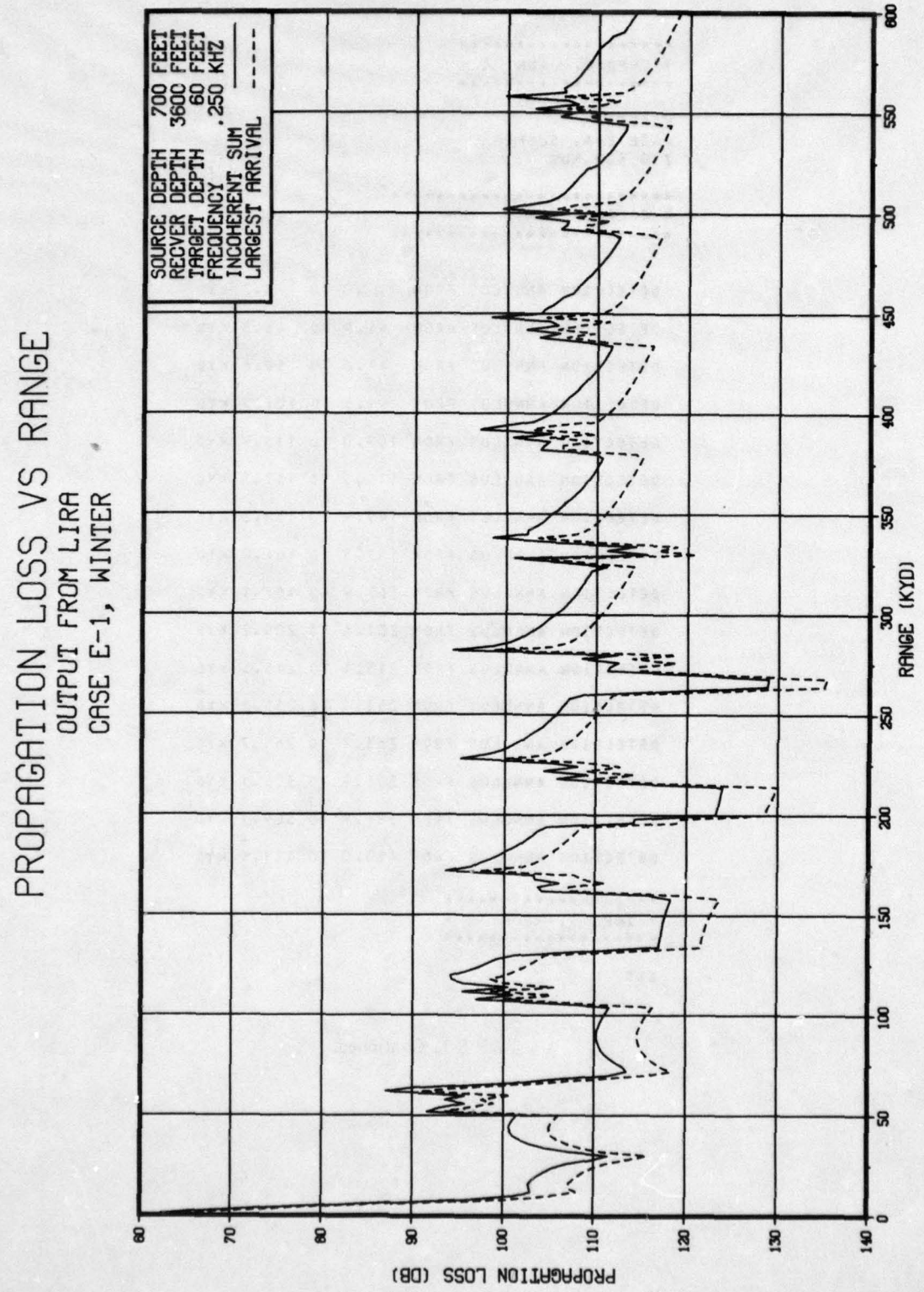

Figure E-3. Propagation loss for CASE E-1.

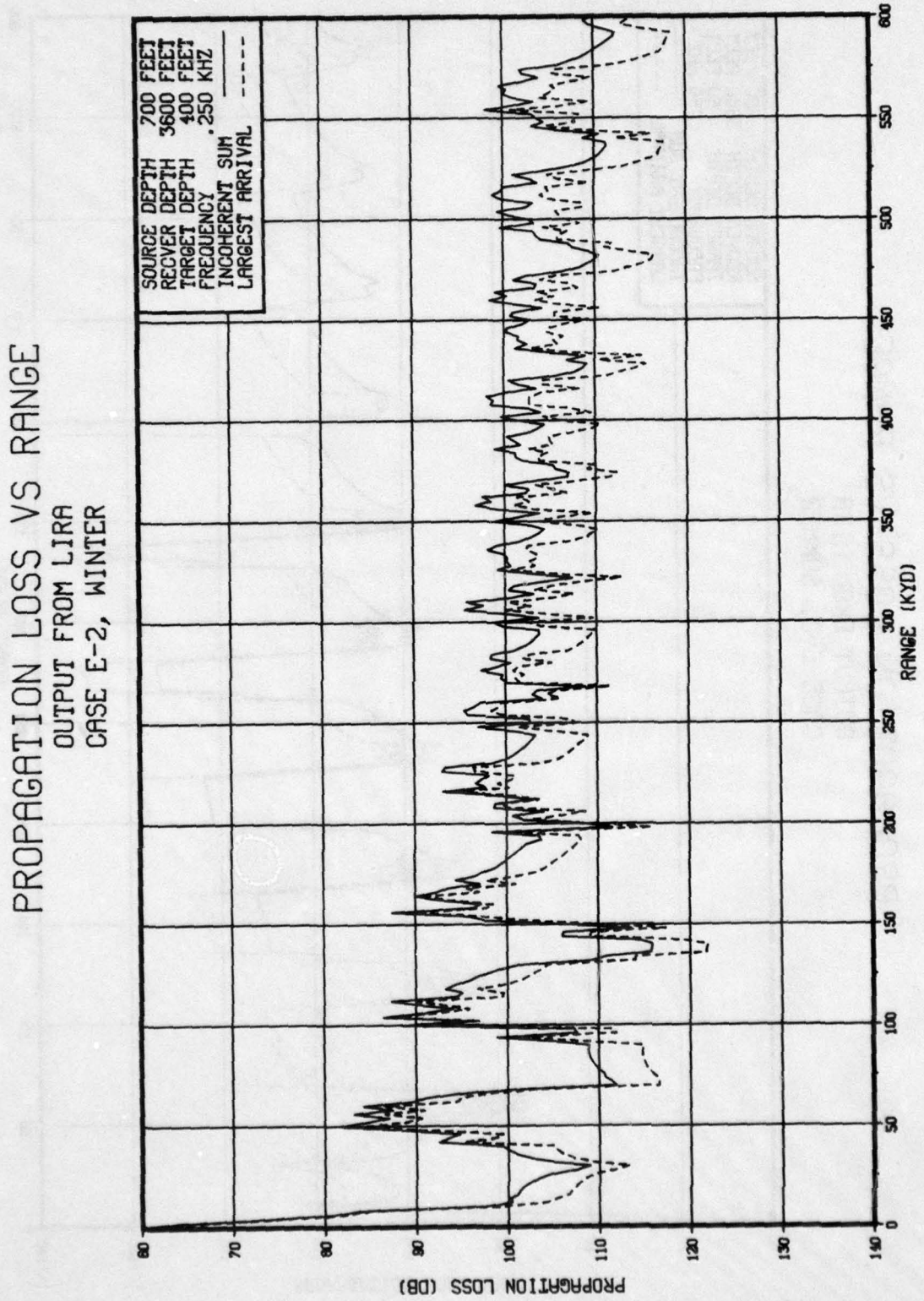

Figure E-4. Propagation loss for CASE E-2.

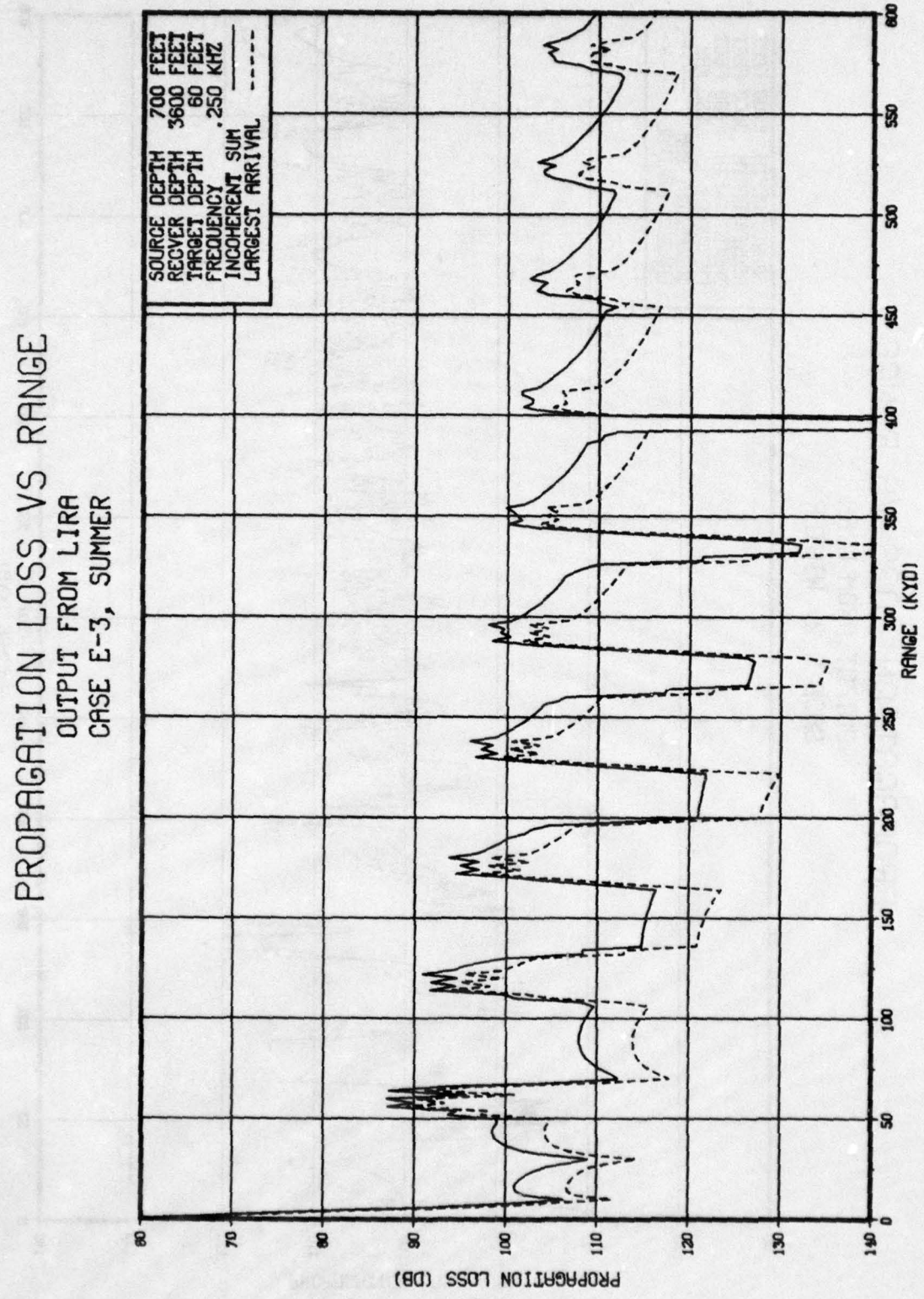

Figure E-5. Propagation loss for CASE E-3.

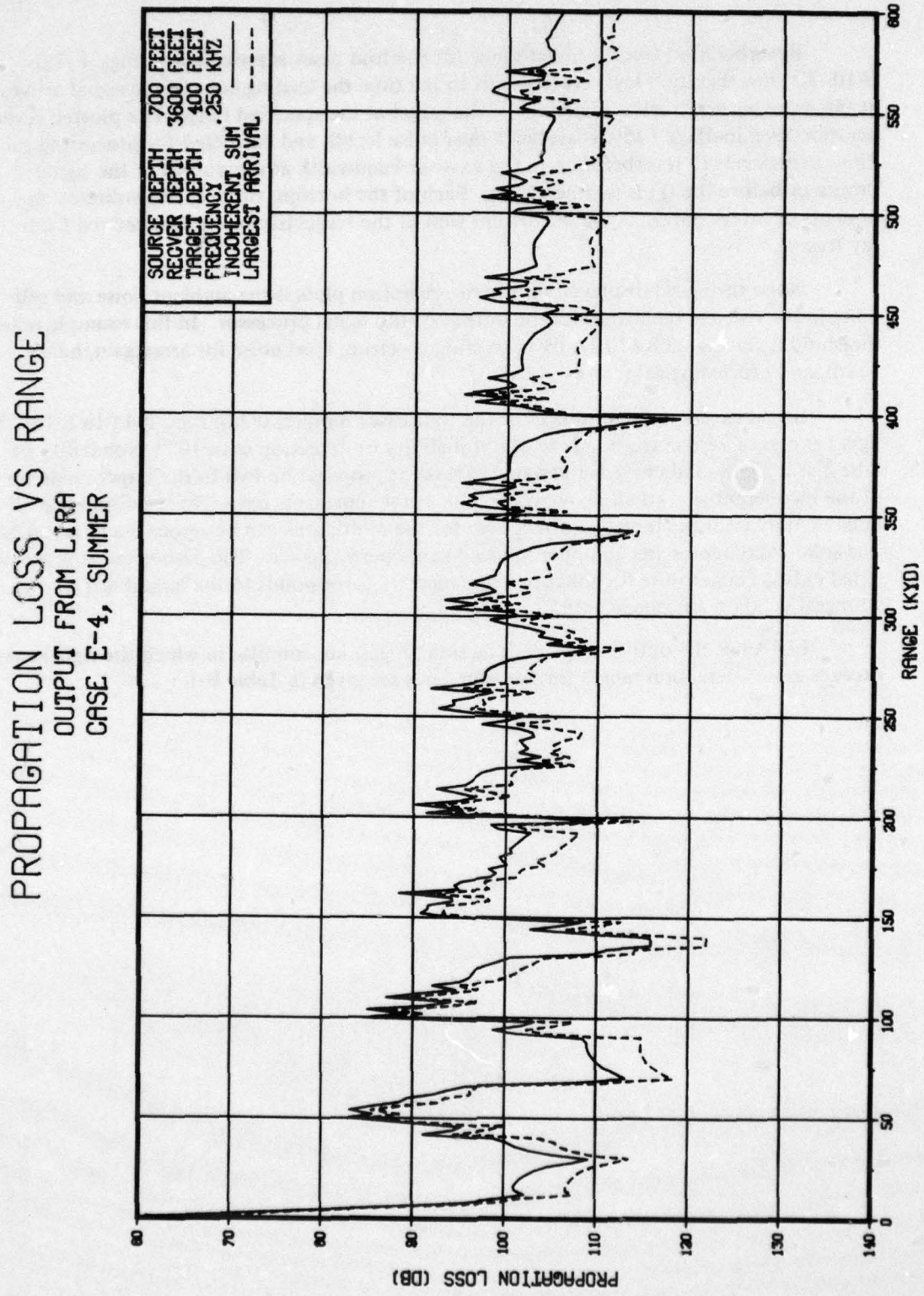

Figure E-6. Propagation loss for CASE E-4.

Reverberation level vs target range for the four cases is presented in Figs. E-7 to E-10. The reverberation level corresponds to the time the leading edge of the signal arrives at the receiving array after bouncing off the target at the specified range. The plotted reverberation level in dB // 1 μPa is averaged over pulse length and corrected for processing gain. This corresponds to reverberation in the receiver bandwidth at the output of the signal processor before the thresholding device. Each of the bottom, surface, and volume components of reverberation is the incoherent sum of the respective intensities derived from ray tracing.

Noise threshold displayed on the reverberation plots is the ambient noise and self-noise in the receiver bandwidth at the output of the signal processor. In this example noise threshold is calculated by LIRA by correcting spectrum level noise for array gain, bandwidth, and processing gain.

Signal excess vs target range for the four cases is presented in Figs. E-11 to E-14. A signal excess of zero corresponds to 0.9 probability of detection with 10^{-4} probability of false alarm. The solid curve is the signal excess for propagation loss to the target made up of the incoherent sum of all ray arrivals. This curve represents optimistic performance obtainable only if all the target-return echoes for the multipaths can be resolved and recombined. The solid curve represents an upper limit on sonar performance. The dashed curve is the proper signal excess curve to use for sonar performance. It corresponds to the largest arrival, the strongest echo on any single path.

LIRA has the option to print detection ranges, i.e., annulae in which the signal excess exceeds zero. Detection ranges for the four cases are given in Table E-1.

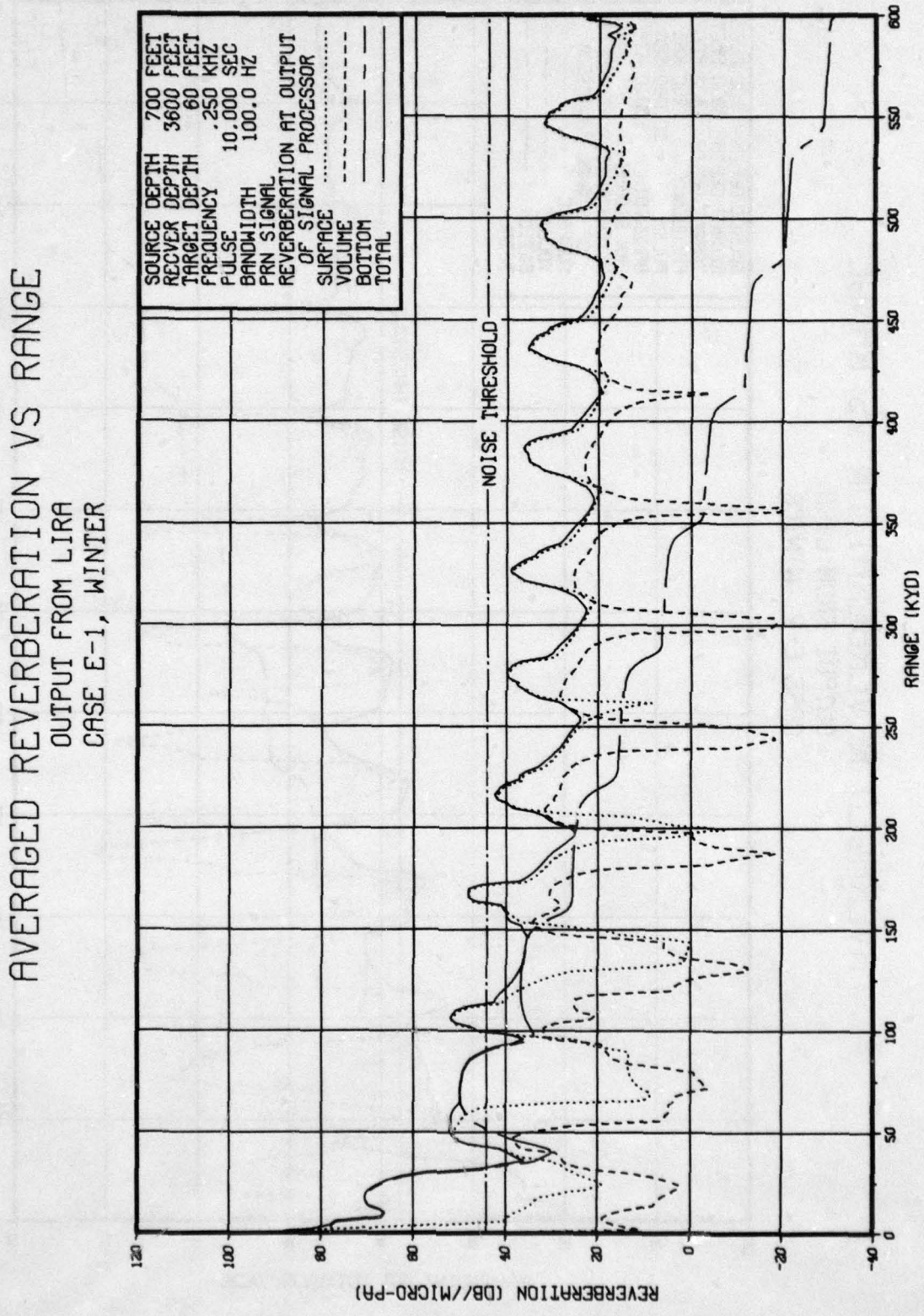

Figure E-7. Reverberation for CASE E-1.

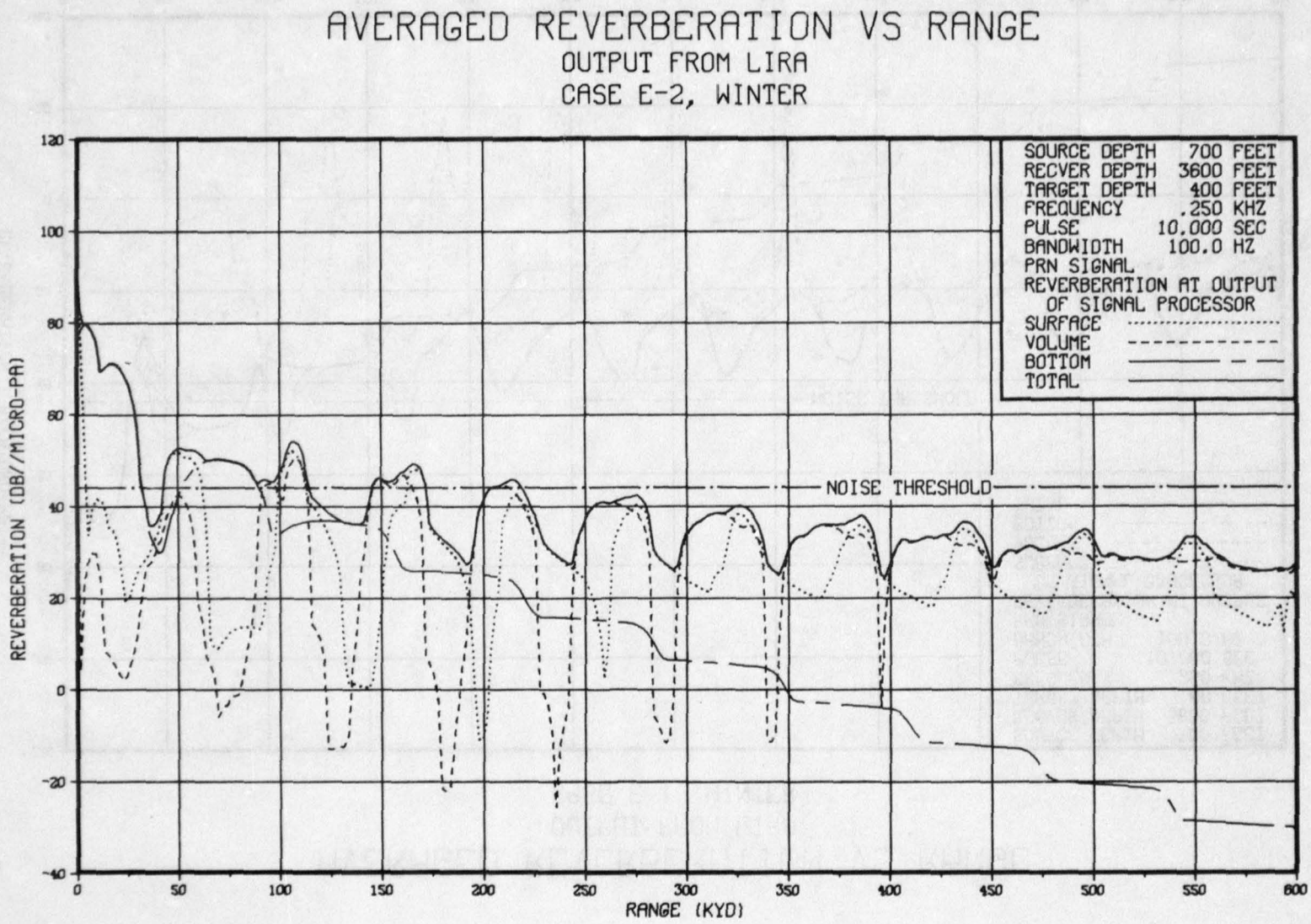

Figure E-8. Reverberation for CASE E-2.

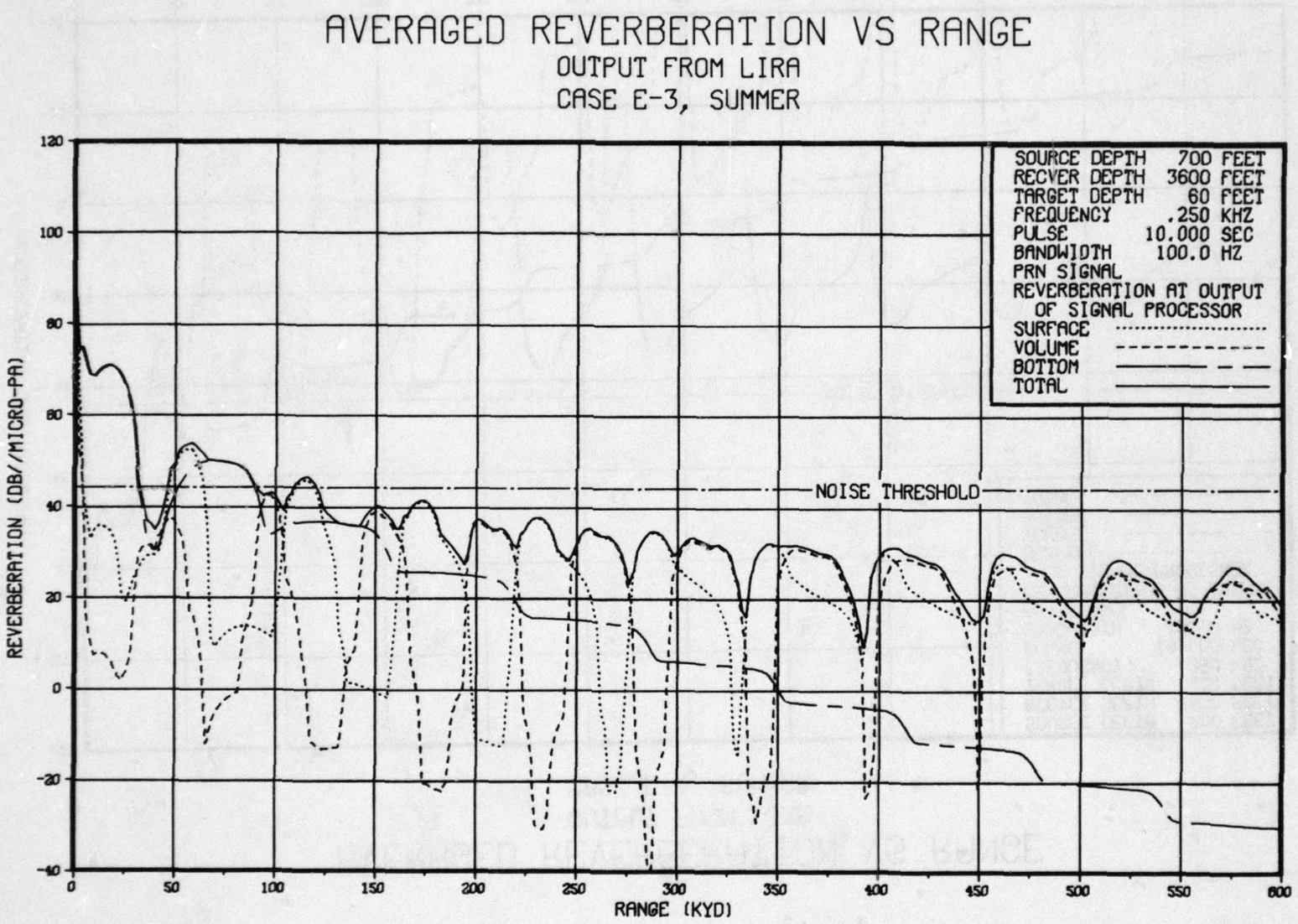

Figure E-9. Reverberation for CASE E-3.

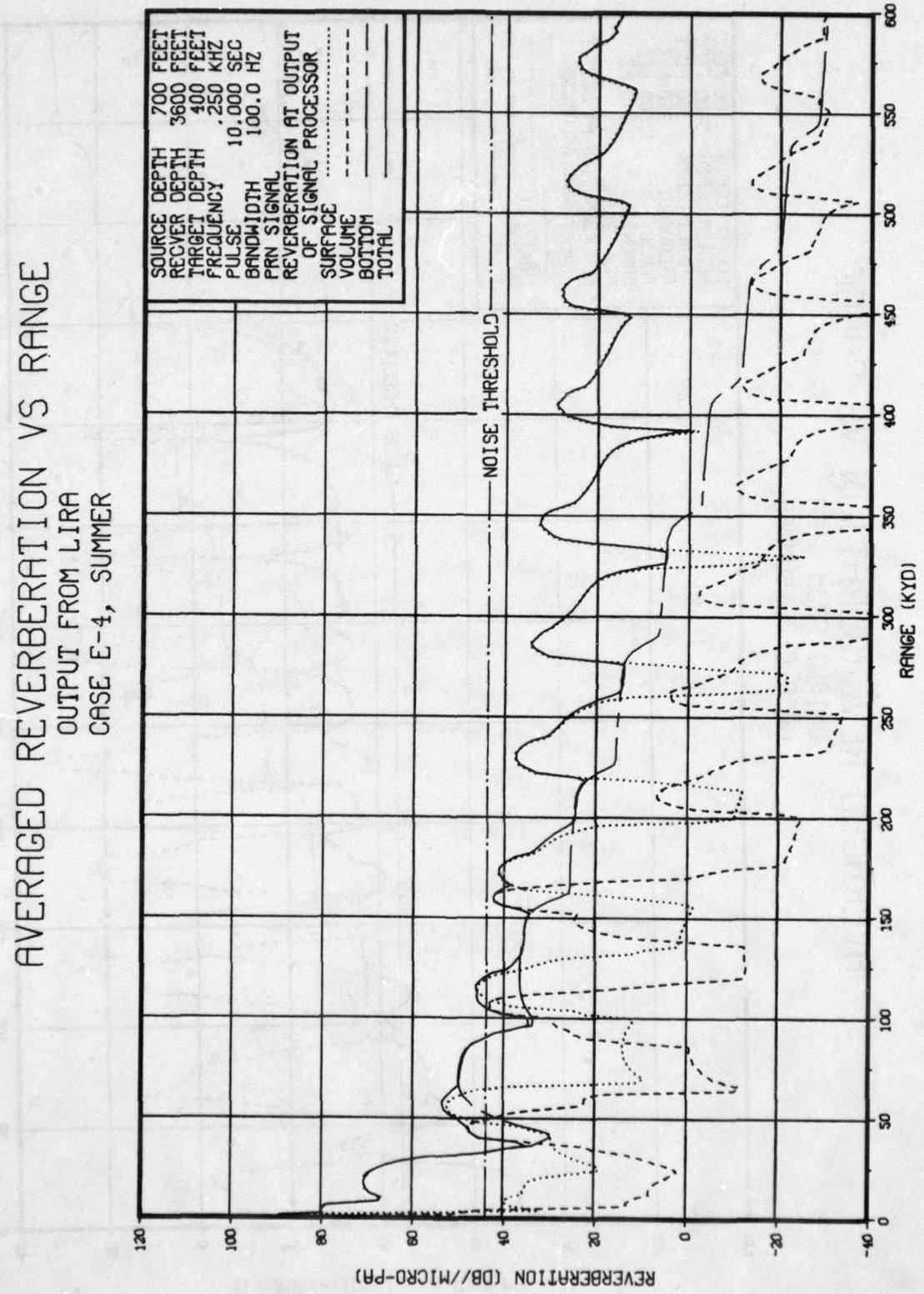

Figure E-10. Reverberation for CASE E-4.

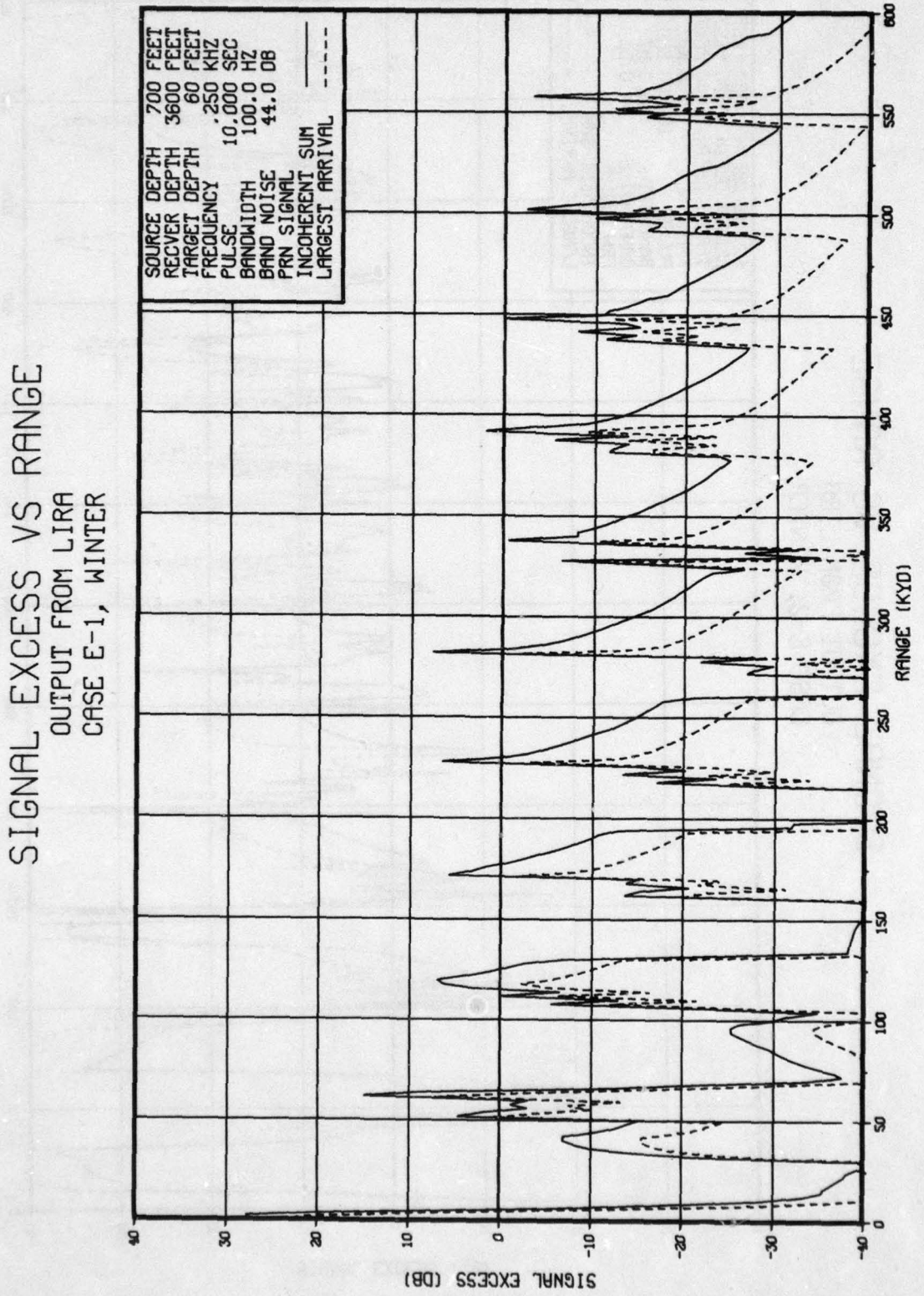

Figure E-11. Signal excess for CASE E-1.

AD-A083 677 NAVAL OCEAN SYSTEMS CENTER SAN DIEGO CA F/G 17/1
LIRA: A MODEL FOR PREDICTING THE PERFORMANCE OF LOW-FREQUENCY A--ETC(U)
JUN 79 D W HOFFMAN
UNCLASSIFIED NOSC/TD-259 NL

2 OF 2
AD A083677

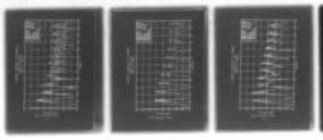

END
DATE FILMED
6-80
DTIC

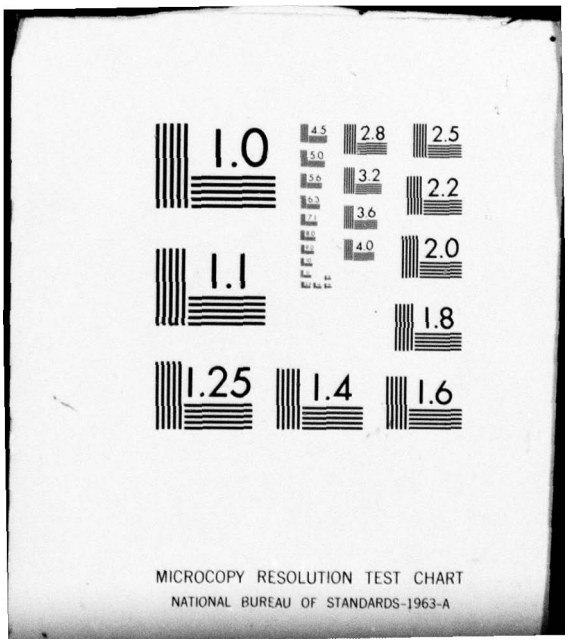
1.0
1.1
1.25
4.5
5.0
5.6
6.3
7.1
2.8
3.2
3.6
4.0
2.5
2.2
2.0
1.8
1.4
1.6
MICROCOPY RESOLUTION TEST CHART
NATIONAL BUREAU OF STANDARDS-1963-A

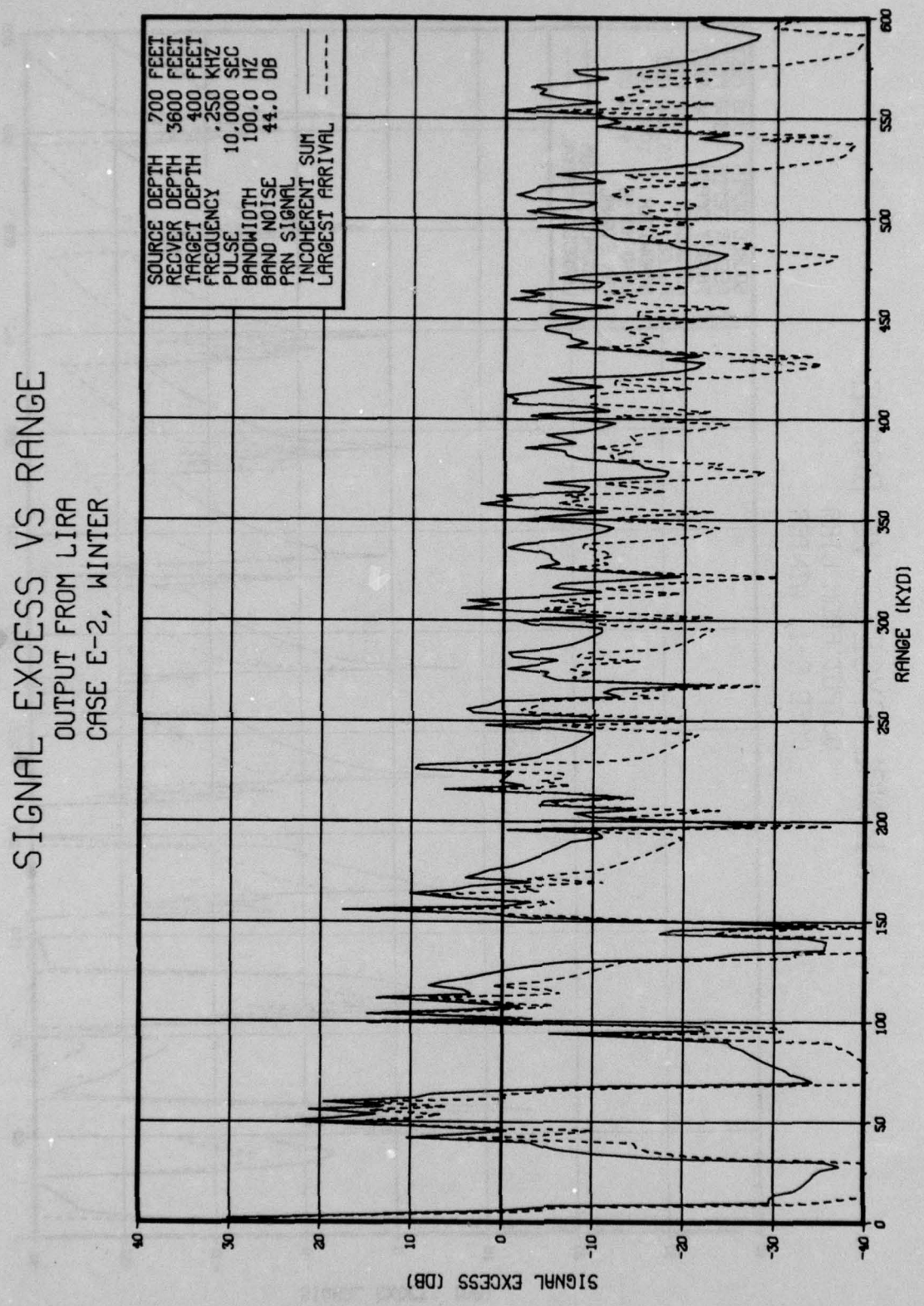

Figure E-12. Signal excess for CASE E-2.

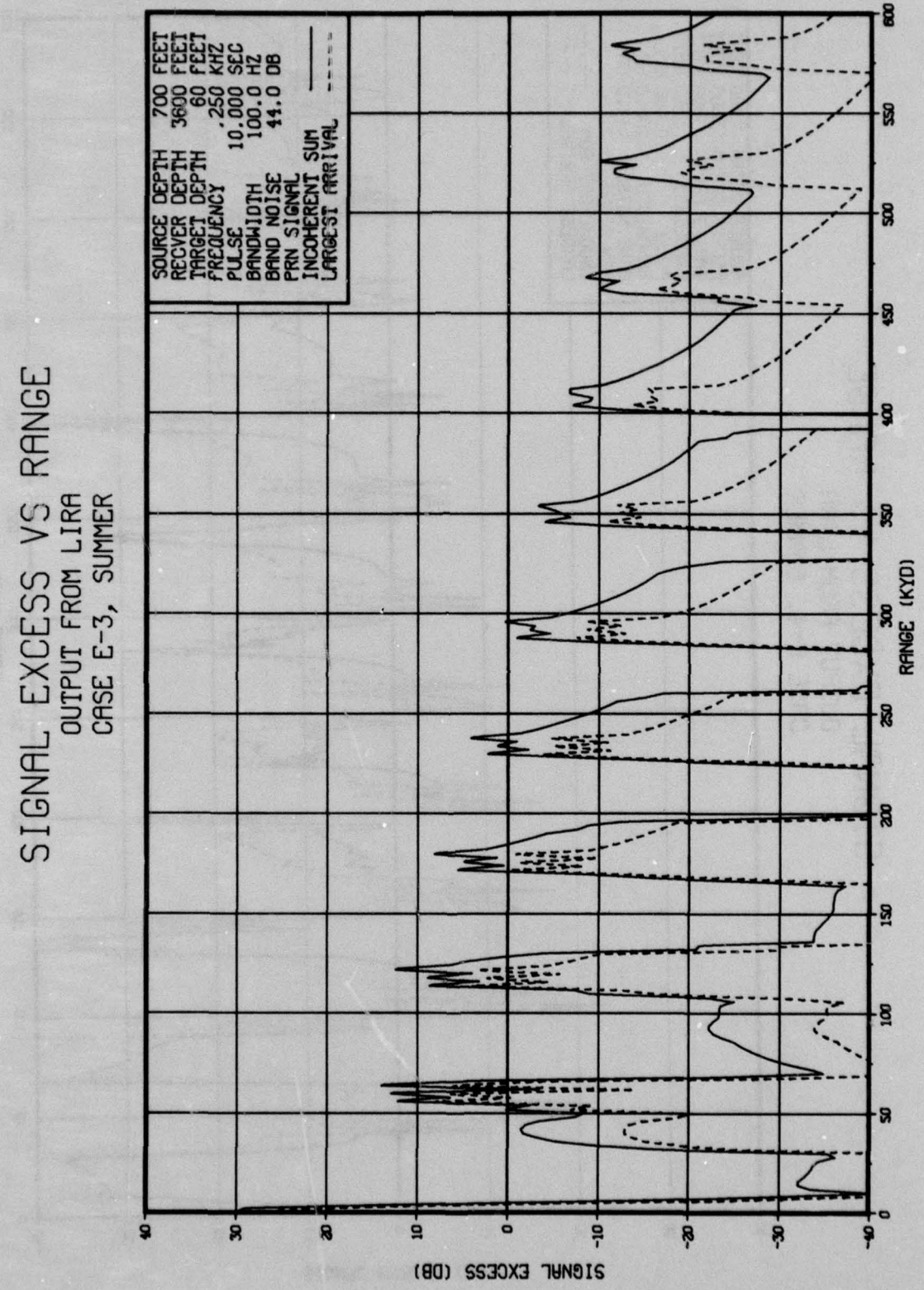

Figure E-13. Signal excess for CASE E-3.

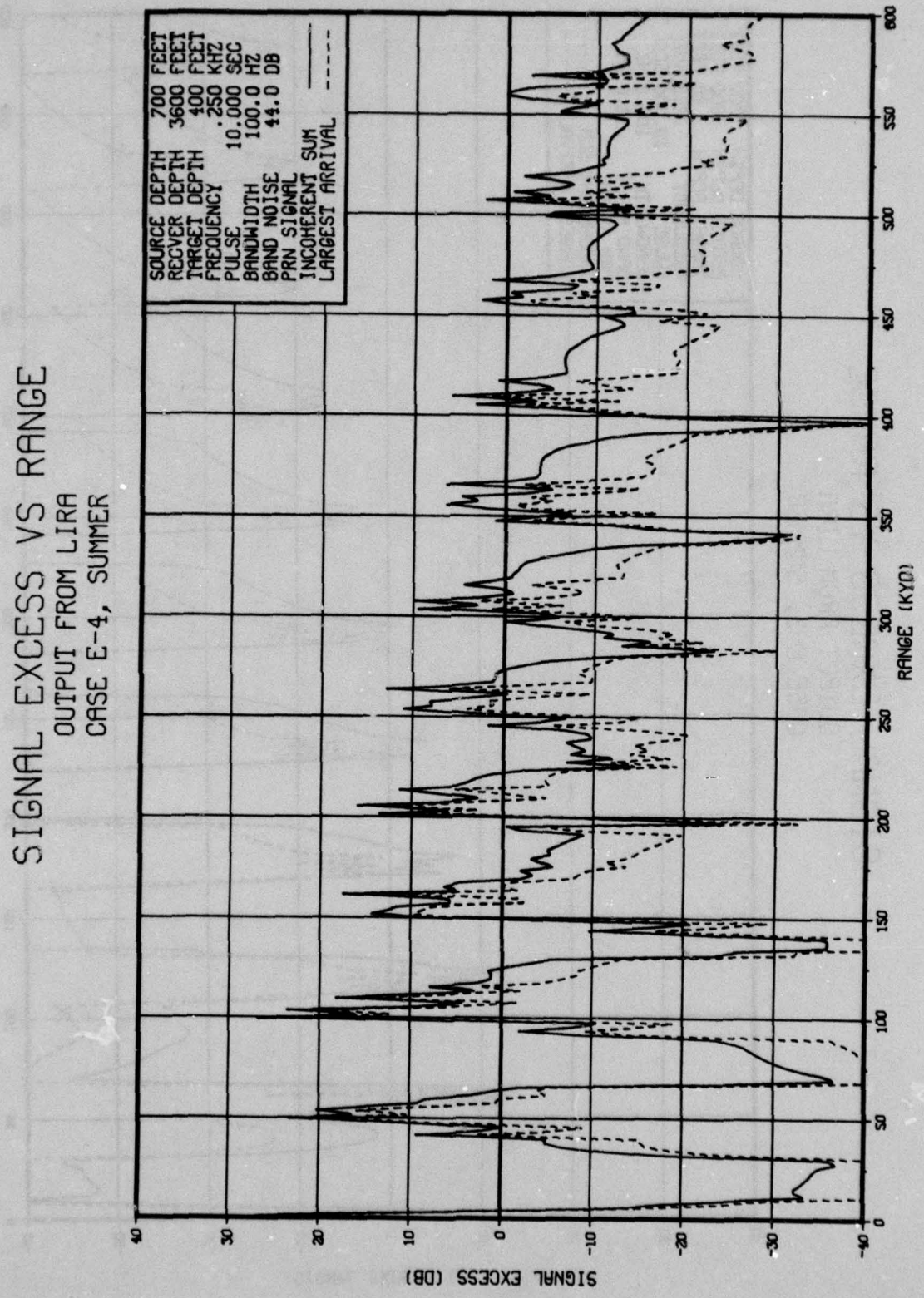

Figure E-14. Signal excess for CASE E-4.

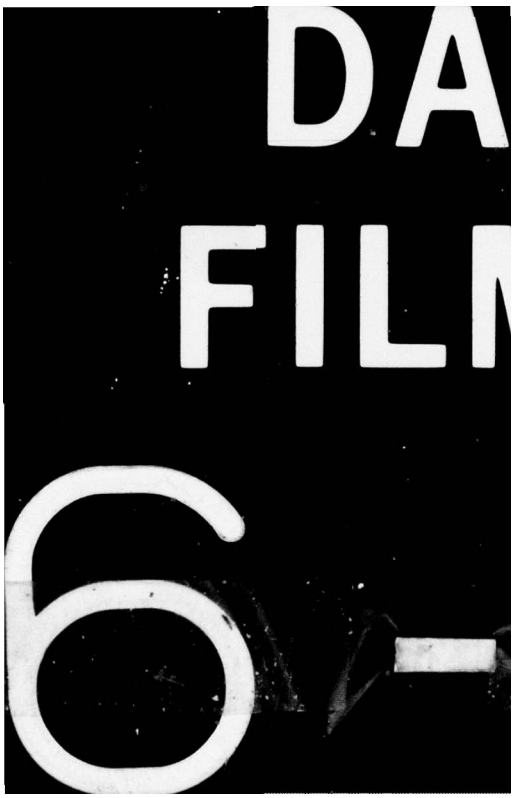
DA
FILM
6-